U. S DEPARTMENT OF COMMERCE
WEATHER BUREAU

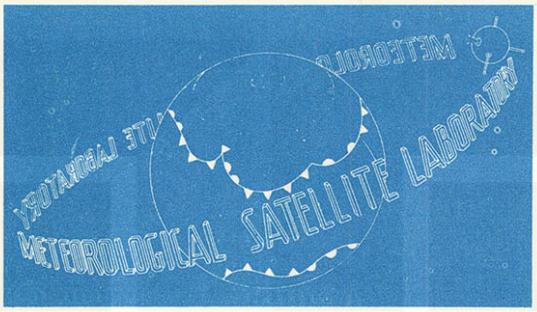

METEOROLOGICAL SATELLITE LABORATORY
REPORT NO. 14

A Technique For Precise Analysis For Satellite Data; Volume I - Photogrammetry

WASHINGTON, D. C.
JANUARY 1963

U. S. DEPARTMENT OF COMMERCE

Luther H. Hodges, Secretary

WEATHER BUREAU

F. W. Reichelderfer, Chief

METEOROLOGICAL SATELLITE LABORATORY

REPORT NO. 14

A TECHNIQUE FOR PRECISE ANALYSIS FOR SATELLITE DATA; VOLUME I - PHOTOGRAMMETRY

by Tetsuya Fujita

This paper also represents Research Paper No. 13 of the Mesometeorology Project, Department of the Geophysical Sciences, the University of Chicago. Sept. 1962

This research has been supported by the Meteorological Satellite Laboratory, U. S. Weather Bureau, under contract Cwb 10215.

Washington, D. C.
January 1963

Table of Contents

LIST OF TABLES

MATHEMATICAL SYMBOLS

a	semimajor axis of satellite orbit; (as IIIrd subscript) reference to apogee
AN	(as superscript) ascending node of satellite
C	(as Ist superscript) celestial
d	great-circle distance of a terrestrial point measured from subsatellite point
d_T	track distance in great-circle distance
e	eccentricity of satellite orbit; (as Ist subscript) earth
e_e	eccentricity of the earth's ellipsoid
E	mean radial distortion of readout image
f	focal distance of positive image; (as IInd subscript) fixed-earth reference
f_e	oblateness of the earth
f_R	focal distance of readout image
F	(as Ist superscript) fixed-earth
G	gravitational constant
GL	(as superscript) sun-glint point
GRE	(as superscript) Greenwich
H	height of satellite above terrestrial ellipsoid
H_c	height of cloud above mean sea-level
i	inclination of projection equator
I	(as Ist superscript) image
L_θ	one-degree length of earth's longitude
L_ϕ	one-degree length of earth's latitude
M_e	mass of the earth
n	(as IIIrd subscript) reference to node
o	(as IInd subscript) orbital motion
P	period in general which is identified by three subscripts
P_{soa}	anomalistic period of satellite
P_{son}	nodal period of satellite
P_{sss}	solar spin-period of satellite
PM	(as superscript) primary point
PP	(as superscript) principal point
r	radius vector of satellite
R	radius of the earth
$\overline{R}$	mean radius of the earth defined by $1/2\ (R_E + R_P)$
R_E	equatorial radius of the earth
R_P	polar radius of the earth

R_R radius of a ring on readout image

$\bar{R}_R$ mean radius of a ring on readout image

s (as Ist subscript) satellite; (IInd subscript) spin motion; (as IIIrd subscript) reference to the sun

SA (as superscript) spin axis

SAT (as superscript) satellite

SP (as superscript) subsatellite point

SS (as superscript) subsolar point

SUN (as superscript) the sun

t time

t_F time of fix

t_S^{MAX} time at the maximum satellite nadir-angle

t_S^{MIN} time at the minimum satellite nadir-angle

T (as Ist superscript) terrestrial

u_S argument of satellite

u_S^{MIN} argument of satellite at the minimum satellite nadir-angle

v true anomaly

VE vernal equinox

w argument of perigee

$\dot{w}$ perigee rate

α azimuth

γ tangential angle in general; primary tangential angle

γ' primary tangential angle

γ_R tangential angle of an object on readout image

γ_T tangential angle of an object on target

γ_V tangential angle of an object on vidicon image

γ^{SN} tangential angle of the sun

δ declination

δ_H dip angle

ΔR excess radius of the earth

Δt actual time less the time of fix ($t - t_F$); OOZ March 21 less time of vernal equinox

$\Delta\rho_e$ excess radius of curvature of the earth

ϵ radial angle in general

ϵ_H horizon distance

ϵ_R radial angle of an object on readout image

ϵ_T radial angle of an object on target

ϵ_V radial angle of an object on vidicon image

$\mathcal{E}$ equation of time

ζ vertical angle

η	nadir angle in general
η_s	satellite nadir-angle
η_s^{MAX}	maximum satellite nadir-angle
η_s^{MIN}	minimum satellite nadir-angle
η_T	track distance in nadir angle
θ	earth longitude
$\textcircled{H}$	fixed-earth longitude
ι	inclination of satellite orbit
ρ_e	local radius of curvature of the earth
τ	tilt
ϕ	latitude in general
ϕ_B	baseplate angle
ϕ_c	geocentric latitude
ϕ_d	geodetic latitude
χ	angle between optical and nodal-spin axes of TIROS camera
ψ	horizontal angle
ψ_i	image horizontal angle
ω	angular velocity in general
ω_{eof}	angular velocity of the earth's orbital motion referred to the fixed-space
ω_{eon}	angular velocity of the earth's orbital motion relative to the nodes
ω_{esf}	fixed-space rotation rate of the earth
ω_{esn}	rotation rate of the earth relative to the nodes
ω_{ess}	mean solar rotation rate of the earth
ω_{ssf}	fixed-space spin-rate of satellite
Ω	right ascension in general
$\dot{\Omega}^{AN}$	right ascension rate
$\overline{\Omega}^{SUN}$	right ascension of the mean sun

INTRODUCTION

The TIROS series of meteorological satellites have added new information of nephsystems viewed from outer space several hundred kilometers above the surface of the earth. In order to utilize these photographs for operational purposes, they have to be analysed as soon as possible after each readout. To meet the operational requirements of quick rectification, Glaser (5) developed a well known method of image rectification which permits us to obtain the patterns of nephsystems with a possible error up to two degrees of the great-circle arc. His method is reported later by Hubert (7) in detail so that anyone who wishes to analyse satellite photographs is able to perform his own rectification using the charts and grids included in the report. They are the focus sheets, one for each TIROS-borne camera; tilt indicators for discrete increments of satellite height; perspective grids for discrete increments of tilt and satellite height; a transfer grid constructed to the scale of a geographic map; and an Oblique Mercator Map Projection. These charts and grids are used at the readout stations to produce quick nephanalysis which are transmitted through facsimile circuits.

For research purposes, however, a need for better accuracy arose on many occasions. This would naturally necessitate accurate determination of satellite attitudes and exposure times. In an effort to determine the spin-axis orientation, Hubert (7) made a survey of the time change of the right ascension and the declination of the TIROS I spin-axis point, reaching a conclusion that an extremely accurate position of the spin axis is essential to obtain the satellite attitude using the TIROS I Orientation Nomogram designed by Ruff (7). Despite the fact that the azimuth and the nadir angle determination is based upon the assumption that a great circle on the nomogram is a straight line, the error is found to be insignificant if the nadir angles fall within about 30 degrees. Beyond this angle, of course, the error, especially in azimuth angles, increases appreciably. The work by Hubert and Ruff led the author to develop a precise method for use in research purposes.

A technique for precise rectification of satellite cloud photographs was reported by Fujita (4) for use at the International Meteorological Satellite Workshop, 13-22 Nov 1961. The technique has been tested for various TIROS photographs with or without landmarks, revealing that the error normally does not exceed 0.2 degrees of the great-circle arc.

Since the first photograph from TIROS I was transmitted back to the earth on 1 April 1960 various terms were applied to express the subjects necessary to investigate meteorological phenomena using satellite data. A glossary of about 50 terms was prepared by the Meteorological Satellite Laboratory for the International Meteorological Satellite Workshop, Nov 1961, in Washington, D. C. These terms contained in the "Glossary of Terms used in Satellite Meteorology" were adopted in the International Workshop and have been widely used.

Because of the necessity of standardizing the terms to be used in the rapidly expanding field of Satellite Meteorology, the author made a survey of terms in addition to these 50 terms. They were then reviewed and discussed in the conference on glossary at the Meteorological Satellite Laboratory, 12 Sept 1962. Participants were Louis Allison (National Aeronautics and Space Administration), William R.

Bandeen (National Aeronautics and Space Administration), Russell C. Doolittle (Meteorological Satellite Laboratory), Tetsuya Fujita (University of Chicago), Arnold H. Glaser (Allied Research), Joseph L. Goldman (University of Chicago), Lester Hubert (Meteorological Satellite Laboratory), David Q. Wark (Meteorological Satellite Laboratory), and Linwood F. Whitney, Jr. (Meteorological Satellite Laboratory). About 200 terms were brought into discussion and adopted by the participants. Included in this glossary are approximately 160 terms which are used in this text dealing primarily with the photogrammetric analysis of satellite cloud photographs.

When the radiation data of TIROS-borne scanning radiometer became available in 1961, it was found that the author's photogrammetric technique can also be used for the precise determination of scan lines and scan spots on the earth. Only one grid which is called the radiometer grid is required in addition to the rectification grids and charts appearing in this report. The radiometer grid when placed on an undistorted image permits us to determine the exact area on the earth, the radiation from which is received within the aperture of the TIROS scanning radiometers.

An attempt was made to compare the infrared radiation with the cloud patterns by plotting the radiation values directly on the corresponding cloud photographs. This would varify the accuracy of both photograph and infrared analysis. The results were that the nephsystems determined by the scanning radiometers are slightly larger in horizontal dimensions than those seen on the photographs. Nevertheless, their locations are found to fit extremely well. This method of radiation data analysis will appear in Vol. II of this report.

This report includes both theories and actual methods of precise rectification. First, the shape of the earth and the orbital characteristics of earth orbiting satellites are discussed leading into the three coordinate systems conveniently used in the analysis. A survey of the characteristics of TIROS-borne cameras is described in an attempt to show users the nature of the distortions and the methods of their correction. The readers will then find various map projections and their matching overlays which are designed to minimize the error coming from the use of improper projection. Before the actual rectification is explained, the attitude of satellite with respect to the sun and the earth is described so that we are able to determine the position of a satellite and the orientation of its spin axis before rectification is performed. It is seen that the prior knowledge of satellite attitudes is very helpful not only to estimate the photographic coverage but also to perform rectification of a picture sereis which include no landmarks.

Finally, the rectification methods are explained step by step dealing first with the precise method which can be performed if we have a landmark in one of the pictures belonging to a series to be rectified. Next, an approximate method applicable to any series of satellite photographs is explained. In fact, such rectification methods should be practiced before they can be applied to the complicated picture series. There are cases that (1) an entire series include no apparent horizon, (2) total number of frames in tape mode series is only a few, (3) there are skips in frame numbers, etc. In case we face such problems, they must be solved individually taking into consideration the various factors such as IPM tracks, attitude changes, and

others. It is expected, however, that the basic knowledge of satellite photographs will help readers to solve the problems in most cases so that any valuable data can be utilized properly.

1. SATELLITE AND THE EARTH

A. DIMENSION OF THE EARTH

For ordinary meteorological problems, the earth may be assumed to be a spheroid. When satellites are involved, however, it becomes necessary to take into consideration the oblateness of the earth. The dimensions of the International Ellipsoid adopted in 1924 by the International Union of Geodesy and Geophysics are

$$\text{Semimajor axis, } R_E = 6378.39 \text{ km,}$$

$$\text{Semiminor axis, } R_P = 6356.91 \text{ km.}$$

The derived quantities from these values are

$$\text{Oblateness, } f_e = (R_E - R_P)/R_E = 0.00337,$$

$$\text{Eccentricity, } e_e = \sqrt{R_E^2 - R_P^2}/R_E = 0.0820,$$

$$\text{Mean Radius, } \frac{1}{2}(R_E + R_P) = 6367.65 \text{ km,}$$

$$\text{Equatorial Bulge, } R_E - R_P = 21.48 \text{ km.}$$

These basic figures describe the shape of the earth, approximated as an ellipsoid. It should be noted that the reference ellipsoids, which are locally determined through detailed geodetic surveys, may slightly differ from the International Ellipsoid. Such a difference is usually so small that it can be neglected in ordinary satellite meteorological problems.

The radius of a terrestrial ellipsoid is expressed by

$$R^2 = R_P^2 / (1 - e_e^2 \cos^2 \phi_c), \tag{1}$$

where ϕ_c denotes the geocentric latitude which is the angle, measured in the meridional plane, between the terrestrial equator and the geocentric radius vector. Equation (1) may be approximated as

$$R^2 = R_E^2 (1 - e_e^2 \sin^2 \phi_c) \tag{2}$$

or

$$R = R_E (1 - f_e \sin^2 \phi_c) \tag{3}$$

or

$$R = R_E (1 - \frac{f_e}{2} + \frac{f_e}{2} \cos 2\phi_c). \tag{4}$$

The earth's radius subtracted by its polar radius is termed the "Excess Radius of the Earth". From Eq. (4) the excess radius can be written as

$$\Delta R = R - R_P = 1/2 \, R_E f_e (1 + \cos 2\phi_c). \tag{5}$$

Table III is prepared to obtain the earth's radius and its excess radius in km as a function of the geocentric latitude. The formulae used are

$$R = 6378.39 (0.998320 + 0.001683 \cos 2\phi_c)$$

and

$$\Delta R = 10.74 (1 + \cos 2\phi_c).$$

B. LOCAL RADIUS OF CURVATURE OF THE EARTH

The radius of the earth, as discussed in the previous section, varies only as a function of the geocentric latitude. The local radius of curvature of the earth, ρ_e , is the function of not only the latitude but also the azimuth along which the curvature is measured. In fact the local radius of curvature takes its maximum value at the poles and minimum at the equator in the meridional direction.

First, the local radius of curvature along a meridian is obtained with the use of a general formula of curvature in rectangular coordinates,

$$\rho_e = \frac{\left\{ 1 + \left(\frac{dz}{dx} \right)^2 \right\}^{\frac{3}{2}}}{\frac{d^2z}{dx^2}} \tag{6}$$

and the equation of the ellipse

$$\frac{x^2}{R_E^2} + \frac{z^2}{R_P^2} = 1 . \tag{7}$$

The absolute value of ρ_e is thus expressed by

$$\rho_e = R_E (1 + f_e - 3 f_e \cos^2 \phi_c) . \tag{8}$$

Its maximum and minimum values are, respectively,

$$\rho_e^{MAX} = R_E (1 + f_e)$$

and

$$\rho_e^{MIN} = R_E (1 - 2 f_e) = R_P (1 - f_e) .$$

It is obvious that the local radius of curvature along a meridian varies equally on both sides of the arithmetical mean of the polar and equatorial radii,

$$\overline{R} = 1/2 (R_P + R_E).$$

Equation (8) can, therefore, be reduced to

$$\rho_e = \overline{R} \left(1 - \frac{3}{2} f_e \cos 2\phi_c \right) . \tag{9}$$

In order to obtain the local radius of curvature in the direction of an arbitrary azimuth angle, α , from a point P in figure 1, we consider a plane which includes the earth's center and the azimuth under discussion. The inclination of this plane with respect to the earth equator is the angle $\angle$COD, where C and D are the points where a meridian perpendicular to this plane intersects the ellipse AP and the earth equator respectively. The geocentric latitude of P is measured along the meridian NB which passes through P. Now we denote the latitude of P by ϕ_c , the angle $\angle$AOP by ℓ , and the inclination $\angle$DOC by I.

The local radius of curvature at P in the direction α can, thus, be solved as that of the inclined ellipse at the same point, P. The semimajor axis OA is obviously equal to R_E, the equatorial radius. However, the semiminor axis, OC, varies

according to the inclination I. The value obtained by substituting ϕ_c in Eq. (3) by I gives

$$OC = R_E (1 - f_e \sin^2 I). \tag{10}$$

Equation (8) may also be applied to the inclined ellipse after a small modification, thus, we have

$$\rho_e = R_E (1 + f_e' - 3 f_e' \cos^2 \ell), \tag{11}$$

where f_e' denotes the oblateness of the inclined ellipse. This oblateness is given by

$$f_e' = (OA - OC) / OA = f_e \sin^2 I. \tag{12}$$

In view of the fact that the oblateness of the earth is small, we may, with high accuracy, apply spherical trigonometric formulae to solve the triangle PBA on the surface of the terrestrial ellipsoid. Thus, we write

$$\tan \ell = \tan \phi_c / \cos \alpha \tag{13}$$

$$\cos I = \cos \phi_c \sin \alpha. \tag{14}$$

Putting Eqs. (12, 13 and 14) into Eq. (11) we obtain

$$\rho = R_E \left\{ 1 + f_e (1 - \sin^2 \alpha \cos^2 \phi_c) \left(1 - \frac{3 \cos^2 \alpha}{\cos^2 \alpha + \tan^2 \phi_c} \right) \right\} \tag{15}$$

which can be reduced, in special cases, to

$$\left(1 + \tfrac{3}{2} f_e \right) \bar{R} \qquad \text{when } \phi_c = 90$$

$$\left(1 - \tfrac{3}{2} f_e \right) \bar{R} \qquad \text{when } \phi_c = 0, \quad \alpha = 0$$

$$\left(1 + \tfrac{1}{2} f_e \right) \bar{R} \qquad \text{when } \phi_c = 0, \quad \alpha = 90$$

$$\bar{R} \qquad \text{when } \phi_c = 45^\circ, \alpha = 0 \text{ and } \phi_c = 0, \alpha = 60^\circ.$$

The deviation of the local radius of curvature from the arithmetical mean radius of the earth

$$\rho_e - \bar{R} = \Delta \rho_e,$$

is called the excess radius of curvature of the earth. The computed excess radius of curvature appears in figure 2. It is seen that the line of zero excess extends from 45 degree latitude and zero azimuth angle to the equator and 60 degree azimuth angle. The area above this line is characterized by positive values which remain + 32.2 km at the pole regardless of the azimuth angle. Near the equator, on the other hand, the variation of $\Delta \rho_e$ with respect to the azimuth is appreciable.

C. POSITION OF SATELLITES IN SPACE

Six orbital elements are required to determine the position of a satellite in orbit at a given time. They are (1) Inclination of orbit, ι; (2) Right ascension of the

ascending node, Ω^{AN}; (3) Argument of perigee, w; (4) Semimajor axis, a ; (5) Eccentricity, e; and (6) Ascending-node time t^{AN}. If the satellite does not suffer perturbations due to the oblateness and the atmosphere of the earth, the elements (1) - (5) remain constant. The ascending-node time, therefore, increases by the nodal period, P, per orbit. The orbital elements of TIROS I-V appears in Table I.

Davis, Whipple and Zirker (3) calculated the effect of the atmospheric drag upon satellite motion, revealing that apogee altitude decreased rapidly while perigee altitude drops gradually. Shortly before a satellite plunges into the earth's atmosphere, the orbit takes almost circular shape. The TIROS series of meteorological satellites were injected into orbits above 500 km; the effect of atmospheric drag is extremely small. Orbital elements of TIROS I by Stafford, Croft, and Marshall (11) were reproduced in Table II. The elements ι, a, and e indicate minor fluctuations resulted partially from tracking errors; nevertheless, they remained fairly constant during the period of a few months. In fact, the expected life of the satellite is 75 years.

Appreciable variations in the right-ascension and the argument of perigee are the characteristics of earth orbiting satellites influenced by the oblateness of the earth. Following the theoretical studies by Spitzer (10) and others, the complete solutions of the precession rate $\dot{\Omega}^{AN}$ and the perigee rate $\dot{w}$, were attempted. The solutions given by Kozai (8) and Danby (2) are

$$\dot{\Omega}^{AN} = -\frac{3\bar{\omega}}{2a^2} J_2 \left(1 + e^2\right)^2 \cos\iota , \tag{16}$$

and

$$\dot{w} = \frac{3\bar{\omega}}{2a^2} J_2 \left(1 + e^2\right)^2 \left(2 - \frac{5}{2}\sin^2\iota\right), \tag{17}$$

where J_2 is a constant indicating the oblateness of the earth, $\bar{\omega}$, the mean angular velocity of the satellite in orbit.

The period, P, of a satellite of infinitesimal mass circling around a central body under the influence of a central force is expressed simply by

$$P = 2\pi\sqrt{\frac{a^3}{G\,M_e}} , \tag{18}$$

where $G = 6.670 \times 10^{-8}$ cm^3 g^{-1} sec^{-2} is the gravitational constant; and $M_e = 5.97 \times 10^{27}$ g, the mass of the central body or the earth. Putting these constants into equation (18), we obtain

$$P = 1.66 \times 10^{-4}\, a^{\frac{3}{2}} \tag{19}$$

the units of which are minutes for period and km for where a denotes the semimajor axis of the satellite orbit, the units of P and a are, respectively, minutes and km. Such a period is too idealistic to be applied to the earth-orbiting satellites. Nevertheless, the periods computed by Eq. (19) was compared with the nodal periods of actual satellites tracked during the years 1957-1960. The results in figure 3 indicate that they agree very well. This suggests that the perturbation in the nodal period is rather small as theoretically expected. The mean angular velocity may, therefore, be written

$$\bar{\omega} = \frac{2\pi}{P} = \sqrt{\frac{G M_e}{a^3}} \tag{20}$$

Putting this period into Eq. (16) and (17) we express both precession and perigee rates as a function of the period, the eccentricity and the inclination, thus

$$\dot{\Omega} = -\lambda P^{-\frac{7}{3}} (1 + e^2)^2 \cos \iota \tag{21}$$

and

$$\dot{w} = \lambda P^{-\frac{7}{3}} (1 + e^2)^2 (2 - \frac{5}{2} \sin^2 \iota), \tag{22}$$

where

$$\lambda = 3 \sqrt[3]{16}\ \pi^{\frac{7}{3}} (G M_e)^{-\frac{2}{3}} J_2 . \tag{23}$$

It follows, therefore, that

$$\lambda P^{-\frac{7}{3}} = \frac{-\dot{\Omega}^{AN}}{(1 + e^2)^2 \cos \iota} = \frac{\dot{w}}{(1 + e^2)^2 (2 - \frac{5}{2} \sin^2 \iota)} \tag{24}$$

can be calculated from satellite tracking data. Scatter diagrams in figure 4 were made by plotting the U. S. and Russian satellites tracked during the years 1957-1960. Using the perigee and precession rates in deg/day, and the nodal period in min., an empirical value of λ obtained by the figure turned out to be

$$\lambda = 3.11 \times 10^5 . \quad (\text{deg/day} \quad \text{min}^{\frac{7}{3}}) .$$

It should be noted that the above difference and perigee rate is zero when the orbital inclination satisfies

$$2 - \frac{5}{2} \sin^2 \iota = 0, \quad \text{or} \quad \sin^{-1} \iota = \frac{2}{\sqrt{5}}$$

namely

$$\iota = 63^{\circ}\ 26' .$$

D. TERRESTRIAL COORDINATES

In order to express the position of a satellite or any other point in space with respect to the earth's surface, frequently used are the terrestrial coordinates which consist of θ, the longitude; ϕ_d, the geodetic latitude; and H, the height.

This coordinate system is well described by introducing the terrestrial subpoint (TSP), the point of intersection of the local vertical through a satellite with the surface of the earth (figure 5). Any reference ellipsoidal surface determined locally by accurate geodetic surveys may be chosen as the earth's surface. It should be noted that NASA uses the International Ellipsoid in computing the Definitive AT MAP which includes subpoint and height data. The earth in this paper also denotes the International Ellipsoid unless otherwise indicated.

The height of a satellite, H, is defined as the closest distance between a satellite and the earth's surface. Namely, the distance between a satellite and its terrestrial subpoint. Thus, the height of a satellite is slightly larger than its geocentric dis-

tance less the radius of the earth at the subsatellite point.

The longitude, θ, of a satellite should always be equal to that of the TSP; because the local vertical through a satellite is included in the meridional plane through the satellite. As in the case of geographic longitudes, the longitudes of satellites and related objects may be measured both eastward and westward from the Greenwich Meridian. It is more convenient, however, to measure longitudes only eastward so that they vary between 0 and 360 degrees.

The geodetic latitude, ϕ_d, is the angle measured in a meridional plane between the local vertical and the equatorial plane of the earth. The geodetic latitude of both the satellite and its TSP should be identical since they are on the same local vertical.

The geocentric latitude, ϕ_c, is not used as one of the terrestrial coordinates. This latitude is smaller, as much as 0.2 deg, than the geodetic latitude, ϕ_d, which appears on geographic maps. The difference, $\phi_d - \phi_c$ can easily be obtained by differentiating the equation of ellipse given by Eq. (7) with respect to x, thus

$$\frac{dz}{dx} = -\frac{R_P^2}{R_E^2}\frac{x}{z} \quad . \tag{25}$$

The relations

$$\tan \phi_c = \frac{z}{x} \quad \text{and} \quad \tan \phi_d = -\frac{dx}{dz}$$

permits us to reduce Eq. (25) to

$$\tan \phi_d = \frac{R_E^2}{R_P^2} \tan \phi_c \quad .$$

Putting, f_e, the oblateness of the earth into the above, and neglecting the terms including f_e^2 and $f_e(\phi_d - \phi_c)$, we have

$$\phi_d - \phi_c = f_e \sin 2\phi_c \fallingdotseq f_e \sin 2\phi_d \quad . \tag{26}$$

It is obvious that the difference between the geodetic and geocentric latitude reaches its maximum value at 45 deg latitude. Table III shows the difference in degrees and minutes computed by

$$\phi_d - \phi_c = 11.59 \sin 2\phi, \quad (\text{in min}) \tag{27}$$

where ϕ may be considered as either geodetic or geodesic latitude.

E. CELESTIAL COORDINATES

The celestial coordinates permit us to express the motion of a satellite or a related point with respect to a coordinate system which does not rotate as the earth does. Since the rotation rate of the earth's ascending node is reasonably small it is convenient to use the celestial coordinates associated with a celestial sphere with its center at the center of the earth. The coordinates, therefore, are r, the geocentric distance; δ, the declination; and Ω, the right ascension. The zero right-ascension is always taken in the direction of the vernal equinox.

The definition of the declination is identical to the geocentric latitude except either N or S is used for the latitude, but the signs + or - are attached to the declination in expressing the Northern or Southern Hemisphere. The declination of a

satellite, δ^{SAT}, and the geocentric latitude of its subpoint, ϕ_c^{TSP}, differs slightly from each other. This difference can be obtained using figure 5 appearing in the previous section. With satisfactory accuracy we may write

$$H(\phi_d^{TSP} - \delta^{SAT}) = R(\delta^{SAT} - \phi_c^{TSP})$$

and rearrange the equation into

$$H\phi_d^{TSP} - (H+R)\delta^{SAT} = -R\phi_c^{TSP}.$$

Dividing both sides by (H + R) after adding $R\phi_d^{TSP}$ to both sides we obtain

$$\phi_d^{TSP} - \delta^{SAT} = \frac{R}{H+R}(\phi_d^{TSP} - \phi_c^{TSP}) \tag{28}$$

which can be expressed as a function of the oblateness of the earth and the latitude using Eq. (26). That is

$$\phi_d^{TSP} - \delta^{SAT} = \frac{R}{H+R} f_e \sin 2\phi_d^{TSP}. \tag{29}$$

This difference, even in an extreme case which occurs at the 45 degree latitude on sea level, does not exceed 12 minutes. Figure 6 represents the value computed from Eq. (29). It is seen that the difference is largest near the 45 degree latitude. Nevertheless, it is insignificant when the height of a satellite is over 5,000 km where the difference is no more then 0.1 degree. When Eq. (29) is applied to a heavenly body of a considerable height, the right side becomes negligibly small so that we may write

$$\phi_d^* = \delta^*,$$

where the superscript asterisk denotes remote objects such as the sun, moon, etc. For instance, the declination of the sun is equal to the geodetic latitude of the subsolar point.

The right ascension of an object is the arc measured eastward along the celestial equator from the vernal equinox to the great circle passing through the celestial poles and the object projected onto the celestial sphere. We may thus write

$$\Omega = \theta + \Omega^{GRE} \tag{30}$$

where Ω denotes the right ascension of an object; Ω^{GRE}, that of the Greenwich Meridian; and θ, the longitude of the object measured eastward from Greenwich. It necessitates, therefore, to obtain the right ascension of the Greenwich Meridian as a function of time.

Now we express a given moment, t, by Y (year), N (day), H (hour), M (minute), and S (second). N, the number of days are counted each year from March 21 being zero. The right ascension of Greenwich at t is expressed by

$$\Omega_t^{GRE} = (H + M + S - 12h)\bar{\omega}_{ess} + (N + H + M + S)\bar{\omega}_{eon} + \mathcal{E}^{VE}\bar{\omega}_{ess} + \Delta t\,\bar{\omega}_{eon}, \tag{31}$$

where Δt is the time difference, OOZ March 21 - time of Vernal Equinox, and $\mathcal{E}^{VE}$, the equation of time at the Vernal Equinox. (Figure 7)

In expressing ω, the angular velocity of various objects, a three-small-letter designator is used. The first letter denotes OBJECTS such as s (satellite), e (earth),

etc; the second, MOTIONS, o (orbit), s (spin), p (precession), n (nutation), etc; and the third, REFERENCES, s (sun), n (line of nodes), a (line of apsides), f (fixed space), p (primary line), etc. $\bar{\omega}_{ess}$ thus denotes the angular velocity of the earth's rotation with respect to the sun. Likewise, ω_{eon} indicates the angular velocity of the earth's orbital motion with respect to the line of nodes.

To make computation easy, Eq. (31) may be divided into

$$\begin{array}{lllllllll} & \text{(Year)} & & \text{(Day)} & & \text{(Hour)} & & \text{(Minute)} & & \text{(Second)} \\ & +\mathcal{E}^{VE}\,\bar{\omega}_{ess} & & & + & H\,\bar{\omega}_{ess} & + & M\bar{\omega}_{ess} & + & S\,\bar{\omega}_{ess} \\ & +\Delta t\,\bar{\omega}_{eon} & & & - & 12\,\bar{\omega}_{ess} & & & & \\ & & + & N\,\bar{\omega}_{eon} & + & H\,\bar{\omega}_{eon} & + & M\,\bar{\omega}_{eon} & + & S\,\bar{\omega}_{eon} \\ \hline \Omega_t^{GRE} & = \Omega_Y & + & \Omega_N & + & \Omega_H & + & \Omega_M & + & \Omega_S \end{array} \qquad (32)$$

The terms Ω_Y, Ω_N, etc., which can be computed individually as a function of the year, the day, etc., are respectively called the

$$\begin{array}{lll} \text{Year Function,} & \Omega_Y = & \mathcal{E}^{VE}\,\bar{\omega}_{ess} + \Delta t\,\bar{\omega}_{eon} \\ \text{Day Function,} & \Omega_N = & N\,\bar{\omega}_{eon} \\ \text{Hour Function,} & \Omega_H = & (H - 12)\,\bar{\omega}_{ess} + H\,\bar{\omega}_{eon} \\ \text{Minute Function,} & \Omega_M = & M(\bar{\omega}_{ess} + \bar{\omega}_{eon}) \\ \text{Second Function,} & \Omega_S = & S(\bar{\omega}_{ess} + \bar{\omega}_{eon}) \end{array} \qquad (33)$$

The right-ascension table in Table XIII gives these functions individually, so that the right ascension of Greenwich at a given moment during the years 1960-1970 is obtained simply by adding these functions.

The right ascension can also be obtained by using the American Ephemeris and Nautical Almanac, or equivalent publications which give the right ascension of the apparent sun daily.

Another simple way is to use the Air Almanac published in three volumes a year. It gives the right ascension of Greenwich at 10 minute intervals thus making it easy to interpolate the needed values at the exact moment.

F. FIXED-EARTH COORDINATE

The third coordinates used in the analysis of meteorological satellite data refer to an imaginary earth whose rotation has been stopped at t_F, the time of fix. It should be noted that the real earth keeps rotating without interruption by the act of fixing the rotation of the imaginary one. A terrestrial object, a point on the rotating earth can be expressed similtaneously by both terrestrial and fixed-earth coordinates.

The height (H) and the latitude (ϕ) of an object as observed from both coordinates should remain unchanged as far as the earth is assumed to be an ellipsoid.

The terrestrial longitude (θ) which is the meridional angle measured eastward from Greenwich on the rotating earth is different from the fixed-earth longitude (Θ). The fixed-earth longitude denotes the meridional angle of an object measured eastward from the Greenwich Meridian on the fixed earth at the time of fix (t_F). That is to say the fixed-earth longitude at a time t is

$$\Theta_t = \Omega_t - \Omega_{t_F}^{GRE}$$

where Ω_t and $\Omega_{t_F}^{GRE}$ denote, respectively, the right ascension of a terrestrial object at t and that of the Greenwich Meridian at t_F.

From Eq. (30) and (31), the right ascension of an object at any moment t is expressed by

$$\Omega_t = \theta_t + (t - 12h)\,\bar{\omega}_{ess} + \bar{\Omega}_t^{SUN} \tag{34}$$

because the sum of the last three terms in Eq. (31) is equal to $\bar{\Omega}_t^{SUN}$, the right ascension of the mean sun at time t. The right ascension of Greenwich at t_F, the time of fix, therefore, is

$$\Omega_{t_F}^{GRE} = 0 + (t_F - 12h)\,\bar{\omega}_{ess} + \bar{\Omega}_{t_F}^{SUN}$$

Substituting this equation from Eq. (34), we have

$$\Theta_t = \Omega_t - \Omega_{t_F}^{GRE} = \bar{\Omega}_t^{SUN} - \bar{\Omega}_{t_F}^{SUN} + (t - t_F)\,\bar{\omega}_{ess} + \theta_t \,. \tag{35}$$

We know, on the other hand, that

$$\frac{d}{dt}\,\bar{\Omega}^{SUN} = \bar{\omega}_{eon} \,,$$

which permits us to write

$$\bar{\Omega}_t^{SUN} - \bar{\Omega}_{t_F}^{SUN} = (t - t_F)\,\bar{\omega}_{eon} \,.$$

Putting this into Eq. (35), we have

$$\Theta_t = (t - t_F)\,(\bar{\omega}_{eon} + \bar{\omega}_{ess}) + \theta_t \,. \tag{36}$$

The sum of the angular velocity of the earth's rotation, relative to the mean sun and that of the earth's orbital motion with respect to the vernal equinox, is the angular velocity of the earth's rotation relative to the line of nodes. Thus, Eq. (36) is reduced simply to

$$\Theta_t = \theta_t + (t - t_F)\,\bar{\omega}_{esn} \,. \tag{37}$$

This equation indicates that the fixed-earth longitude is obtained by adding the angle of the earth's rotation between a given time and the time of fix to the longitude of an object.

These three coordinate systems are interchangeably used during the analysis of meteorological satellite data. It will, therefore, be convenient to summarize the coordinates for the purpose of quick references.

Coordinates	Terrestrial		Fixed-earth		Celestial	
Objects	SAT	TSP	SAT	TSP	SAT	TSP
Height or Radius	H^{SAT}	0	H^{SAT}	0	r^{SAT}	R^{TSP}
Longitude or Right-Ascension	θ^{SAT}	$= \theta^{TSP}$	Θ^{SAT}	$= \Theta^{FSP}$	Ω^{SAT}	$= \Omega^{TSP}$
Latitude or Declination	ϕ_d^{SAT}	$= \phi_d^{TSP}$	ϕ_d^{SAT}	$= \phi_d^{FSP}$	δ^{SAT}	$> \delta^{TSP}$

The conversions between these coordinates as already discussed are made by using:

$H + R = r$	(Height or Radius)
Eq.(30), (31), and (37)	(Longitude or Right-Ascension)
Eq.(29)	(Latitude or Declination).

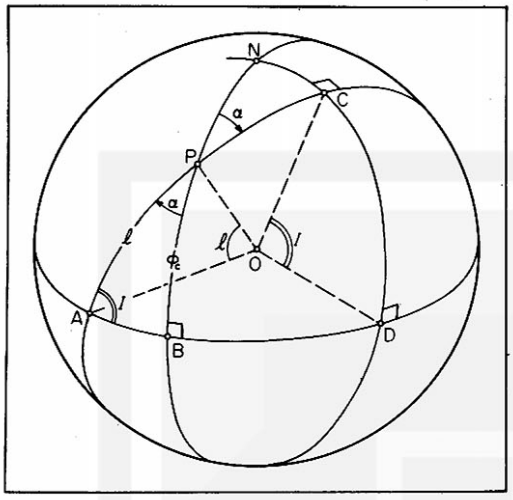

Figure 1. To obtain the radius of curvature of the earth as a function of the latitude and azimuth angle.

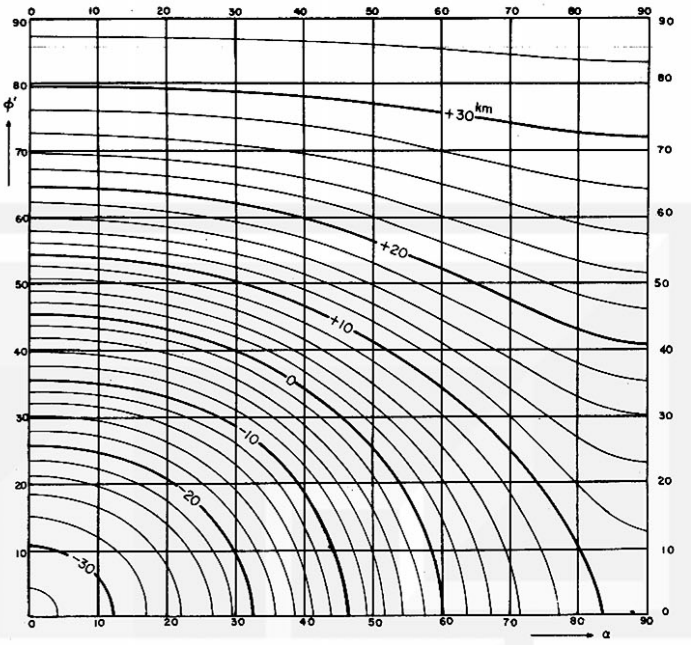

Figure 2. The excess radius of curvature of the earth expressed as a function of the latitude (ϕ) and the azimuth (α). Extreme values are +32.2 km at the poles and -32.2 km at the equator in the direction of meridians.

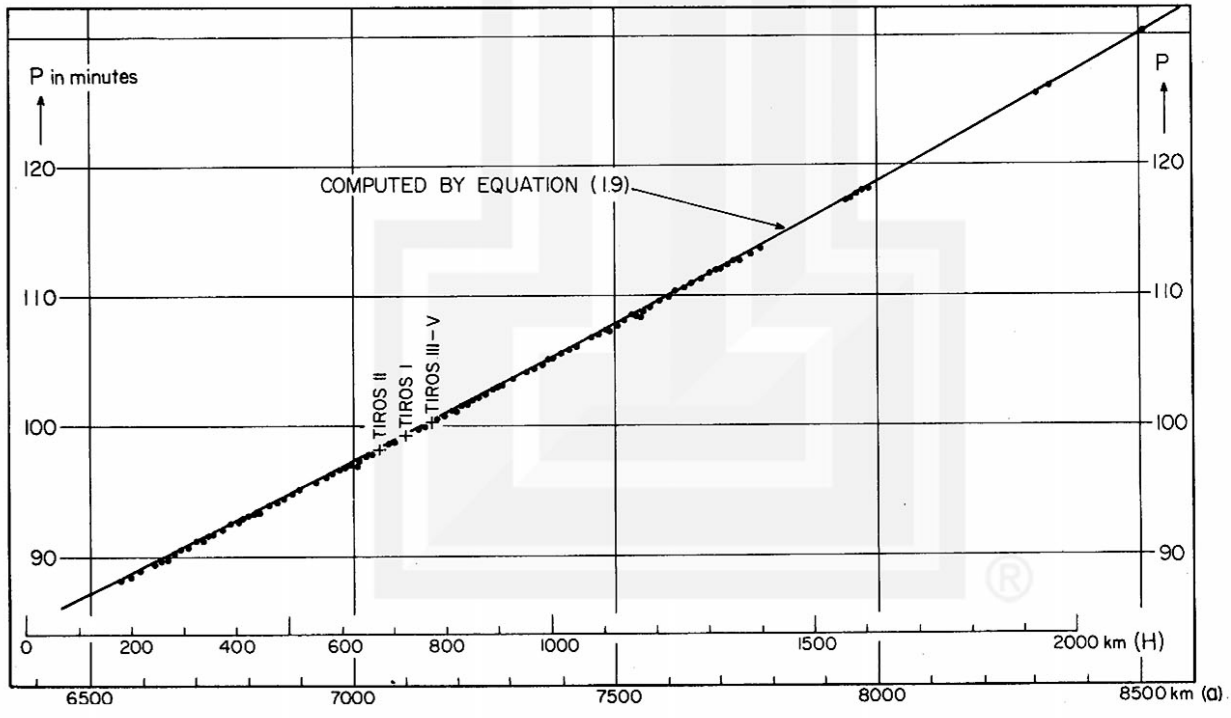

Figure 3. Nodal period (P) of the artificial satellites tracked during the years 1957-1960. The TIROS series of meteorological satellites are given in + symbols.

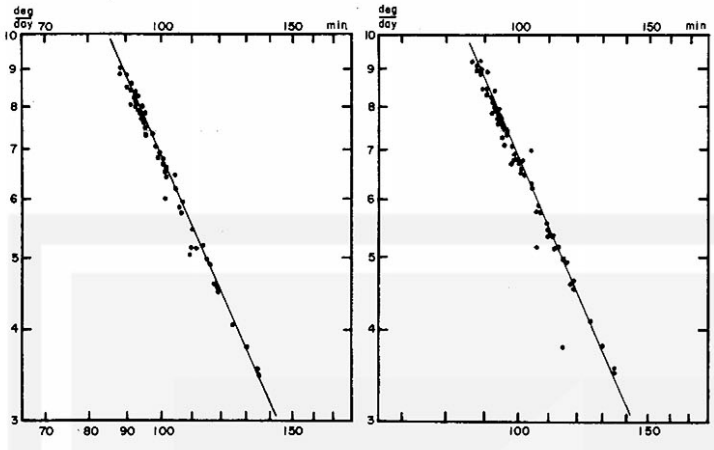

Figure 4. The values of $\dot{\Omega}^{AN} / (1 + e^2)^2 \cos i$ (left) and $\dot{w} / (1 + e^2)^2 (2 - 5/2 \sin i)$ plotted as a function of nodal periods. The charts are in logarithmic scales.

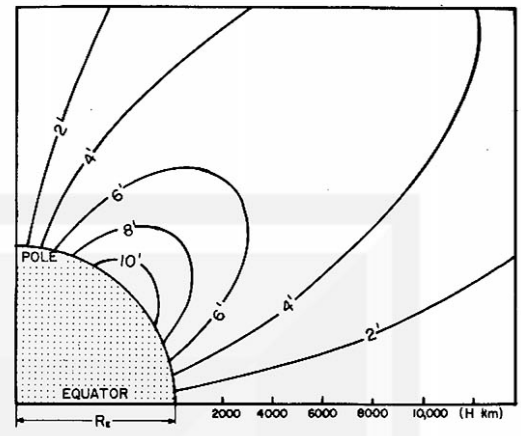

Figure 6. The difference between the geodetic latitude of a subsatellite point and the declination of the satellite. Unit in minutes.

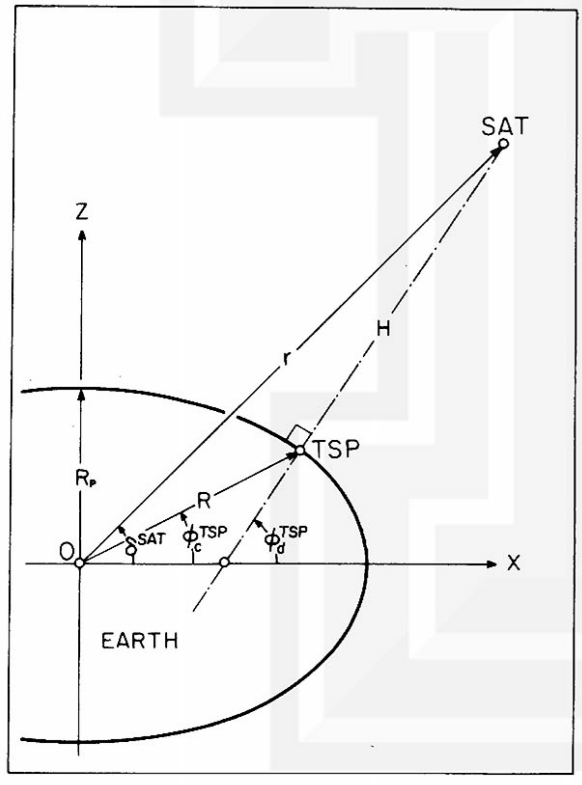

Figure 5. To clarify the relationship between the declination of satellite (δ), geodetic (ϕ_d), and geocentric (ϕ_c) latitudes of the TSP.

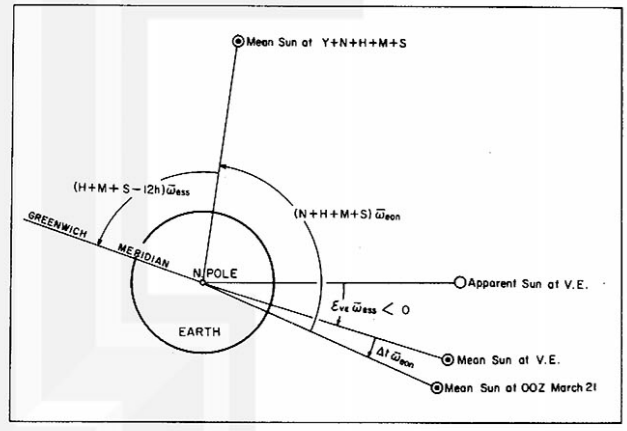

Figure 7. To obtain the right ascension of the Greenwich Meridian as a function of the year, day, hour, minute, and second. V. E., vernal equinox; $\bar{\omega}_{ess}$, mean solar rotation rate of the earth; $\bar{\omega}_{eos}$, mean angular velocity of the earth's orbital motion with respect to the line of nodes.

2. SATELLITE PHOTOGRAPHS

A. POSITION OF TIROS CAMERAS

The TIROS-borne cameras placed on the baseplate are designed in such a manner that the optical axes of the cameras are parallel to the spin axis of the vehicle. Alignment measurements by RCA (9), however, revealed that the direction of the optical axes of the TIROS cameras are up to 44' off from that of the spin axes. Actual deviations for each camera of five TIROS are given in Table IV.

To evaluate further the consequence of such a deviation of optical axis figure 8 was prepared. A vector through the front nodal-point of the camera lens and parallel to the vehicle's spin axis is called the nodal spin-axis. The nodal spin-axis intersects the positive image plane at the image primary-point (IPM), and the surface of the earth at the terrestrial primary-point (TPM). These two points could slightly be off from the image principal-point (IPP) and the terrestrial principal-point (TPP), respectively. Let the angle of deviation be χ and the focal distance of the positive image plane be f, the distance of IPP and IPM is given by

$$f \tan \chi \tag{38}$$

which would reach 1.3 mm when f = 10 cm and χ = 44'. The distance between TPM and TPP depends upon various factors such as the height of the satellite and the angle of the optical axis; however, it is worthwhile to note that it reaches about 10 km while viewing straight down from 750 km.

The spin and orbital motions of a satellite result in helical track of TPP while TPM follows along a smooth path if we neglect the nutation of the satellite spin-axis. The loci of these points are called TPP track and TPM track. In case the angle of deviation, χ is very small, it becomes unnecessary to distinguish the nodal spin-axis from the optical axis. Therefore, both IPP and TPP are used in lieu of IPM and TPM, respectively.

It has been estimated that the nutation of a satellite immediately after the launch is considerably large-in the order of 0.5 degrees-but after about 100 orbits or so it dumps out to only 0.1 to 0.2 degrees. Due to the quick change in both gravitational and magnetic field, impacts of micrometeorites, firing of spin-up rockets, a satellite may suffer additional perturbations which might result in an appreciable nutation.

The angular position of the camera optical-axis with respect to the vehicle's spin axis is conveniently expressed by the polar angles on the baseplate, abbreviated as baseplate angle (figure 9). The baseplate angle, ϕ_B, increases clockwise when viewed from the satellite top. As tabulated in Table IV, the baseplate angles of the axes of cameras 1 and 2 are approximately 170 and 290 varying a few tenths of a degree from camera to camera.

Another important angle associated with the baseplate and camera orientation is the polar angle around the optical axis of each camera. This angle is called the principal tangential-angle, γ . It increases clockwise on the positive image. The direction of the zero tangential angle of each camera does not always point precisely toward the spin axis of TIROS. For some cameras, the exact directions were not measured prior to the launch. Nevertheless, the tangential angle could play an important role should the sun angles be used for the determination of principal lines. Since an image rotates around the IPM rather than IPP the tangential angle is sometimes measured after translating the center of the polar grid from IPP to IPM. The tangential angle relative to the IPM is called the primary tangential-angle (γ'). The radials with identical γ' and γ remain parallel to each other on the image plane.

B. TOTAL IMAGE DISTORTION

Prior to the launch of each satellite, both direct and tape-mode photographs of a test-polar target were made by simulating the actual readout processes of TIROS photographs. Arranged in figure 10 are the direct readout photographs of polat targets. The tape-mode photographs are obtained by looking at them upside-down. Indicated at the bottom of each polar-target image are the angles labeled on the target (in parenthesis) and those obtained through calibration measurements. These target images reveal that the readout images include distortions both in radial and tangential directions.

A diagram shown in figure 11 illustrates the steps in which the lens and electronic distortions deform the test polar target into an actual televised image. In the figure P_T, P_V, and P_R, respectively, are the principal points on the target, the vidicon, and the readout image. The angle $P_T L C_T$ in the figure represents the true object angle between C_T and P_T viewed from the front nodal-point of the camera lens. This angle is called the radial angle of target (ϵ_T). Let the tangential angle and the radial angle of the object C_T be γ_T and ϵ_T , these angles change into γ_V and ϵ_V upon projection on vidicon surface. The changes in these angles define the optical distortions, which are

$$\text{Tangential distortion of vidicon image} = \gamma_V - \gamma_T \tag{39}$$

$$\text{Radial distortion of vidicon image} = \tan\epsilon_V \,/\, \tan\epsilon_T \ . \tag{40}$$

Due to the large angle of TIROS wide angle lenses, the radial distortion for each camera is normally much less than 1.00 resulting in an appreciable barrel shaped image. Both tangential distortion and the radial distortion of narrow angle cameras are insignificant.

In the process of televising the vidicon images back to the earth, a slight pincushion distortion is introduced. This is partially because of the curvature of image raster lines while the original raster of the vidicon used in TIROS is a series of

straight parallel lines. Such a pincushion distortion moderates to a certain extent the barrel lens distortions. Nevertheless, the direct comparison of the targets and the readout images indicates the existence of a fair amount of barrel distortion. Such a combined distortion is called the optical and electronic distortions, which can be expressed as

$$\text{Tangential distortion of readout image} = \gamma_R - \gamma_T \tag{41}$$

$$\text{Radial distortion of readout image (E)} = \tan\epsilon_R \,/\, \tan\epsilon_T. \tag{42}$$

As shown in the photographs of figure 10, the concentric rings on readout images are not the true circles as appear on the original test targets. Therefore, the mean distortion characteristics should be obtained from the mean radius of the rings defined by

$$\bar{R}_R = \frac{1}{2\pi}\int_0^{2\pi} R_R \, d\gamma_R . \tag{43}$$

As shown in figure 11, the mean radial angle, $\bar{\epsilon}_R$, of a ring on a readout image may be defined as

$$\tan\bar{\epsilon}_R = \bar{R}_R / f_R , \tag{44}$$

where f_R represents the hypothetical principal distance applicable to the readout image. As a result of the radial distortion this principal distance varies with the radial angle. Without definition, therefore, a unique principal distance does not exist for a distorted readout image.

Under the assumption that the distortions in the vicinity of the principal point are the least significant, we may assume that

$$\lim_{\epsilon_R \to 0} \tan\bar{\epsilon}_R = \lim_{\epsilon_T \to 0} \tan\epsilon_T . \tag{45}$$

This equation, when combined with Eq. (44) defines the principal distance of a readout image. Namely, we write

$$f_R = \lim_{\epsilon_T \to 0} \frac{\bar{R}_R}{\tan\epsilon_T} . \tag{46}$$

A graphical method of determinging the focal distance, f_R, of a readout image of a test polar-target appears in figure 12. The coordinates consist of $\tan\epsilon_T$ and $\bar{R}_R$ for both positive and negative values so that the curves are drawn through the origin thus making it possible to draw an accurate tangential line through the origin. It is obvious that the focal distance can be obtained by drawing a vertical line of $\tan\epsilon_T = 1.00$ and measuring the length of the line segment between the abscissa and the tangential line.

After the determination of the focal distance of the readout image (f_R), the image of a polar target is reduced or enlarged until the focal distance becomes identical to f_T. Then the readout image is superimposed upon the target with its focal distance f_T, in order to determine the vector shifts of the objects on the target due to the optical and electronic distortions. Figure 13 presents an example of the vector shifts obtained by this method. It is seen that the image far from the principal point suffer both shrinkage and twisting deformations.

The mean radial distortion of a readout image is defined by

$$\overline{E} = \tan \overline{\epsilon}_R \; / \; \tan \overline{\epsilon}_T \tag{47}$$

which is identical to Eq. (42) which defines the radial distortion. From Eq. (44), however, the mean tangential angle of any concentric ring on a readout image can be obtained, making it possible to determine the mean radial distortion from

$$\overline{E} = \frac{\overline{R}_R}{f_R \tan \epsilon_T} \tag{48}$$

where f_R denotes the focal distance of the readout image, $\overline{R}_R$, the mean radius of a concentric ring on the readout image, and ϵ_T, the radial angle of the corresponding circle on the target. Table IV includes the calculated mean radial distortion as a function of the radial angle ϵ_T.

Using the information of TIROS cameras given in Table IV the distortion curves for 10 TIROS-borne cameras (figure 14) were completed. The distortion of camera lenses is known to be barrel shaped, however, the additional electronic distortion turns the final distortion into pincushion especially when the field of view of a lens is medium or narrow.

C. FIDUCIAL AND DISTORTION-FREE FIDUCIAL GRID

Test target images, which were discussed in the previous section, reveal quantitatively the displacement of object points due to optical and electronic distortions. The actual photographs televised from satellites do not include the image of the polar target. Instead, they show fiducial marks of which four at the corners are L-shaped and the one at the center is + shaped. These fiducial marks are the enlargement of miniature marks placed on the focal plane of each TIROS vidicon cameras. In fact, these fiducial marks are also scanned together with the clouds. Thus, they undergo distortion in exactly the same manner in which cloud images are distorted.

It is extremely important to realize that the exact tangential and the radial angles of the fiducial marks can be reproduced on a target image by transcribing the fiducial marks on a readout image to the target image, with the help of the polar grid. The upper diagram in figure 15 represents the fiducial marks transcribed from the readout image in the lower chart. Notice that the position of the fiducial marks relative to the distorted (lower) and the distortion-free (upper) polar grids are precisely identical. The electronic distortion may change from frame to frame, however, the fiducial marks transcribed on the target image using the polar target will never change in both shape and position. As a result, we may assume that a permanent pattern of the fiducial marks for each camera exists on a distortion-free target image.

In order to transfer the object points on an image plane (distorted) to the target plane (undistorted), it is necessary to produce a corresponding grid on both image

and target planes, because the cloud photographs do not include the lines of a polar grid which appeared in the test photographs taken before the launch of each satellite. Fujita (4) proposed a "Fiducial Grid" on an image plane, which is drawn on an image plane by using the L and + shaped fiducial marks seen on each photograph.

Figure 16 demonstrates a method of producing a fiducial grid. After the completion of the main box A' B' C' D', the shortest distances, a, b, c, and d, between the central cross point and the curved sides are measured. The four curved sides are then cut off from both ends by the lengths a, b, c, and d in the manner shown in figure 16. Thus, a short segment is left near the center of each of the four sides. The midpoints of these segments are designated as P', Q', R', and S'. Now, each of the lengths, A' S', S' B', B' P', ----, and R' A' is divided into four equal parts. Likewise the distances O' P', O' Q', O' R', and O' S' are divided into four, so that the main box A' B' C' D' can be divided into 16 small sections. The area outside the main box may also be divided by extrapolating the four curved sides of the main box.

By superimposing the fiducial grid upon the image of the test polar target, the lines of the fiducial grid are transcribed onto the test polar target. As shown in the figure the grid thus completed on an undistorted plane takes the shape of a pincushion. Any object on this grid coordinates preserves its exact radial and tangential angles, hence the grid is called the distortion-free fiducial grid.

Extensive research on the distortion-free fiducial grid for the TIROS cameras was made, leading the author to make designs of the grid including tangential and radial angles in addition to the grid lines.

The distortion-free fiducial grids for 10 TIROS cameras appear in figures 17-26 in which the black dot at the center represents IPM, the point at which the nodal spin-axis penetrates the image plane. The tangential angles indicated around the distortion-free fiducial grid are the primary tangential angles. The image principal point (IPP) shown in small circle appears in the vicinity of the IPM. In the case of TIROS I camera 1 and 2, the amount of deviation of IPM from IPP is known, but the direction of the deviation is still uncertain. Therefore, the distortion-free fiducial grid was constructed placing IPP at the center. The original sizes of these distortion-free fiducial grids are made to fit f = 94.7 mm for medium and wide angle cameras, and f = 947 mm, for narrow angle cameras.

D. TILT GRID

Transcriptions of objects on an image plane onto a distortion-free fiducial grid with the use of fiducial grid eliminate both optical and electronic distortions, permitting us to proceed with the photogrammetric analysis on the distortion-free image plane. Unlike the cases of regular aerial photogrammetry, it is always necessary to take the curvature of the earth into consideration. In view of this, it is found convenient to express the coordinates on images by the nadir angle, η, and the horizontal

angle, ψ . The nadir angle is defined as the angle measured at the perspective center between a specified ray and the local vertical. The horizontal angle denotes the azimuth angle relative to the direction of the principal plane.

The geometry for computing the isoline of both ψ and η on an oblique image plane is presented in figure 27. The nadir angle of the camera optical-axis is called the tilt, τ, which is the standard term used in aerial photogrammetry. The point of intersection of the local vertical with the image plane is the image subsatellite point (ISP); likewise the image principal point is defined as the intersection of the image plane and the optical axis of the camera. These points are located on the principal line on the image.

The isoline of ψ on the image plane is a straight line defined by the intersection of the image plane and a vertical plane of horizontal angle, ψ . The angle between this straight line and the principal line is the image horizontal angle, ψ_i , which is, with the use of the symbols in figure 27, obtained as

$$\tan \psi_i = HJ/AH = \tan\psi \cos\tau . \tag{49}$$

The values of ψ_i computed as a function of the tilt (1^o increment) and the horizontal angle (10 increment) are given in Table VI.

The isolines of η on an image are a group of ellipses which are the intersection of the image plane and a group of cones with various η , the half angle of the cone. It is, of course, possible to calculate analytic geometrically the x and y coordinates of the ellipses. However, the use of the vertical angle, ζ , which is the tilt of a plane perpendicular to the principal plane, makes the determination of the ellipses extremely simple. With the use of the symbols in the figure, the vertical angle is solved as

$$\tan \zeta = A'N'/SA' = \tan \eta \cos\psi . \tag{50}$$

All points designated by the letters with (') are located on a horizontal plane intersecting the image plane with an axis of homology. The values of ζ computed by Eq. (50) are given in Table VII.

A grid on an image plane consisting of the isolines of both ψ and η at certain intervals are called the tilt grid. It is, of course, desirable to prepare tilt grids at close intervals, such as one degree or less. Taking into consideration the errors, which could be introduced from various sources, the interval of 2^o was chosen within a range of 0^o and 120^o of tilts.

Figure 28 indicates a method of tilt grid construction using Table VI and VII. These tables give us both image horizontal angle, ψ_i , and vertical angle, ζ , for given nadir, horizontal, and tilt angles. In order to construct a tilt grid, which fits the distortion-free fiducial grid of focal distance, f, the principal line is first marked with $f \tan\epsilon$, at one degree intervals of ϵ , the radial angle. Through these marks are drawn a group of straight lines perpendicular to the principal line. The image subsatellite point is then obtained on the principal line by selecting a mark, the radial angle of which is equal to the tilt, τ. As shown in the figure, the vertical angle is zero at the ISP, while the radial angle is zero at the IPP.

The intersections of the isolines of vertical angles ζ_0 , ζ_1 , ----and those of image horizontal angles ψ_{i0} , ψ_{i1} , ----are successively obtained. Naturally, these points of intersection define the ellipse of given nadir angle on image. Figure 29 presents actual tilt grids in reduced size. The original size is, of course, made to fit the distortion-free fiducial grids for TIROS cameras.

E. PERSPECTIVE TILT GRID

The tilt grid consists of a group of radials passing through the image subsatellite point and a set of ellipses drawn on an image plane. It is known that the rectification can also be performed with slightly less accuracy, but much quicker, if a set of grids called "Perspective Tilt Grid" is applied to the images to be rectified.

A schematic diagram of this grid geometry appears in figure 30. The grid includes the isolines of two sets of vertical angles; one is oriented in the direction of the principal plane, and the other to that of a perpendicular to the principal plane. In fact we are replacing a cone in figure 27 by a pyramid with its half-angle of vertex identical to ζ , the vertical angle. The figure reveals that one group of the isolines of ζ is parallel to the true horizon. These parallel lines intersect the principal line at the radial angles of

$$\eta \pm \zeta \ .$$

The other group of the isolines of ζ departs from H, the intersection of the principal plane and the true horizon on the image plane and reach the axis of homology at T'. Let the intersection of the principal line and the axis of homology be S'; the tangent of the angle ψ' is expressed by

$$\tan \psi' = \frac{TS'}{HS'} = \tan \zeta \ \sin \tau \ , \qquad (51)$$

where $HS' = SA' \csc \tau$, and $T'S' = a = SA' \tan \zeta$.

As shown in figure 31, perspective 0° tilt grid consists of two sets of parallel lines intersecting orthogonally. As the tilt increases, the image subsatellite point (ISP) displaces downward away from the IPP, moving out of the chart boundary before the tilt of 60° is reached. The vanishing point, which is located always at the intersection of the principal line and the true horizon, comes within the chart boundary at the tilt of 40°. The radials from the vanishing point are exactly at the 10° intervals when tilt is 90°, for which the optical axis points horizontally.

Perspective tilt grids do not inlcude the isolines of nadir angles. For the determination of track distances, which appear later in figure 65 and 66, large and small dots along a circle are provided. The track distances in nadir angle are thus measured on the perspective tilt grid immediately.

F. DISTORTED TILT-GRID

Under certain circumstances one may prefer to analyse a large quantity of pictures rather than worrying too much about the preciseness. One solution to this speed-up analysis can be obtained by distorting tilt grids to fit the mean radial distortions. Due to the fact that we alwyas have to rotate a tilt grid until its principal line coincides with that of readout image, no tangential distortion and perturbed radial distortion can be taken into consideration. Such distortions are, theoretically, correctable in a fixed orientation of the principal line.

The mean radial distortions of the 10 TIROS cameras, shown in figure 14 and Table IV, can be used to distort the tilt grids to fit the distortion characteristics of each camera. Five cameras, TIROS I - camera 2, II - 2, III - 1, III - 2, and IV - 1, indicate almost identical mean radial distortions permitting us to apply only one distortion for all of them. The average values of these five cameras are:

0^{o}...1.00, 10^{o}...0.99, 20^{o}...0.97, 30^{o}...0.91, 40^{o}...0,82, and 50^{o}...0.72.

Examples of 0^{o} and 60^{o} tilt and perspective tilt grids distorted to these mean radial distortions are presented in figure 32. These distorted tilt grids are to be placed on top of the images for quick but less accurate analysis. Experience shows that the error due to the use of these distorted tilt grids is about 1-2 degrees of latitude in cloud fixes, while the precise method using distortion-free grids cut the error down to 0.1-0.2 degrees of latitude. In using these distorted grids, the fiducial marks on an image must fit as accurately as possible to those on each distorted tilt grid.

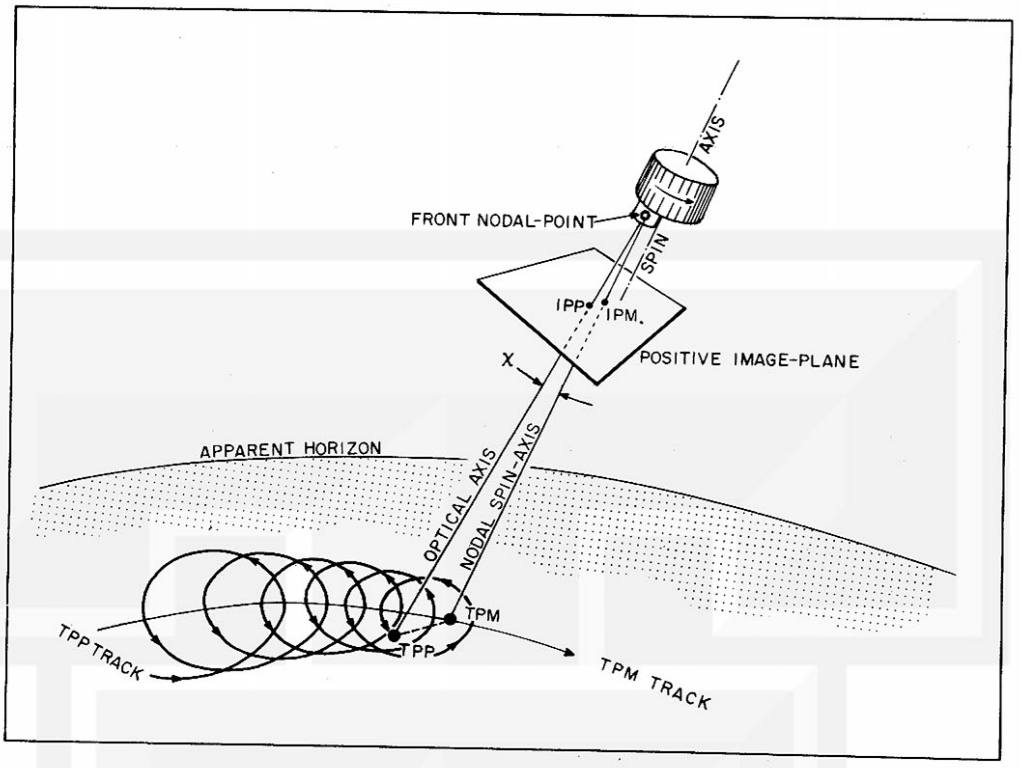

Figure 8. To define the image principal point (IPP), the point of intersection of the camera optical axis with the image, and the image primary point (IPM), the point of intersection of the nodal spin-axis with the image. If there is no nutation, TPM forms a smooth track on the earth, while TPP spins around TPM several times a minute.

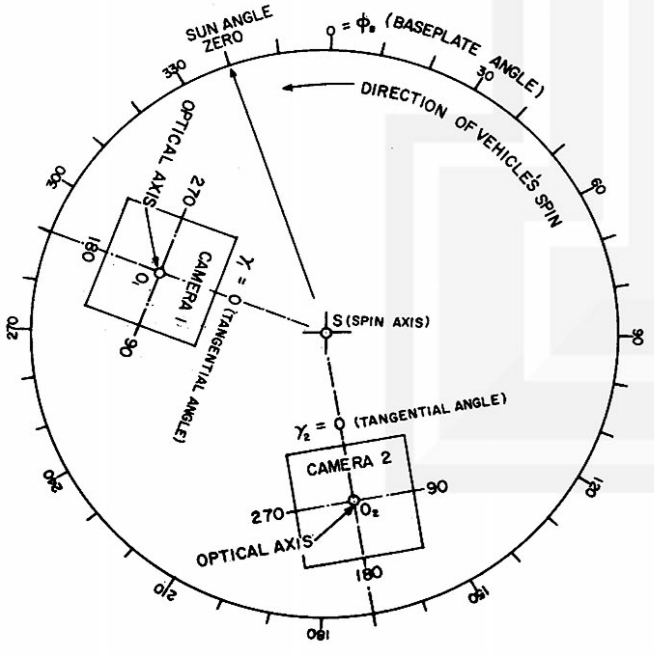

Figure 9. The position of TIROS-borne cameras 1 and 2. The baseplate is viewed from the satellite top. The tangential angles of these cameras, therefore, indicate those on positive images. The radials of zero tangential angle are oriented as close as possible toward the vehicle's spin axis.

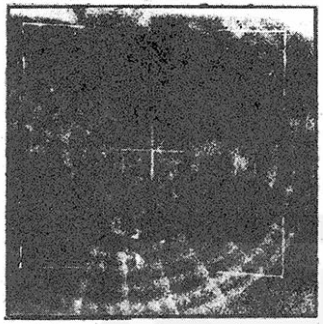

(I) CAMERA 1

(1) 1.00 (6) 5.98
(2) 2.00
(3) 3.00
(4) 3.98
(5) 5.98

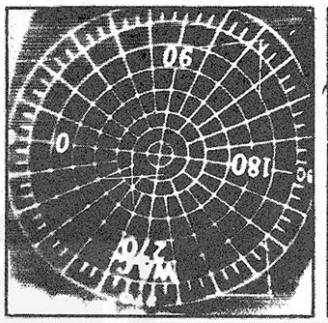

(I) CAMERA 2

(3) 2.68
(6) 5.67
(10) 8.98
(15) 13.52
(20) 18.08

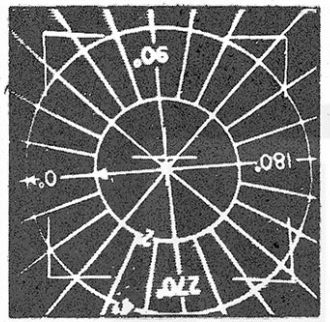

(II) CAMERA 1

(2) 2.00
(4) 4.00
(6) 6.00

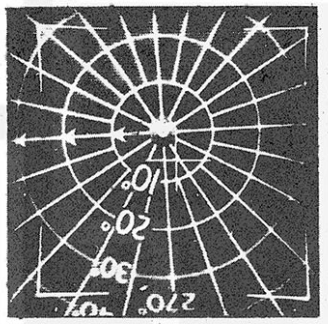

(II) CAMERA 2

(10) 9.83
(20) 19.31
(30) 28.90
(40) 38.63
(50) 48.58

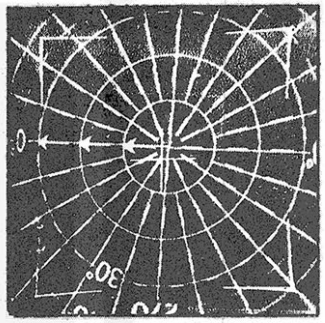

(III) CAMERA 1

(10) 9.50 (45) 42.97
(20) 18.83 (50) 47.98
(30) 28.33
(35) 33.15
(40) 38.02

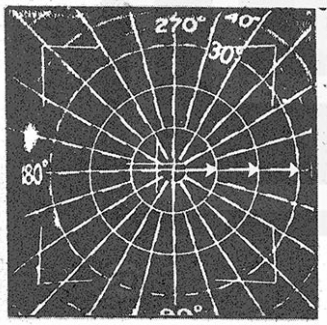

(III) CAMERA 2

(10) 9.62 (45) 43.33
(20) 19.07 (50) 48.35
(30) 28.63
(35) 33.48
(40) 38.38

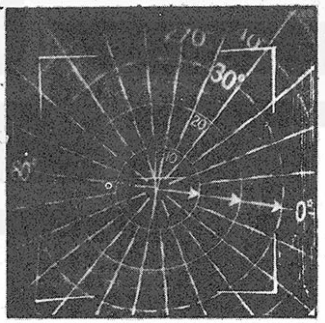

(IV) CAMERA 1

(10) 9.18 (4) 37.05
(20) 18.23 (45) 41.97
(25) 22.82 (50) 46.98
(30) 27.50
(35) 32.24

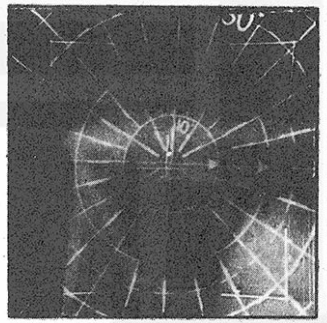

(IV) CAMERA 2

(10) 9.08
(20) 18.05
(25) 22.58
(30) 27.23
(35) 31.95

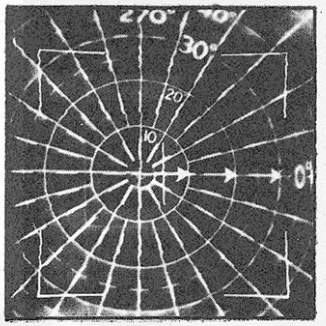

(V) CAMERA 1

(10) 10.52 (40) 40.96
(20) 20.73 (45) 45.97
(25) 25.83 (50) 50.97
(30) 30.88
(35) 35.95

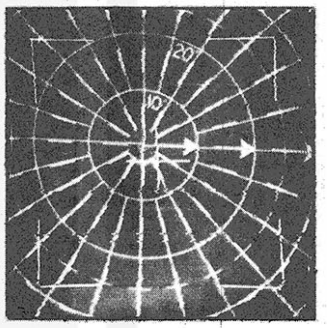

(V) CAMERA 2

(10) 10.25
(20) 20.23
(25) 25.22
(30) 30.22
(35) 35.20

Figure 10. Test target images from 10 TIROS-borne cameras.

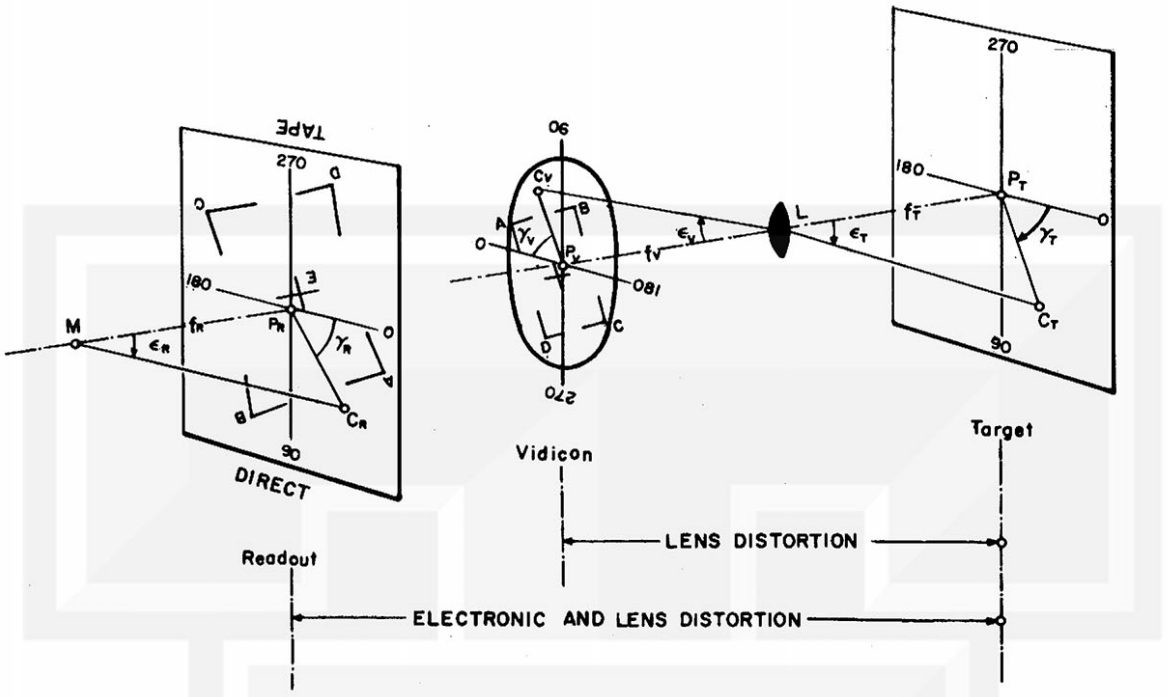

Figure 11. Schematic diagram of target, vidicon, and readout planes. The lens, L, distorts the target objects radially upon forming the image on a vidicon surface. The final readout images include both lens and electronic distortions which should be eliminated as much as possible when a precise rectification is desired.

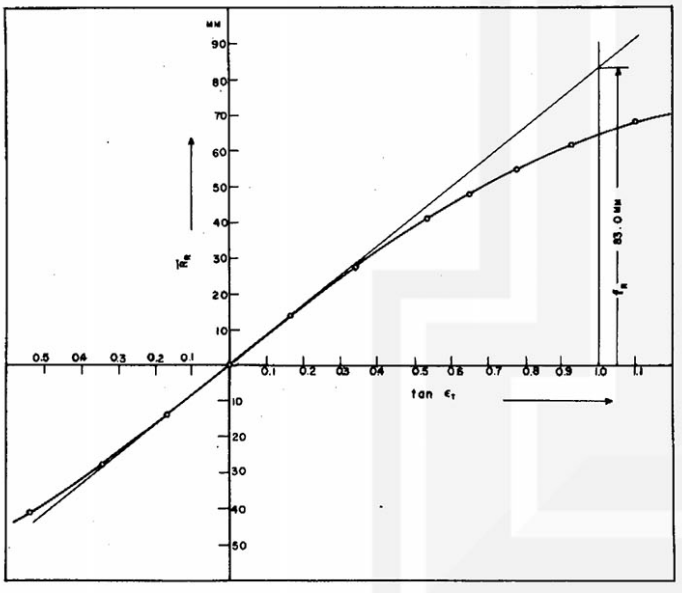

Figure 12. Showing a method to compute the principal distance (f_R) of a readout image. The values of mean radii of concentric rings ($\bar{R}_R$) on a readout image is plotted against tangent of the radial angle (ϵ_T) of the target circles viewed from the front nodal-point.

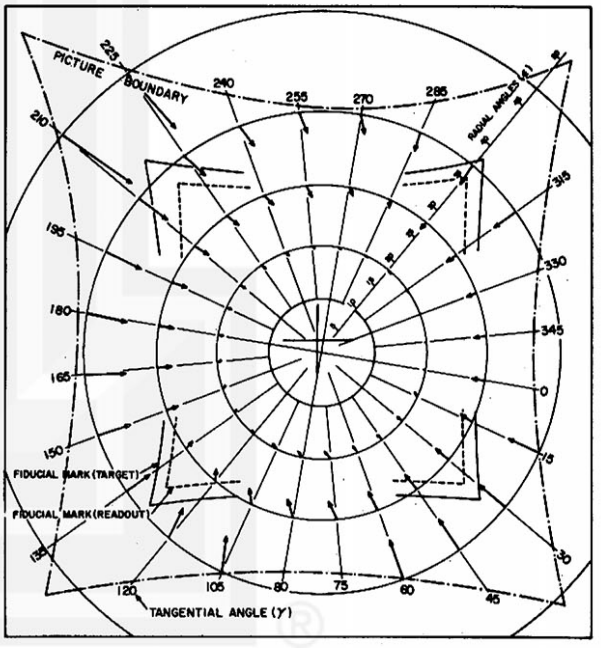

Figure 13. Vector shift of the objects on a polar target when a readout image is obtained by simulating the televising processes on the ground prior to the launch.

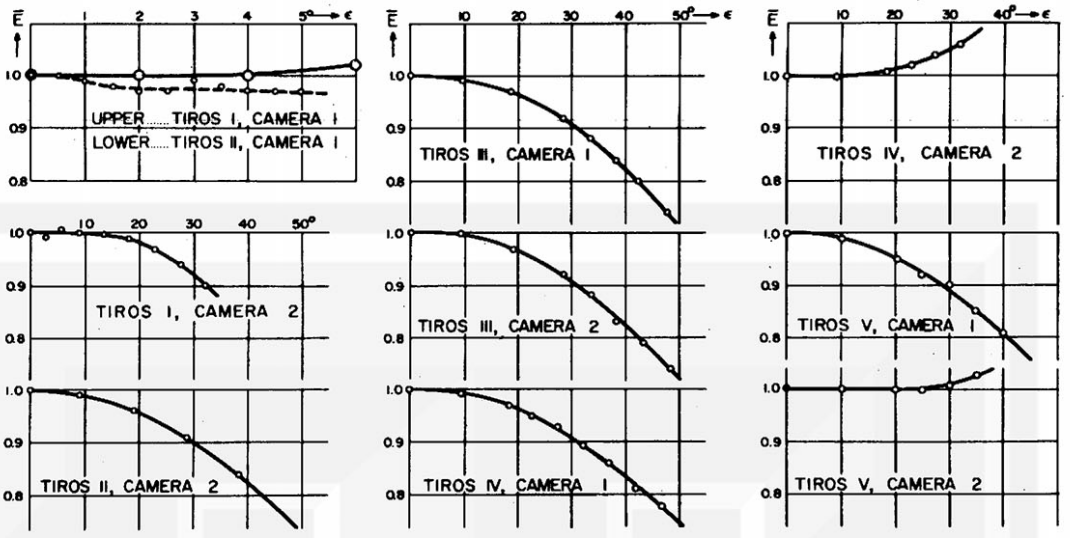

Figure 14. Mean distortion of the 10 TIROS-borne cameras.

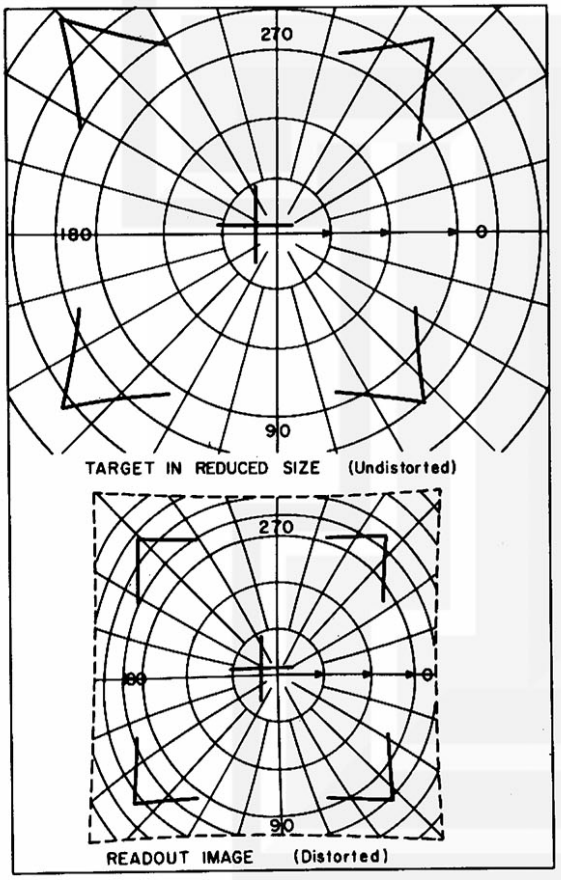

Figure 15. Transcript of fiducial marks on a test-target readout image onto the polar target which is not distorted. The example shown is that of TIROS III, camera 2.

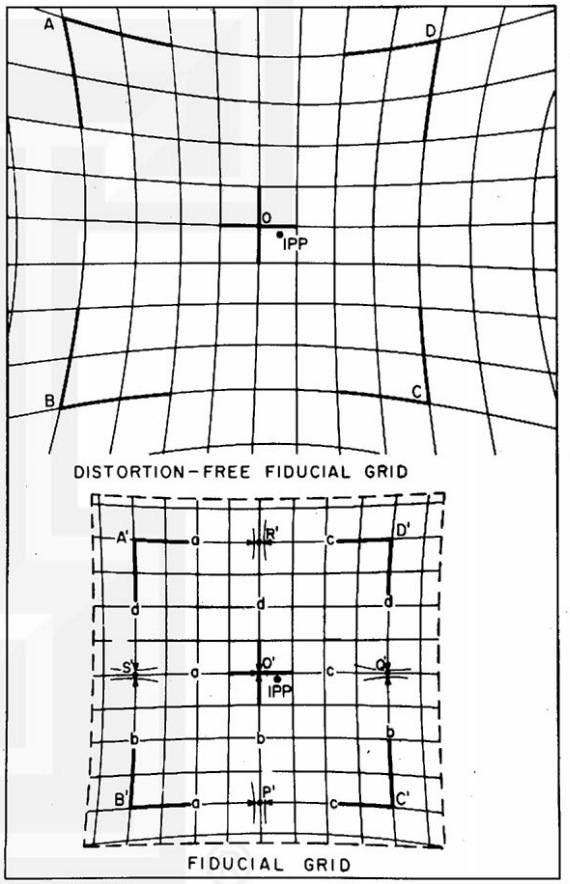

Figure 16. A fiducial grid and the corresponding distortion-free fiducial grid. The distances of four sides, A'B', B'C', C'D', and D'A' from the central + mark are a, b, c, and d, respectively. The example shown is that of TIROS III, camera 2.

Figure 17-26. Distortion-free fiducial grids for TIROS-borne cameras. These figures are the collection of the distortion-free fiducial grids constructed by using the method as shown in figures 15 and 16.

In case of TIROS I, the image principal point (IPP), indicated by a small open circle, is placed at the grid center, because the direction of the vector connecting IPP with IPM is not known. The angles surrounding the grid indicate the principal tangential angle (γ). We may assume that the IPP moves along a small circle due to the apparent image rotation.

For TIROS II-V, the image primary point (IPM), indicated in painted circle, is placed at the grid center. The IPP, thus, spins around the IPM. The angles surrounding the grid are primary tangential angle (γ') obtained by translating the center of the tangential angle coordinates from IPP to IPM.

The act of transferring any object from an image (fiducial grid) to a proper distortion-free fiducial grid will eliminate both lens and electronic distortions.

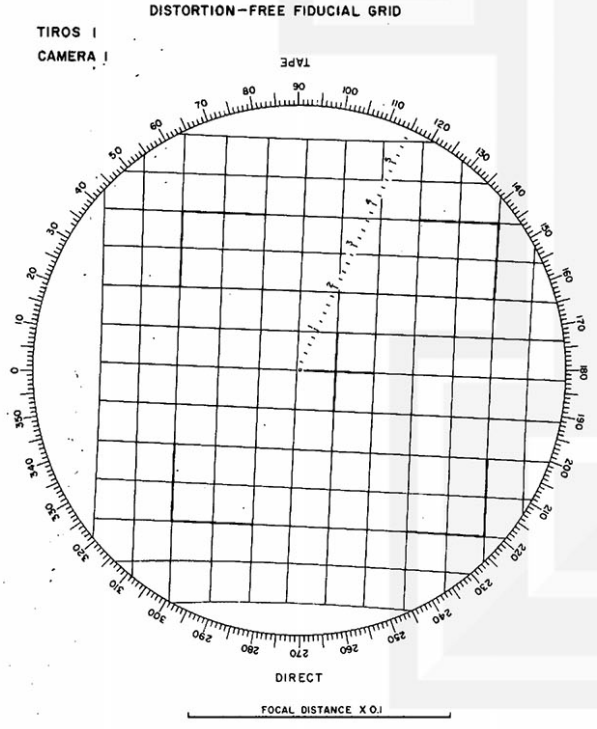

Figure 17. Distortion-free fiducial grid of TIROS I, camera 1.

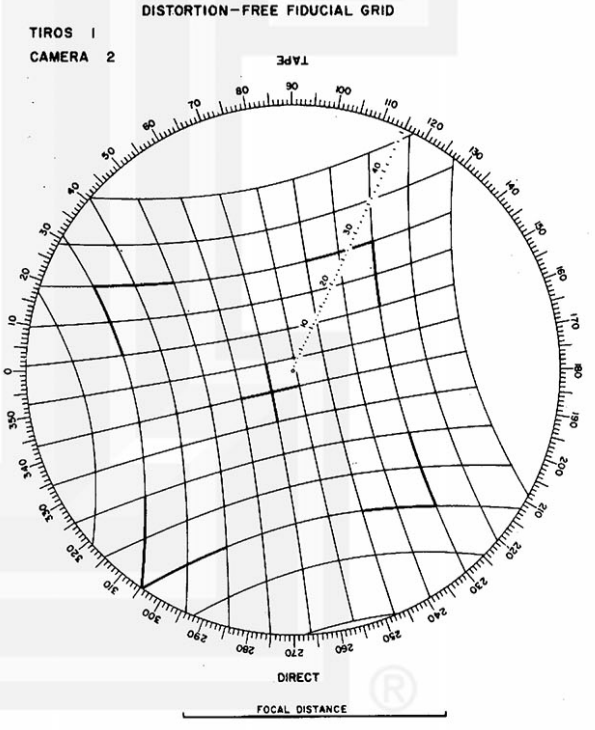

Figure 18. Distortion-free fiducial grid for TIROS I, camera 2.

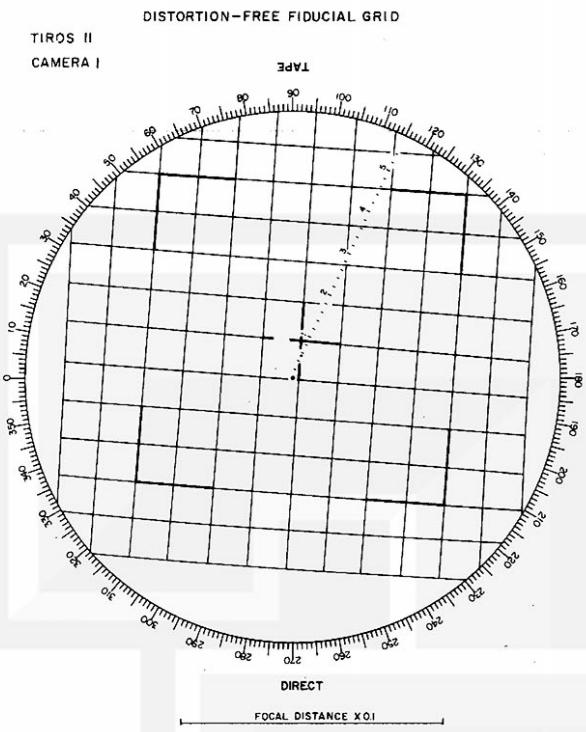

Figure 19. Distortion-free fiducial grid of TIROS II, camera 1.

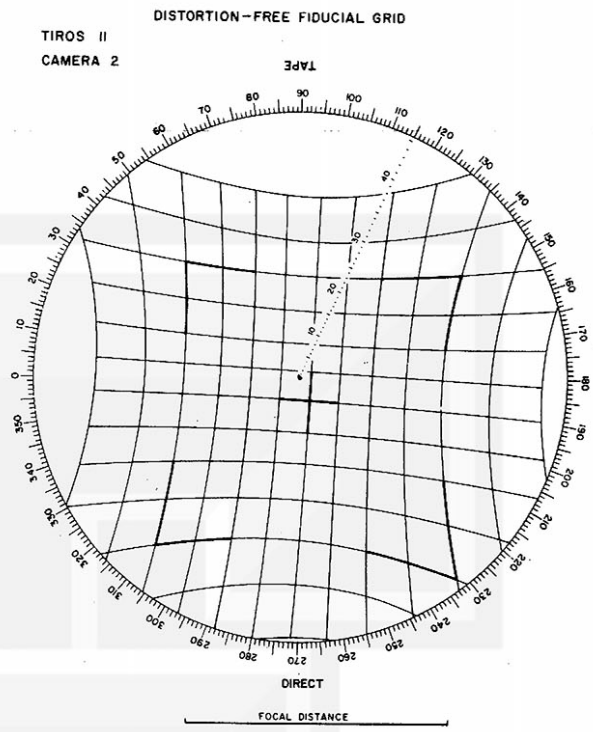

Figure 20. Distortion-free fiducial grid of TIROS II, camera 2.

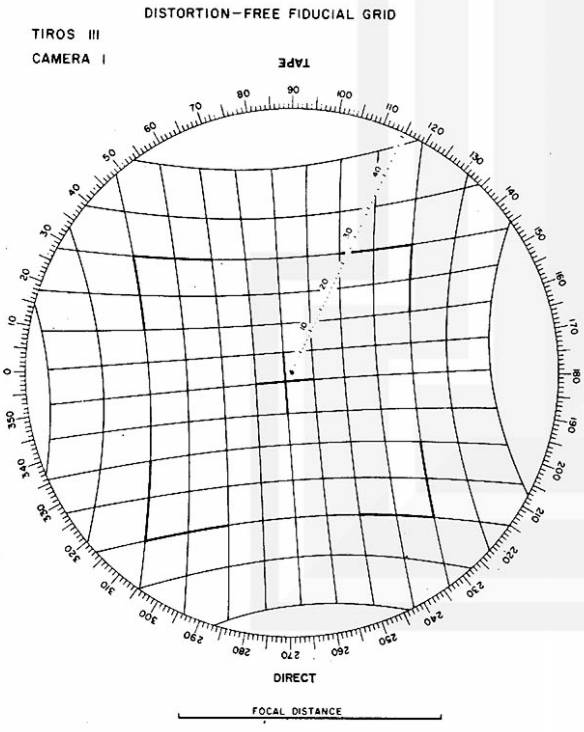

Figure 21. Distortion-free fiducial grid of TIROS III, camera 1.

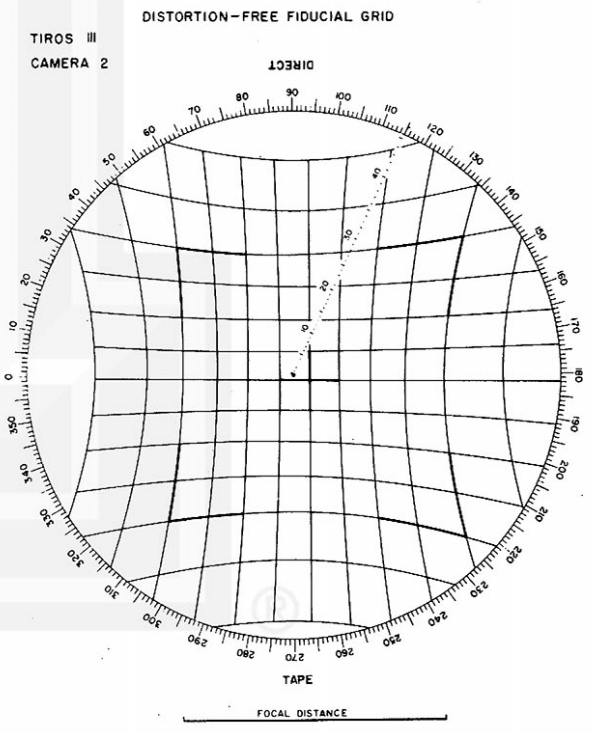

Figure 22. Distortion-free fiducial grid of TIROS III, camera 2.

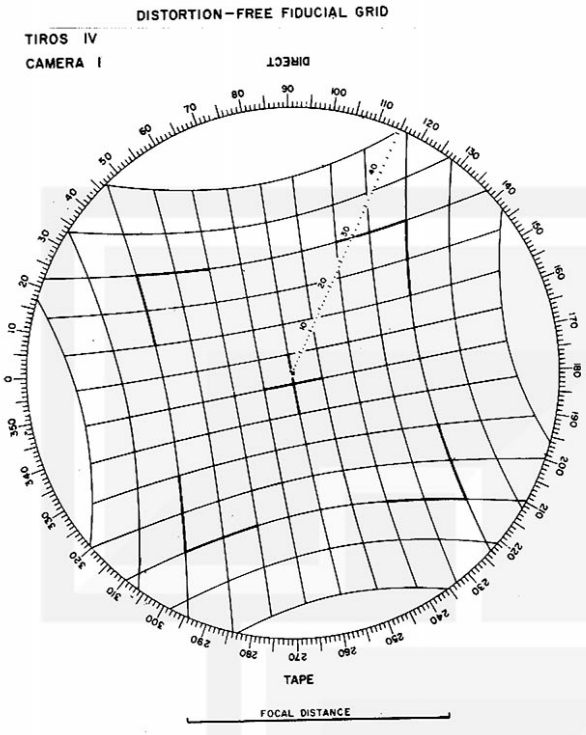

Figure 23. Distortion-free fiducial grid of TIROS IV, camera 1.

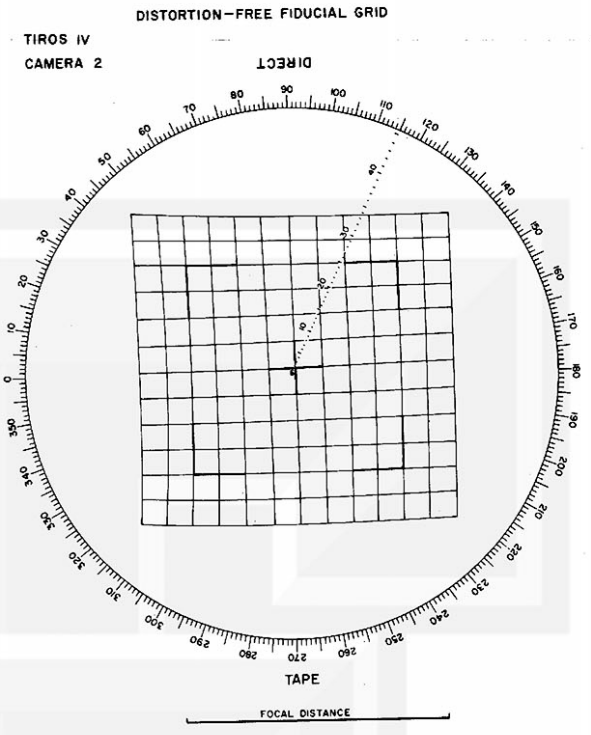

Figure 24. Distortion-free fiducial grid of TIROS IV, camera 2.

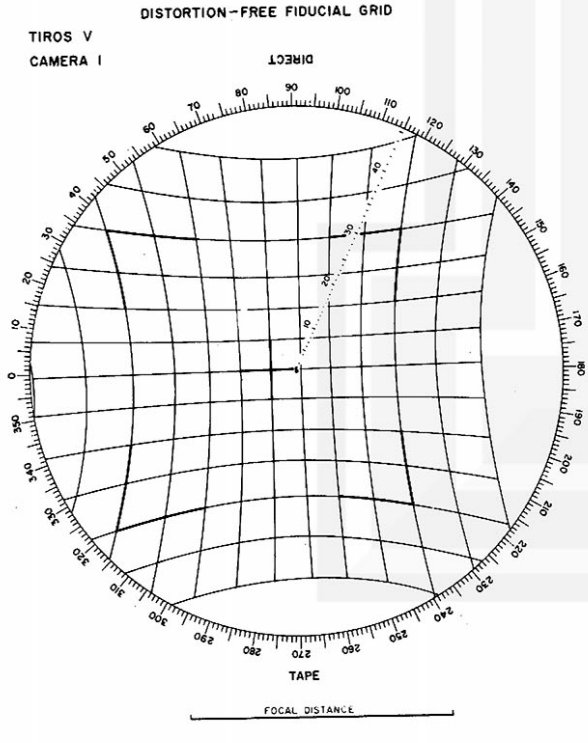

Figure 25. Distortion-free fiducial grid of TIROS V, camera 1.

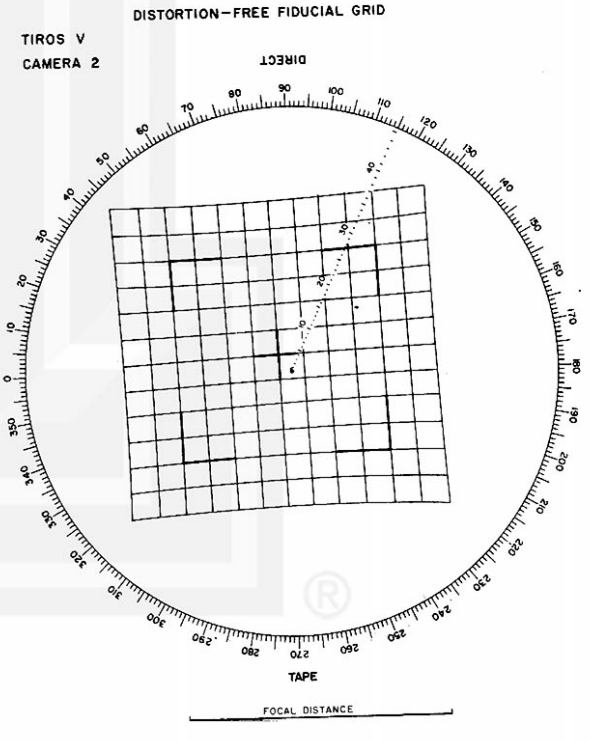

Figure 26. Distortion-free fiducial grid of TIROS V, camera 2.

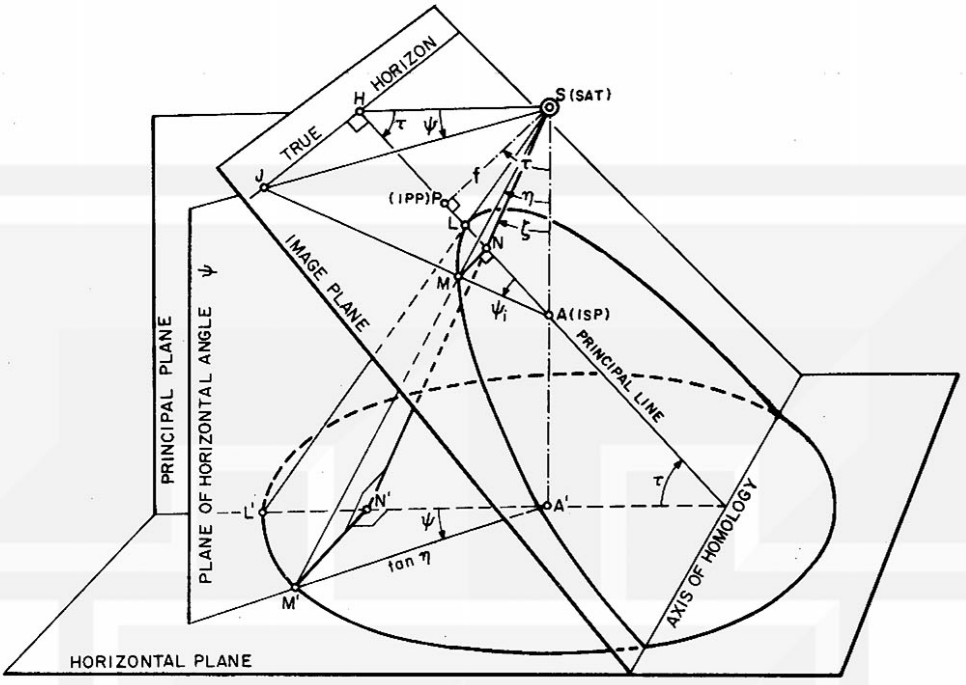

Figure 27. Geometry of constructing a tilt grid. The grid consists of a group of iso-horizontal angle lines and that of iso-nadir-angle lines. If the principal distance (f) of the image remains unchanged, the lines on the grid can be determined as a function of tilt only.

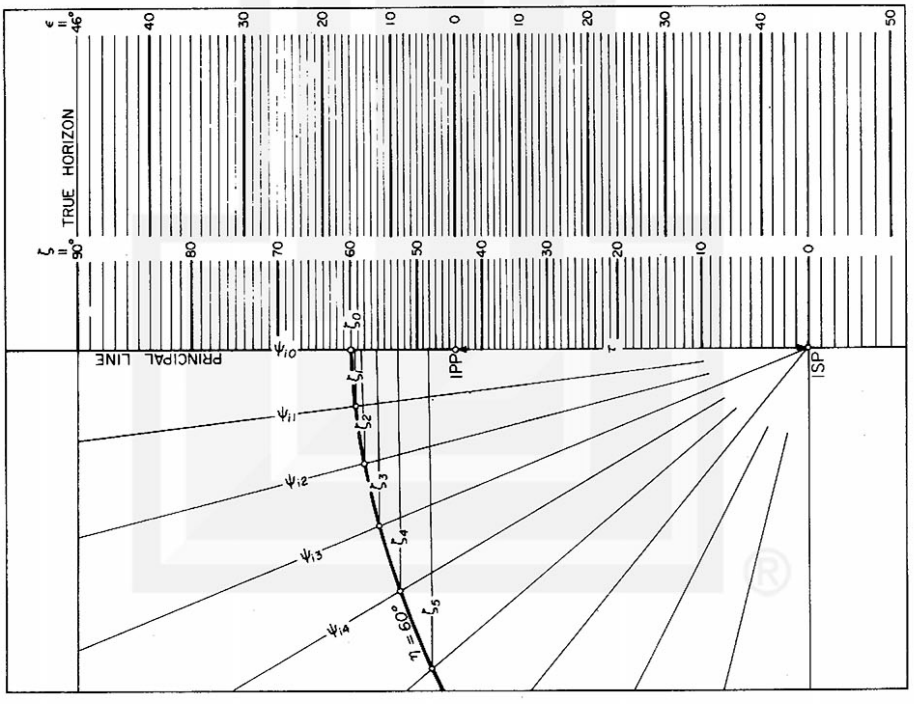

Figure 28. A method of constructing a tilt grid using Tables VI and VII.

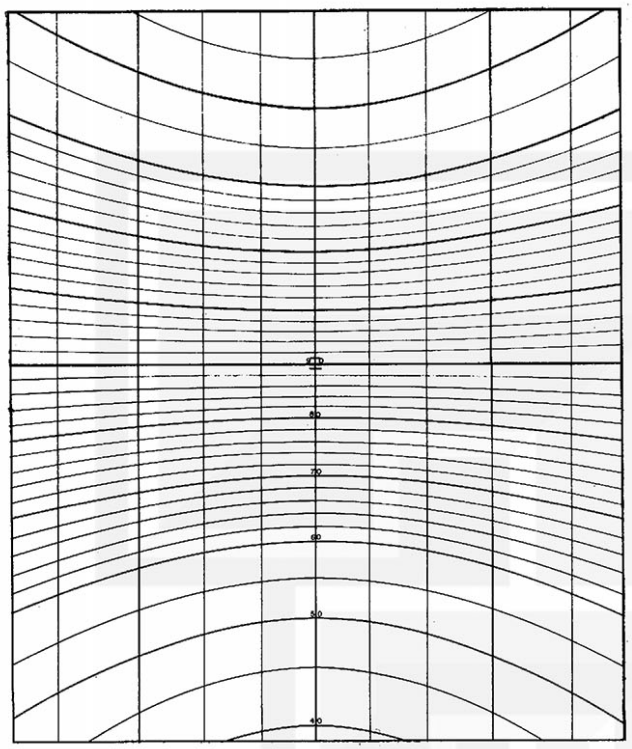

TILT GRID (90^{o})

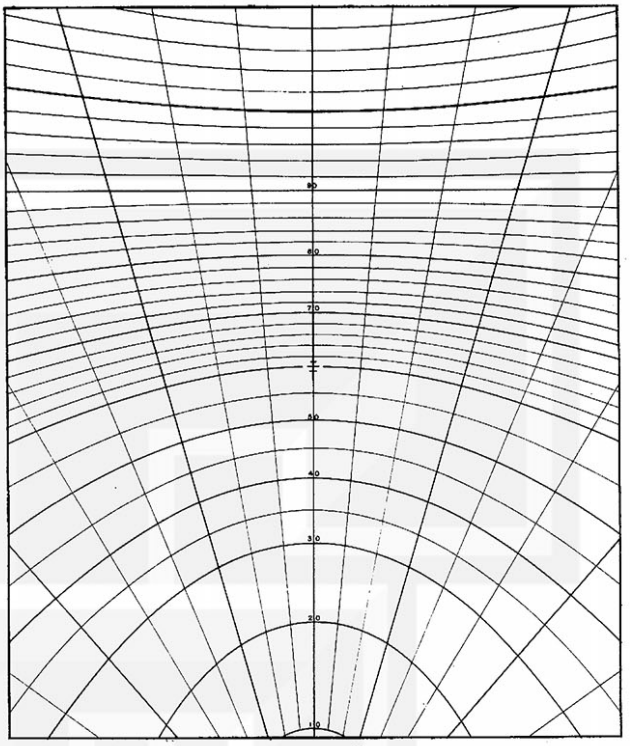

TILT GRID (60^{o})

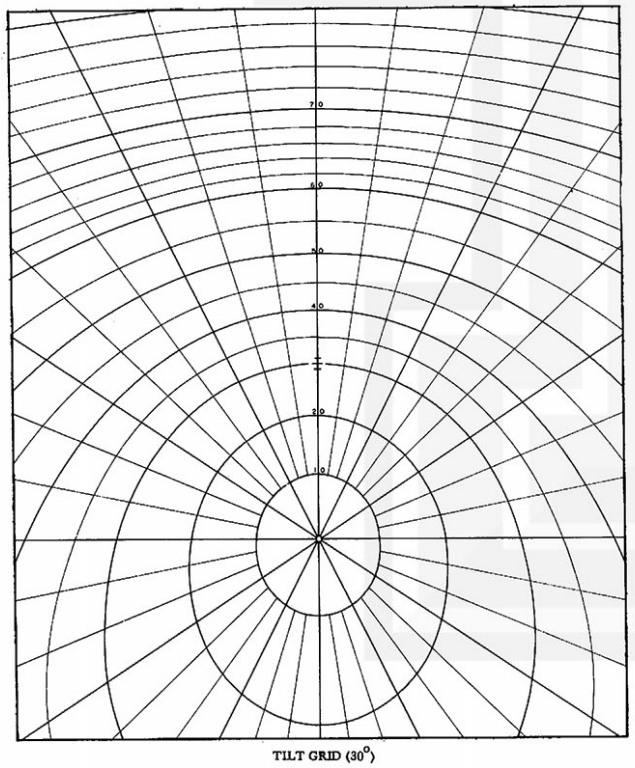

TILT GRID (30^{o})

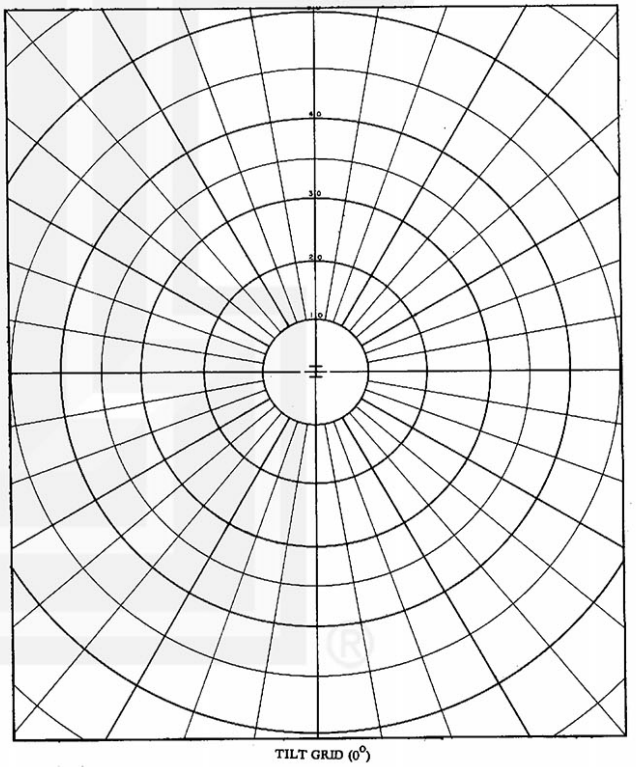

TILT GRID (0^{o})

Fig 29 Examples of tilt grid in reduced size.

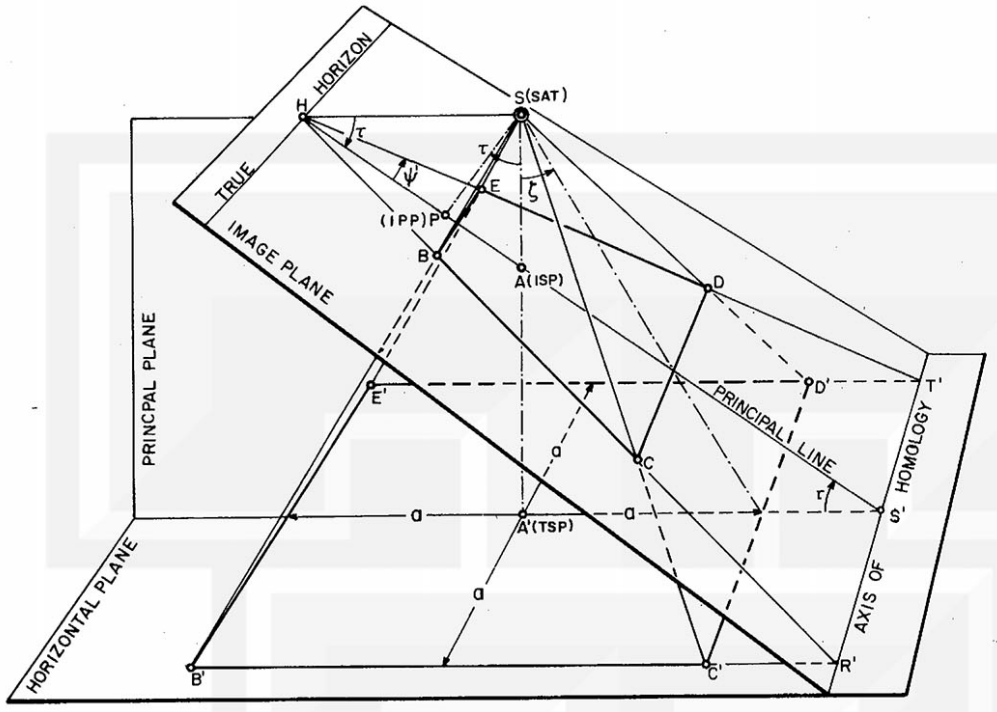

Figure 30. Geometry of a perspective tilt-grid. The grid lines are all straight since they are the intersections of pyramids with different vertical angles and the image plane. The one group of the iso-vertical-angle lines departs from the intersection of the principal line and the true horizon, while the others are always parallel to the true horizon.

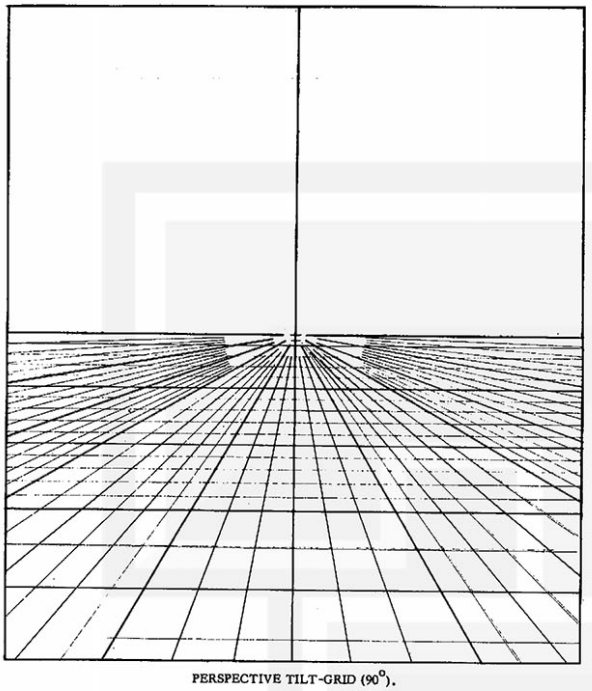

PERSPECTIVE TILT-GRID (90°).

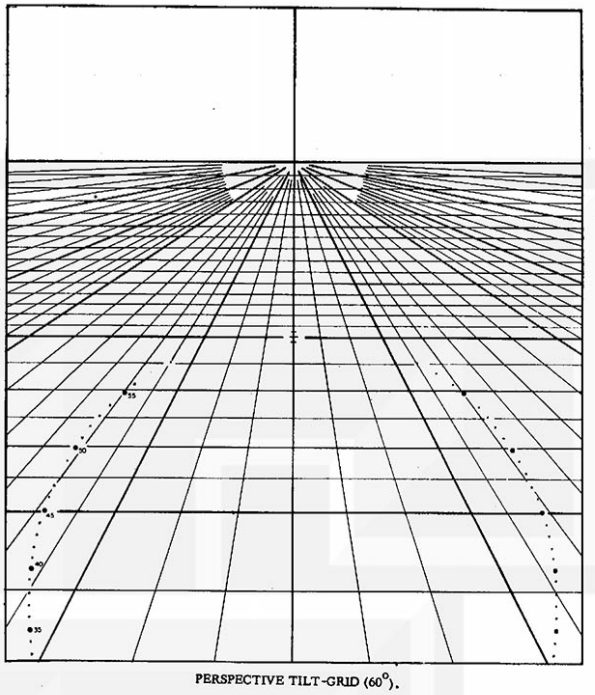

PERSPECTIVE TILT-GRID (60°).

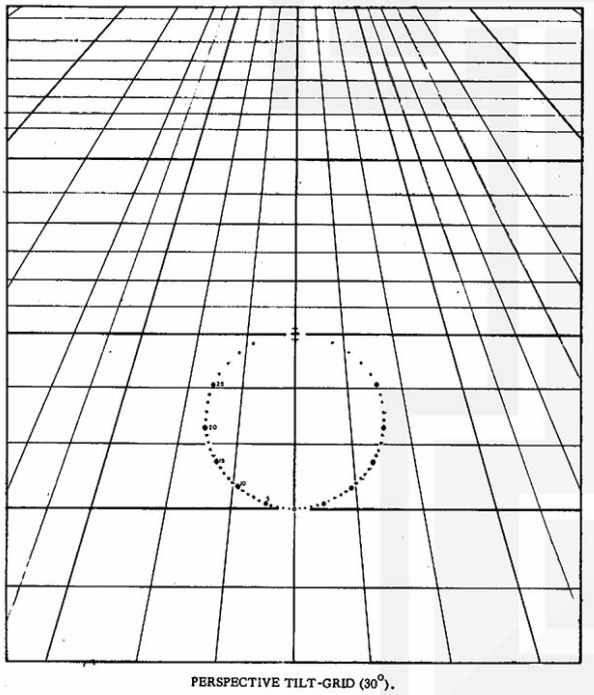

PERSPECTIVE TILT-GRID (30°).

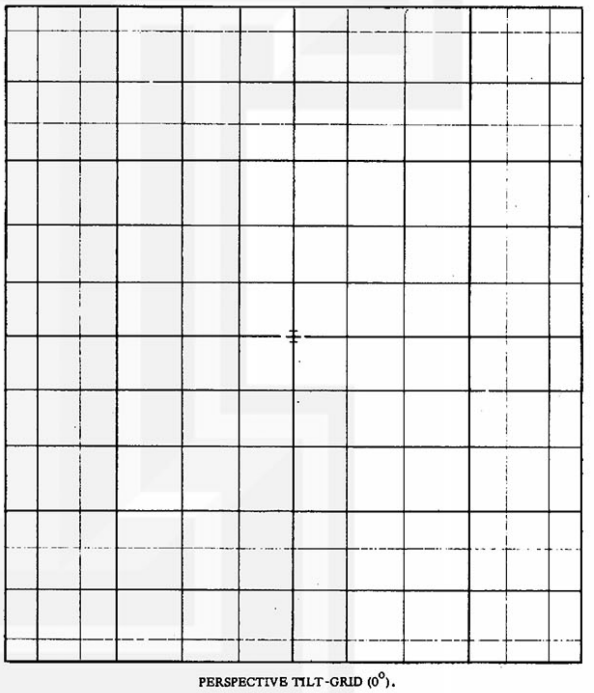

PERSPECTIVE TILT-GRID (0°).

Fig 31 Examples of perspective tilt-grid for distortion-free image plane.

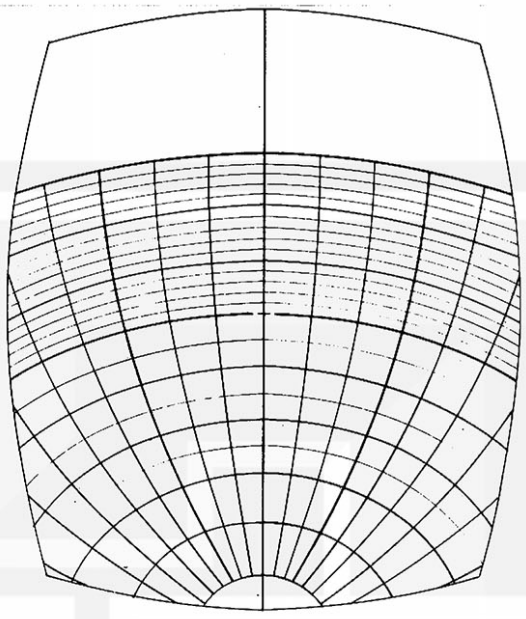

DISTORTED TILT-GRID (60^{o})

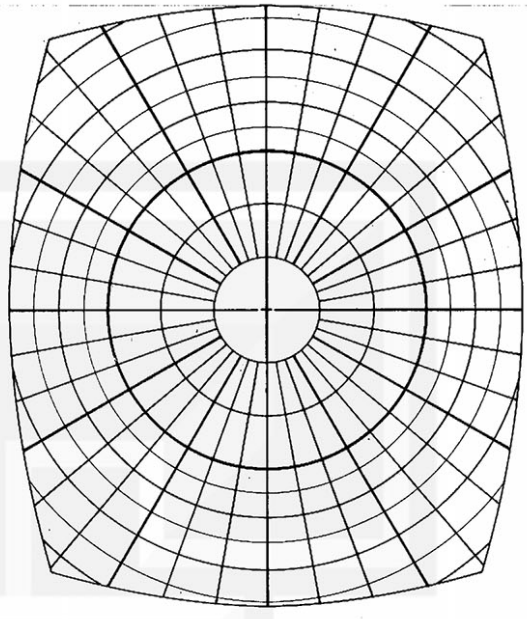

DISTORTED TILT-GRID (0^{o})

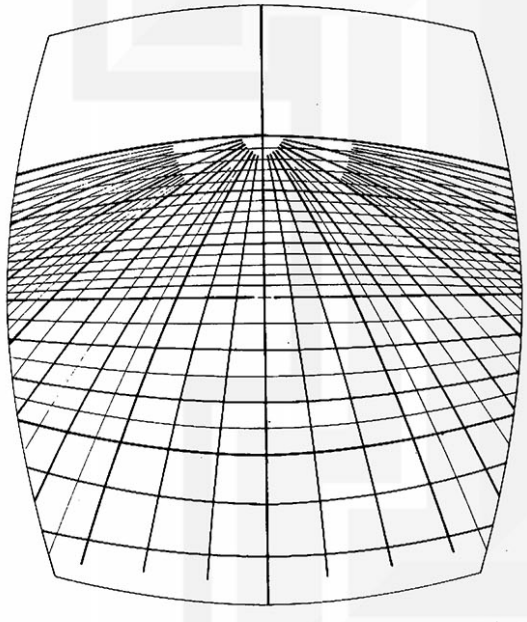

DISTORTED PERSPECTIVE TILT-GRID (60^{o}).

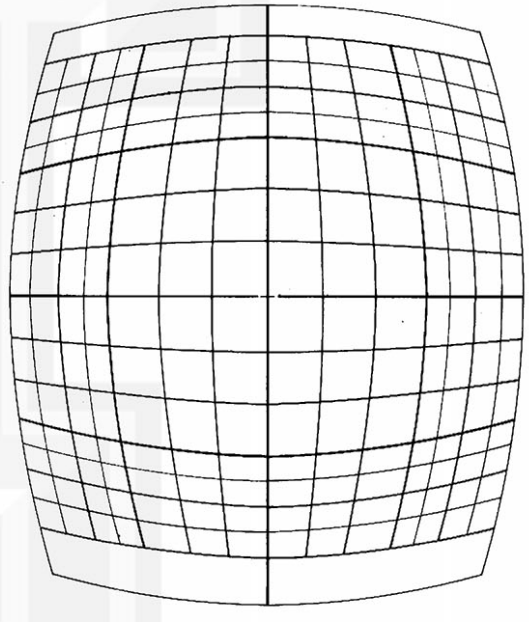

DISTORTED PERSPECTIVE TILT-GRID (0^{o}).

Figure 32. Examples of distorted tilt-grids. Both tilt and perspective tilt grids can be distorted to fit the mean radial distortion.

3. MAP PROJECTION AND HEIGHT GRID

A. HEIGHT GRIDS ON ZENITHAL EQUIDISTANT PROJECTION

One of the simplest yet most accurate map projections of a small portion of the earth beneath a satellite at one moment is the "Zenithal Projection" in which the objects are projected onto a plane tangent to the earth's surface at Q, the TSP (figure 33). Naturally, the least projection error occurs in the vicinity of the TSP.

Due to the orbital motion of the satellite, TSP moves around the earth once in every nodal period. It becomes, therefore, necessary to construct zenithal projection charts for all TSPs whenever photographs are taken by satellite-borne cameras. The easiest way of synthesizing these zenithal projection charts is to combine them into a cylindrical projection with the satellite orbit as the projection equator, along which a cylinder makes contact with the earth's surface. This problem will be discussed later, in detail, however, it should be noticed that a cylindrical projection results in an equidistant projection along the projection equator.

It will be found later, in the rectification processes, that we adjust the azimuth of the primary line by rotating the line around TSP. An equidistant projection on a plane tangent to the earth at a TSP will, therefore, have definite advantages, since the distance of arc between TSP and an object P to be projected remains practically constant in all azimuths viewed from the TSP.

Height grid in zenithal equidistant projection In order to transfer object positions on an image plane, distorted or undistorted, onto a plane of a map projection with the use of a tilt grid, it is required to have a perspectively corresponding grid on the map plane. Because of the fact that the tilt grids consist of lines representing nothing but the angles viewed from a satellite, the corresponding grids on the map plane should be determined solely by the height of the satellite. We call these grids the height grid.

Height grids on a zenithal equidistant projection include isolines of the horizontal angles, which are azimuth lines passing through the TSP. The angle between the azimuths is identical to the difference of the horizontal angles designating these azimuths. Another group of lines included in a height grid is the isolines of nadir angles, which are concentric circles with their radii, d, expressed implicitly by

$$H + \bar{R} = \bar{R} \left(\cos\frac{d}{\bar{R}} + \sin\frac{d}{\bar{R}} \cot\eta \right)$$

which is rearranged as

$$H = \bar{R} \left(\sin\frac{d}{\bar{R}} \cot\eta + \cos\frac{d}{\bar{R}} - 1 \right), \qquad (52)$$

where η denotes the nadir angle; R, the mean radius of the earth; d, the great circle distance of an object from TSP. This implicit equation is used in obtaining the great circle distances to be used in making height grids for various heights.

The numerical values of H from Eq. (52) tabulated in Table XII are used in constructing the height vs great circle distance diagram in figure 34. In order to obtain the arc distance for a given nadir angle, η, we simply draw a horizontal line passing through the satellite height until it meets the isoline of η. The length of the line segment measured from the ordinate represents the distance of arc between TSP and the object. Three scales under the abscissa are used for unit conversions. Also presented in figure 35 is an enlarged portion of the previous diagram to show more accurately the arc distances for the height of TIROS I-V. All isolines of η terminate at the true horizon to the right where dip angles, δ_H, are indicated.

Figure 36 shows an example of height grids drawn to fit a zenithal equidistant projection. For different heights the diameter of concentric circles change accordingly; however, the radials drawn for every 10 degrees of horizontal angle remain the same for any height grid.

Perspective height grid in zenithal equidistant projection A perspective height grid includes the lines of equal vertical angles oriented in four horizontal directions perpendicular to each other. Figure 37 shows both horizontal and vertical projection of a plane of vertical angle, ζ. This plane intersects the terrestrial spheroid with a small circle. The arc distance, d^*, between the TSP and a point P on the small circle is designated by x when it is projected onto the horizontal plane. We know that

$$x = \bar{R} \sin \frac{d^*}{\bar{R}} . \tag{53}$$

The length O'Q' = c is written as

$$c = (\bar{R} + H) \sin \zeta \cos \zeta = \frac{1}{2}(\bar{R} + H) \sin 2\zeta . \tag{54}$$

On the other hand, the distance P'Q' = p is a radius vector of an ellipse whose semimajor and semiminor axes respectively are a_1 and $a_1 \sin \zeta$. Therefore, we have

$$p^2 = \frac{b_1^2}{1 - e^2 \sin^2 \phi} = \frac{a_1^2 \sin^2 \zeta}{1 - \sin^2 \phi \cos^2 \zeta} , \tag{55}$$

where ϕ denotes the angle O'Q'P' and a_1, is expressed by

$$a_1^2 = (H + \bar{R})^2 \cos^2 \zeta - H (H + 2\bar{R}). \tag{56}$$

Solving the Δ O'Q'P', we write

$$\bar{R}^2 \sin^2 \frac{d^*}{\bar{R}} = c^2 + p^2 - 2cp \cos \phi \tag{57}$$

where $\cos \phi$ can be obtained from

$$\sin \phi = \frac{x}{p} \sin \psi . \tag{58}$$

The solution of d^* as a function of ζ and ψ is rather complicated. Nevertheless, the numerical values are obtained by solving Eq. (57) after putting the computed values of c, p, and ϕ into the equation. Figure 38 represents an example of such a grid.

Effects of cloud height and curvature of the earth: In the actual use of height grid, it is important to take into consideration the cloud height which may vary between 0 and probably 15 km or occasionally much larger. If we know the cloud height, H_c, the projection error can mostly be eliminated with the use of a height grid, $H - H_c$.

Another error which could be introduced by the radius of curvature of the earth expressed in Eq. (19), varies according to the latitude and the azimuth. Now we shall evaluate the effect of the earth's curvature. Figure 39 represents y_1 and y_2, the heights of the earth's surface below the true horizon viewed from the TSP. The equation of circles with the radius of curvature ρ_e and $\overline{R}$ in the figure are

$$\begin{aligned} x^2 + (\rho_e - y_1)^2 &= \rho_e^2 \\ x^2 + (\overline{R} - y_2)^2 &= \overline{R}^2 . \end{aligned} \tag{59}$$

Since ρ is usually much larger than x, Eq. (59) can be reduced to

$$y_1 = \frac{x^2}{2}\left(\frac{1}{\rho_e}\right) \quad \text{and} \quad y_2 = \frac{x^2}{2}\left(\frac{1}{\overline{R}}\right). \tag{60}$$

Thus the difference, $y_2 - y_1$, is expressed by

$$\begin{aligned} y_2 - y_1 &= \frac{x^2}{2}\left(\frac{1}{\overline{R}} - \frac{1}{\rho_e}\right) \\ \text{or} \qquad &= \frac{x^2}{2}\,\frac{\Delta\rho_e}{\rho_e \overline{R}} = \frac{x^2}{2}\,\frac{\Delta\rho_e}{\overline{R}^2} \end{aligned} \tag{61}$$

where $\Delta\rho_e$ denotes the excess radius of curvature of the earth. Table XI computed from this formula indicates that the above difference, $y_2 - y_1$, does not exceed 4 km within the limit of $x = 3{,}000$ km. Such a distance is far beyond the arc distance of the apparent horizon visible from the height of TIROS I-V. It is, therefore, reasonable to assume that the earth's radius is represented by its mean value, $\overline{R} = 6{,}367$ km.

B. CYLINDRICAL PROJECTION

It has been stated that a cylindrical projection will be favoralbe in synthesizing the zenithal projection charts tangent to the earth's surface at a series of TSPs, suggesting that a cylindrical projection could be made by selecting a satellite orbit as a projection equator. Strictly speaking, however, the earth is an ellipsoid, the shape of which would prohibit us, theoretically, from wrapping it by a cylindrical surface unless the earth's equator is taken as the projection equator.

Spheroid Approximation A question will arise then if it is plausible to approximate the terrestrial ellipsoid by a spheroid with its radius equal to $1/2\ (R_E + R_P)$. The tracking data of a satellite gives the longitude (θ) and the geodesic latitude (ϕ_d) of TSP as indicated in figure 40. Upon geocentric projection of TSP onto the spheroid in such a manner that the geodesic latitude of B is identical to the geocentric

latitude of B', the terrestrial subpoint and the satellite shift from B to B' and A to A', respectively. The angle OBO' = $\phi_d - \phi_c$, the difference between the geocentric and geodetic latitude at B or TSP, is given by Eq. (26). The height of the TSP at B above the surface of the spheroid with the mean radius is expressed by

$$BB'' = R - \bar{R} = R_E \frac{f_e}{2} \cos 2\phi . \tag{62}$$

As far as the TSPs are concerned, there will be no error in their positions relative to the terrestrial topography such as coastal lines and mountains which are also shifted by Eq. (62). The satellite A, as well, undergoes the same amount of the shift. The only error in the relative position could be introduced by the variation of the one-degree length of the longitude, L_θ, and that of the latitude, L_ϕ. These lengths are different from $\bar{L}'_\theta$ and $\bar{L}'_\phi$, the mean values computed for the terrestrial spheroid with mean radius $\bar{R}$.

$$\begin{aligned} L_\theta &= 111.418 \cos\phi - 0.094 \cos 3\phi \\ \bar{L}'_\theta &= 111.136 \cos\phi \\ L_\phi &= 111.136 - 0.562 \cos 2\phi \\ \bar{L}'_\phi &= 111.136. \qquad \text{(unit in km)} \end{aligned} \tag{63}$$

The differences in a one-degree arc are, therefore,

$$\begin{aligned} \bar{L}'_\theta - L_\theta &= 0.282 \cos\phi + 0.094 \cos 3\phi \\ \bar{L}'_\phi - L_\phi &= 0.562 \cos 2\phi . \qquad \text{(unit in km)} \end{aligned} \tag{64}$$

indicating that the difference in the length of the longitudinal arc at the equator is about 0.3 km/deg. The latitudinal difference, however, may reach up to 0.6 km/deg or 12 km per 20 degree-latitude, the maximum distance of objects from TSP, within which the usual satellite photogrammetric analyses are carried out.

It may be summarized that the spheroid approximation, using the mean radius of the earth, creates no error in the positions of TSPs relative to the terrestrial topography. The error of cloud positions, however, may reach 12 km at a distance of 20 degrees of arc in the meridional direction from TSP near the equator of the pole of the earth.

Projection of partial track: In rectifying TIROS photographs it is not necessary to make a projection of the one complete orbit on a cylindrical projection chart; instead, a partial orbit covered by the length of about a 20 min track of subsatellite points will suffice. Such a portion of an orbit would include all subpoints for the 32 tape-mode photographs, which are usually in a series.

As shown in figure 41 we consider the FSP and TSP tracks which intersect at the point E on the terrestrial spheroid. Then the time of the satellite passages over A, E, and C are expressed by t^{AN}, t^{E}, and t, respectively. If the orbit is assumed to be circular the angular velocity of the satellite in orbit with respect to the fixed space (ω_{sof}) is constant. Expressing the geocentric angles AOE and EOC by u_o and

u', we write

$$u_o = \omega_{sof} \ (t^E - t^{AN}) \text{ and } u' = \omega_{sof} \ (t - t^E).$$

In view of the fact that $(t - t^E)$ is only up to 10 minutes, the solutions of d_o and h_o can be obtained by assuming that the triangle ΔBCL is a plane triangle with straight sides. Now the distance, h_o, is written as

$$h_o = d_o \cos \alpha \tag{65}$$

where α denotes the azimuth of the celestrial orbit at C when the argument of satellite is $u_o + u'$. We express, ϕ_d, the latitude of TSP, the angle $\angle BCD = \delta\theta$ and α, the azimuth angle by

$$\begin{aligned} \sin \phi_d &= \sin \iota \ \sin \ (u_o + u') \\ \delta\theta &= \frac{\omega_{esf}}{\omega_{sof}} u' \quad \text{and} \quad d_o = \delta\theta \cos \phi_d \\ \text{and} \quad \cot \alpha &= \tan \iota \ \cos \ (u_o + u') \end{aligned} \tag{66}$$

in order to calculate h_o from Eq. (65).

These equations are reduced, in case of a polar orbit, to

$$\begin{aligned} \phi_d &= \omega_{sof} \ (u_o + u') \\ d_o &= \frac{\omega_{esf}}{\omega_{sof}} u' \cos \phi_d \\ h_o &= d_o \end{aligned} \tag{67}$$

and for an equatorial orbit to

$$\begin{aligned} \phi_d &= 0 \\ d_o &= \frac{\omega_{esf}}{\omega_{sof}} u' \\ h_o &= 0. \end{aligned} \tag{68}$$

Figure 42 represents the variation of h_o as a function of time past E, the intersection of the FSP and TSP tracks. The upper and lower charts, showing respectively the cases of $\iota = 48.4°$ and $\iota = 90.0°$, are similar in patterns, but the values of h_o is considerably large in the case of a polar orbit. In fact, h_o is extremely small when u_o is selected as either 60° or 240°. There is, of course, no choice in selecting u_o since it is determined by the time of satellite photographs. When u_o is approximately zero the TSP deviates appreciably in proportion to the time passage. Nevertheless, the maximum deviation does not exceed 2.5° even in case of a polar orbit. When the inclination of orbit decreases, the deviation becomes less significant, finally reaching zero for equatorial orbits. The deviation, h_o, we have obtained is fairly small for the partial orbit under consideration. It is, therefore, quite satisfactory to use a cylindrical projection with the inclination of the projection equator identical to that of the satellite orbit.

C. EQUIDISTANT CYLINDRICAL PROJECTION AND ITS OVERLAY

The first cylindrical projection used in rectifying successive TIROS photographs was constructed by Glaser (5), who adopted an oblique mercator projection with its projection equator identical to the FSP track. This projection has contributed significantly to the operational analysis of TIROS photographs at the readout stations. When it is used in solving precise rectification problems, the difference of arc lengths along the projection equator and the projection meridians introduces some error, especially when the primary line is rotated about the TSP. It is, therefore, desirable to design a cylindrical projection chart on which the isolines of nadir angles form the concentric circles around a subsatellite point. On such a chart the primary line may be rotated while maintaining the same object nadir angle.

OEC projection The oblique equidistant cylindrical projection (OEC projection) chart was designed by Fujita (4) for use at the International Meteorological Satellite Workshop in Washington, 1961. The inclination of the projection equator in this projection is identical to ι, the inclination of the satellite orbit (figure 43). As the name of this projection represents, the coordinates, x and y, of a projected point C' on the chart represent the lengths in great circle arc of AB and CB, respectively. Expressing the arc AC by ℓ and the angle $\angle$DAC by λ, we solve the spherical triangles CDA and CBA, thus

$$\begin{aligned} \cos \ell &= \cos \phi \cos \theta \\ \cot \lambda &= \cot \phi \sin \theta \end{aligned} \tag{69}$$

and

$$\begin{aligned} \tan x &= \tan \ell \cos (\lambda - i) \\ \sin y &= \sin \ell \sin (\lambda - i), \end{aligned} \tag{70}$$

where ϕ is the latitude, and θ denotes the longitude measured from A. The OEC projection charts were made to fit the orbital inclination of 48.4° (TIROS I-IV) and 58.3° (TIROS V). They appear in reduced scale in figures 44 and 45 (Table VIII and IX).

By changing the inclination of the projection equator from i to 90°, the projection equator passes through both north and south poles. Such a projection is called the transverse equidistant projection (TEC Projection). This projection chart, shown in figure 47 can be used conveniently for various purposes (Table X).

OEC overlay On an equidistant cylindrical projection chart the distance measured in the great cirle arc is preserved in the direction of the projection equator and the projection meridians. The distance in other directions is larger than that of true arc length on the spheroid. By viewing a TEC projection chart, it will be seen that the isolines of latitudes represent those of various arc distances from the pole. At the same time, the terrestrial meridians on the TEC chart give precisely the

horizontal angles viewed from the point directly above the pole. A TEC chart whose latitudes and longitudes are labeled as the great circle distance (in deg) and horizontal angles, respectively, is called the OEC overlay. The FSP and TSP on the overlay is placed on top of the FSP or TSP on the equidistant cylindrical projection chart in order to determine the arc distances, horizontal angles, and principal or primary lines with respect to these subpoints. The subpoints should be located as close as possible to the projection equator.

The error in position determination using an overlay is significant if the TSP is far off from the OEC projection equator. Let the distance between the TSP and the OEC projection equator be b; the position of C, determined by the overlay with its origin at the TSP and its projection equator parallel to that of OEC, differs from the true relative position, which could be measured by rotating the terrestrial spheroid around the pole, P, until TSP rests on the OEC projection equator. Through this rotation the point, C, moves to C' while maintaining the polar distance, k. With the use of the symbols in figure 48 the component errors (true - measured), ΔX and ΔY will be obtained.

From the spherical triangle, PC'D and PCD, we have

$$\sin Y = \sin k \sin \alpha$$

and

$$\sin Y' = \sin k \sin (\alpha - b),$$

where $Y' = Y + (\Delta Y - b)$ in which the value $(\Delta Y - b)$ is only up to a few degrees. This permits us to use an approximation

$$\cos (\Delta Y - b) = 0, \text{ and } \sin (\Delta Y - b) = \Delta Y - b$$

obtaining finally, the y component of the error

$$\Delta Y = b (1 - \cos X). \tag{71}$$

A similar calculation starting from the equations,

$$\cos k = \sin X \cos Y$$

$$\cos k = \sin (X + \Delta X) \cos (Y + \Delta Y - b)$$

leads us to obtain

$$\Delta X = - b \sin X \tan Y. \tag{72}$$

The absolute value of the vector shift is calculated as

$$\sqrt{\Delta X^2 + \Delta Y^2} = b \left\{ (1 - \cos X)^2 + \sin^2 X \tan^2 Y \right\}^{\frac{1}{2}} \tag{73}$$

which can be reduced, for small values of X and Y to

$$\sqrt{\Delta X^2 + \Delta Y^2} = b \frac{X}{2} \sqrt{X^2 + 4Y^2} \quad \text{(in radians)} \tag{74}$$

or

$$= 0.00015\ b \cdot X \sqrt{X^2 + 4Y^2}. \quad \text{(in degrees)} \tag{75}$$

This might result in an error of 0.03b, when $X = Y = 10^{\circ}$; 0.13b, when $X = Y = 20^{\circ}$;

and 0.52b, when $X = Y = 30^{\circ}$.

Proper use of OEC overlay In the rectification processes of satellite photographs, an OEC overlay is used frequently in drawing a great circle line connecting a TSP with other points, and in measuring the great circle distance from the TSP. It has been shown that the origin of an overlay may be placed on the TSP if the great circle distance to be measured is only a few degrees. When a measurement of relatively large great circle distance is required it is necessary to use the overlay properly, otherwise the error might be too large to tolerate.

Figure 49 indicates the proper uses. First an overlay is so placed on the OEC chart that their projection equators coincide. Then let the projection equator of the overlay slide on top of the other until both TSP and the object, C, lie on an azimuth line. The great circle distance, j, of the object from TSP is calculated by

$$j = j_c - j_T .$$

At the same time, the horizontal angle, ψ, is measured on the overlay.

It should be noted that this method does not involve approximation and exact values are obtained. In case the deviation of the TSP from the OEC projection equator is less than one or two degrees or the object to be measured lies within a few degrees of the great circle distance from the TSP, we may place the origin of an overlay right on the TSP so that the measurement can be accomplished through only one step.

D. HEIGHT GRID ON OEC PROJECTION

The height grids which fit an OEC projection are very similar to those on a ZE projection. Figures 50 and 51 give the examples of OEC height grids. The outermost boundary of the grid denotes the apparent horizon viewed from the satellite altitude.

In fact, the isolines of horizontal angles on any OEC height grid are identical to those on an OEC overlay which fits the OEC projection chart. Therefore, the slightly curved radials on the height grids can be traced off from the OEC overlay. It is evident that an OEC height grid does not fit the OEC projection chart if we rotate the grid around its origin. A semidisc on the apparent horizon on a height grid, thus, indicates the direction which should be kept parallel as much as possible to the projection equator of the OEC projection.

The great circle distance (d) between TSP and the isoline of specific nadir angle is a function of both H and η. It is obtained from Eq. (52) which can be reduced to

$$H = \bar{R} \csc\eta \quad (\sin\frac{d}{\bar{R}} \cos\eta + \cos\frac{d}{\bar{R}} \sin\eta) - \bar{R}$$

or

$$H = -\bar{R} + \bar{R} \csc\eta \sin(\frac{d}{\bar{R}} + \eta).$$

Thus, we have

$$\frac{d}{\bar{R}} = -\eta + \sin^{-1} (\frac{H+\bar{R}}{\bar{R}} \sin\eta). \tag{76}$$

The left side of this equation denotes the geocentric angle of the great circle distance, d.

An OEC overlay includes the isolines of this geocentric angle at one degree intervals. These isolines are almost perfect circles with their centers at the origin of the OEC overlay. Even for the angles of 25 and 30 degrees, the deviations from the great circle are only 0.1 and 0.3 degrees, respectively.

The geocentric angle of the great circle arc, d, may also be obtained from figures 34 and 35. Then the isolines of specific nadir angles may be approximated as concentric circles, since the great circle distances of the apparent horizons viewed from the heights, 650 and 1000 km, respectively, are 25 and 30 degrees.

In case the satellite height exceeds about 1000 km, it becomes necessary to use the isolines of a specific great circle distance on an OEC overlay. They deviate from the true circles considerably when the great circle distance becomes larger than 30 degrees. It should be noted, however, that the isolines of horizontal angles, ψ, remain the same on all height grids, as far as the scale of the matching OEC chart remains unchanged.

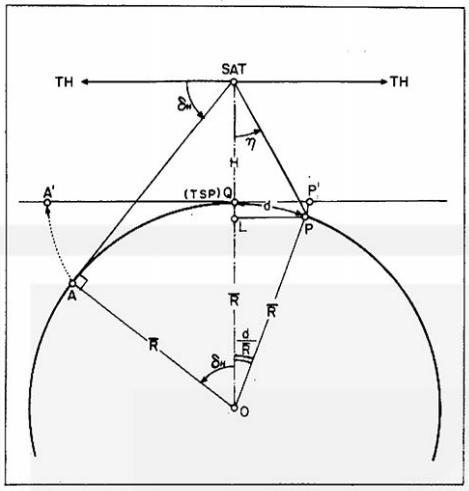

Figure 33. Geometry of computing a height grid to fit a terrestrial spheroid. Symbols in the figure are δ_H, the dip angle; η, nadir angle; d, great circle distance of an object from the TSP; R, radius of terrestrial spheroid.

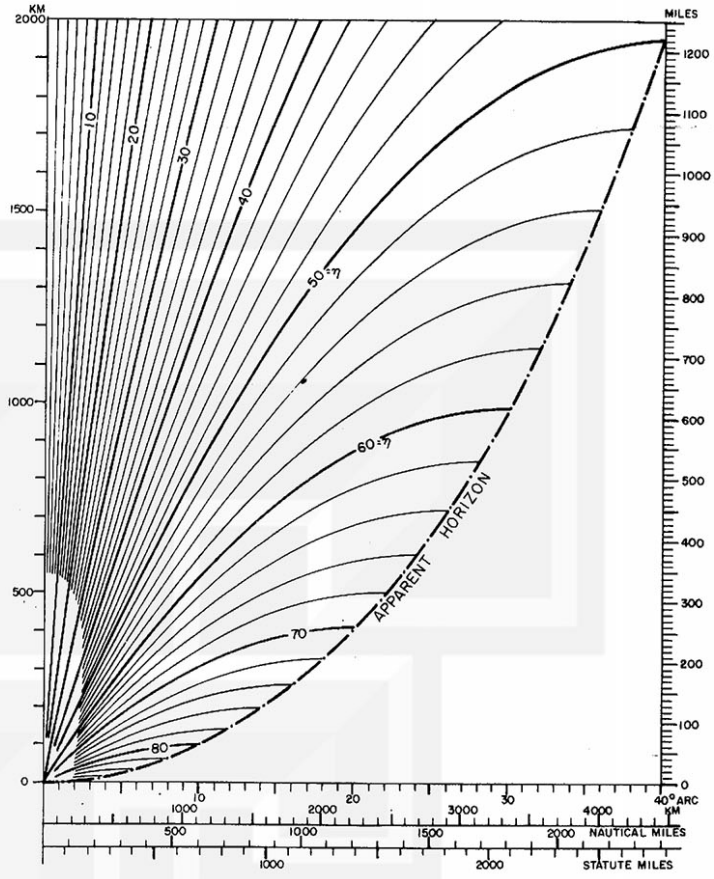

Figure 34. Height of a satellite vs great-circle distance from TSP of objects with different nadir angles. The great-circle distance for a given satellite height and a nadir angle is obtained by drawing a horizontal straight line through the satellite height. The abscissa of the points of intersection of the line and the curves of each nadir angle represent the great-circle distance from TSP.

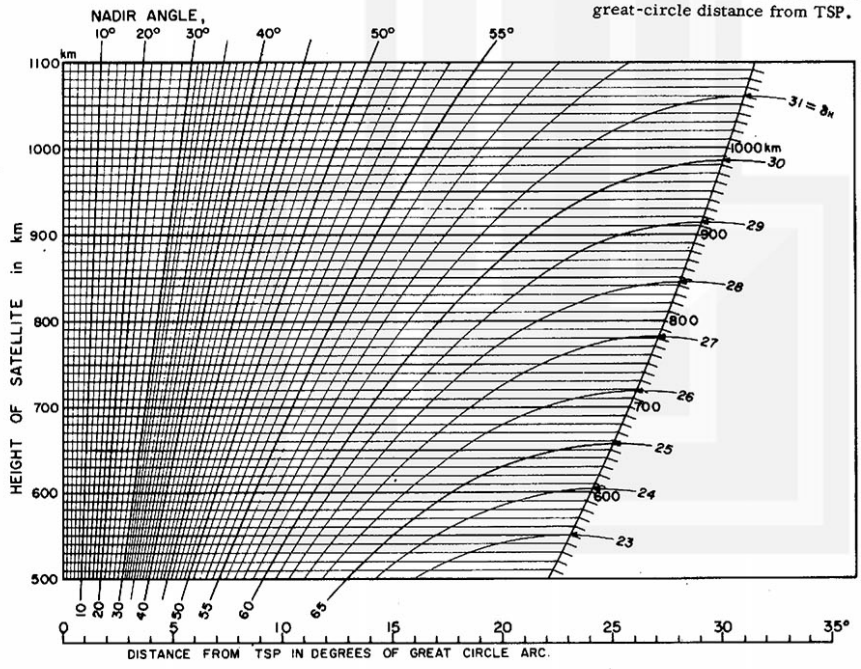

Figure 35. An enlarged section of the previous diagram. This diagram covers the heights and nadir angles needed for TIROS I-V.

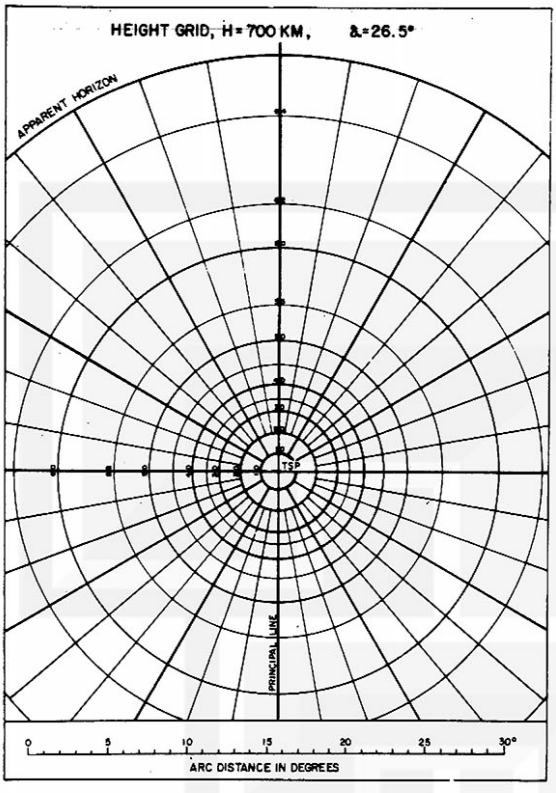

Figure 36. An example of a height grid drawn to fit a zenithal equidistant projection.

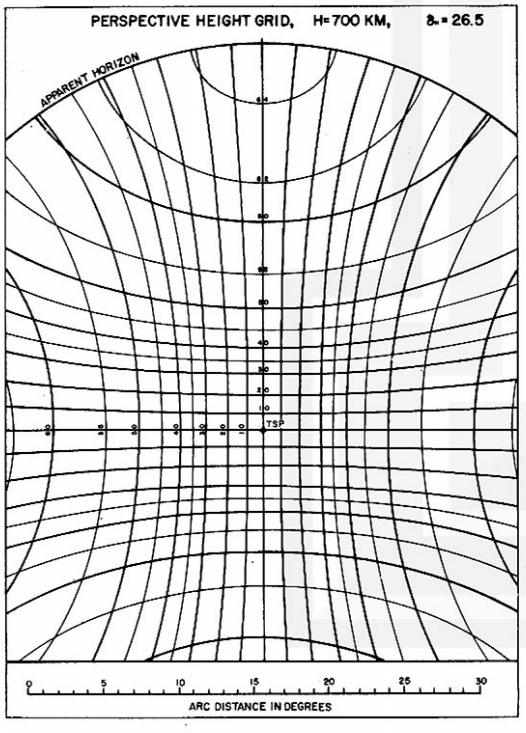

Figure 38. An example of perspective height grids.

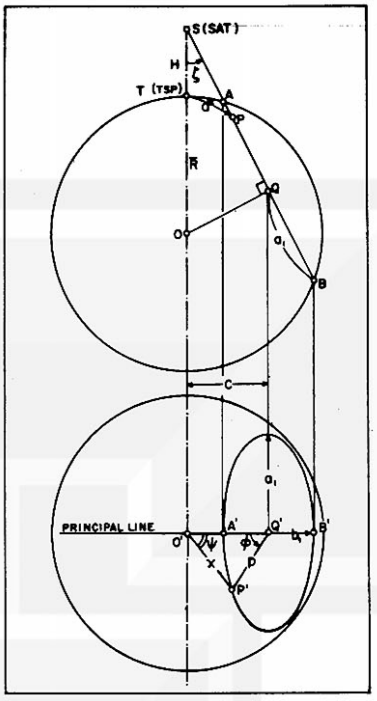

Figure 37. Geometry for calculating grid points of perspective height grid in zenithal equidistant projection.

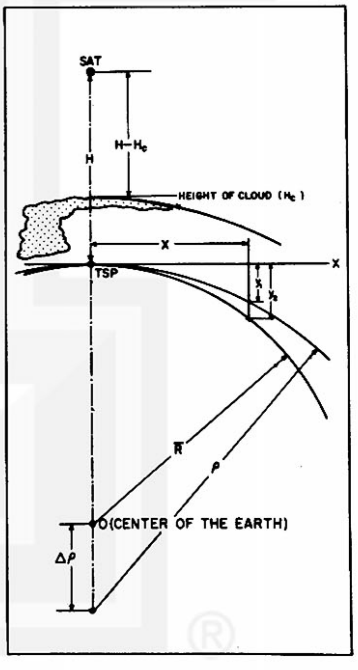

Figure 39. Showing the effects of cloud height and curvature of the earth upon rectification geometry. The difference, $y_2 - y$, appears in Table XI.

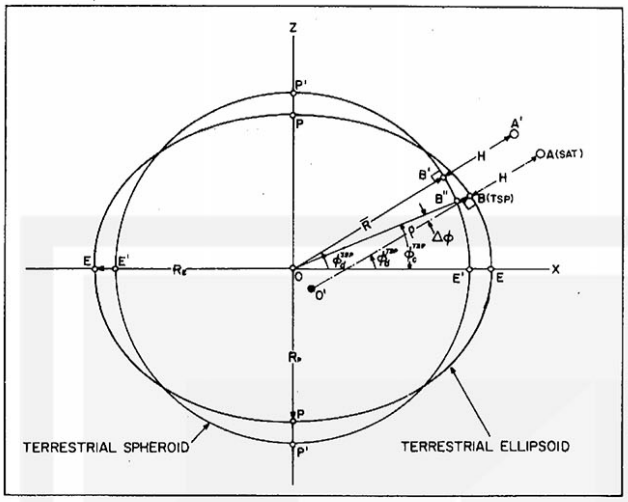

Figure 40. Change in satellite position resulted by the use of the terrestrial spheroid. The change does not affect the relative positions of a subsatellite point and clouds or landmarks.

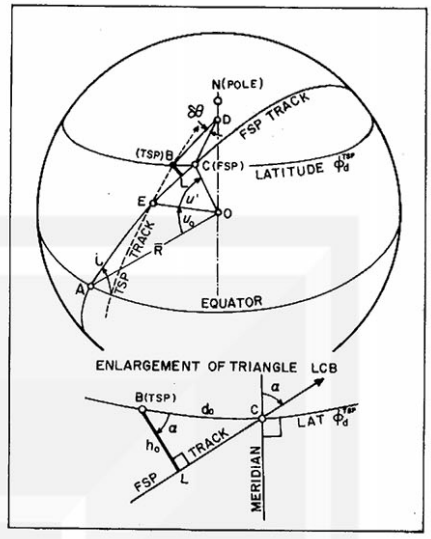

Figure 41. To evaluate the deviation of TSPs from the OEC projection-equator when a partial orbit is plotted on an OEC chart. E denotes the point where TSP track crosses the projection equator.

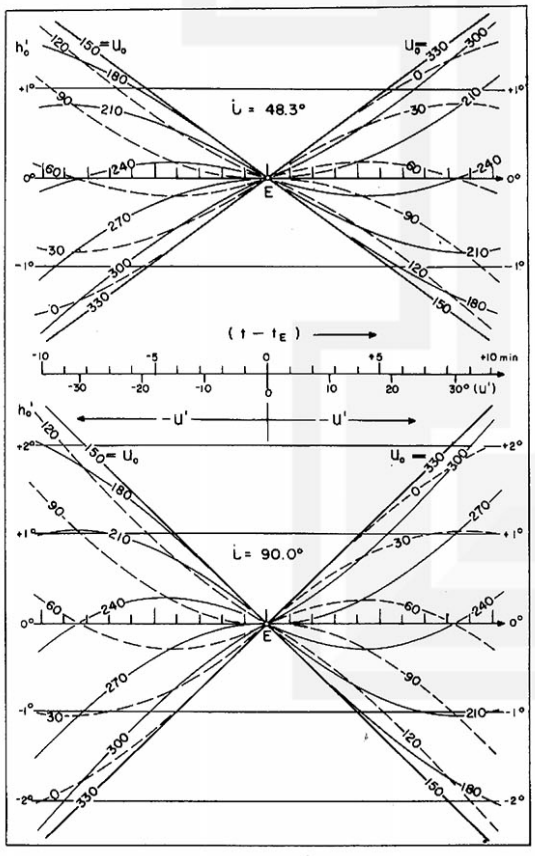

Figure 42. Calculated amount of deviation of TSPs from the OEC projection equator. E denotes the point where TSP track crosses the projection equator. The argument of E was changed at 30 degree intervals between 0 and 360 degrees.

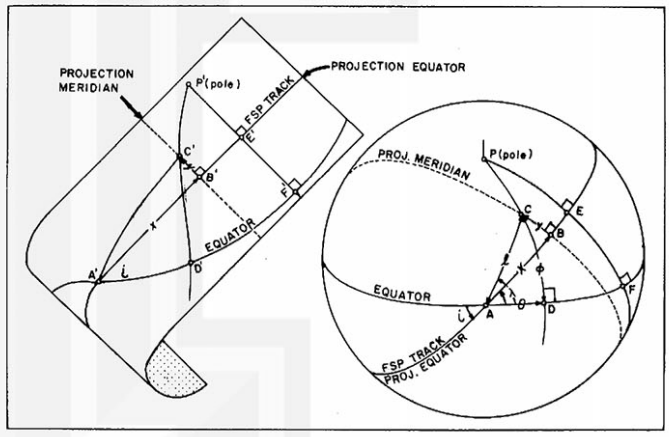

Figure 43. Geometry to construct an OEC projection chart.

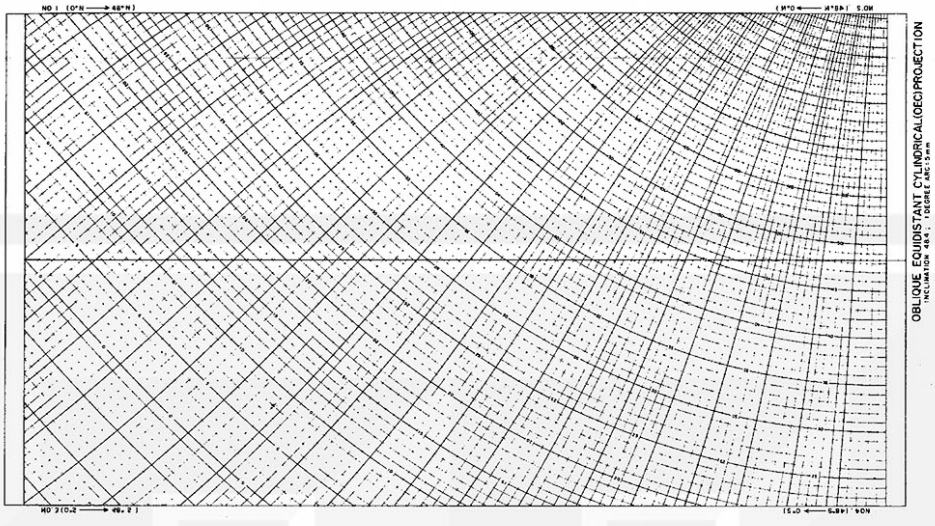

Figure 44. An example of OEC projection chart with 48.4° inclination of the projection equator.

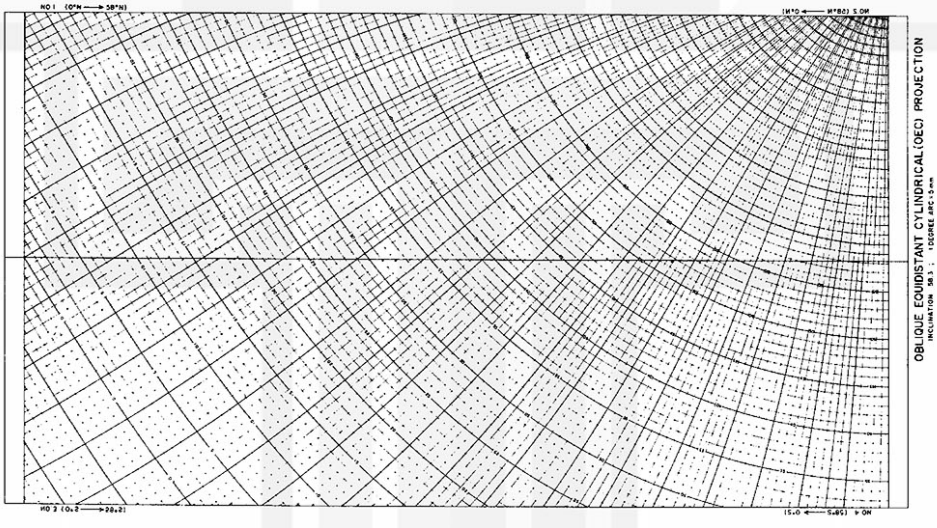

Figure 45. An example of OEC projection chart with 58.3° inclination of the projection equator.

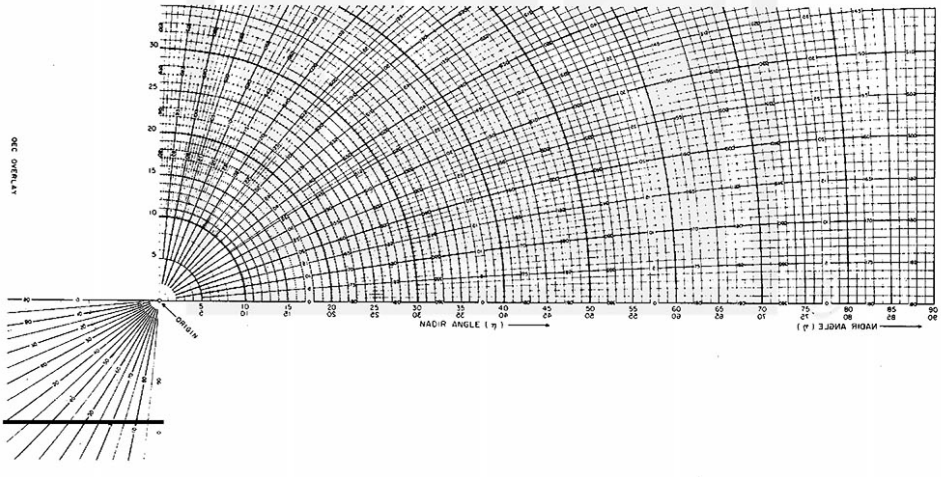

Figure 46. An overlay to OEC chart made to fit the OEC chart in figures 44 and 45.

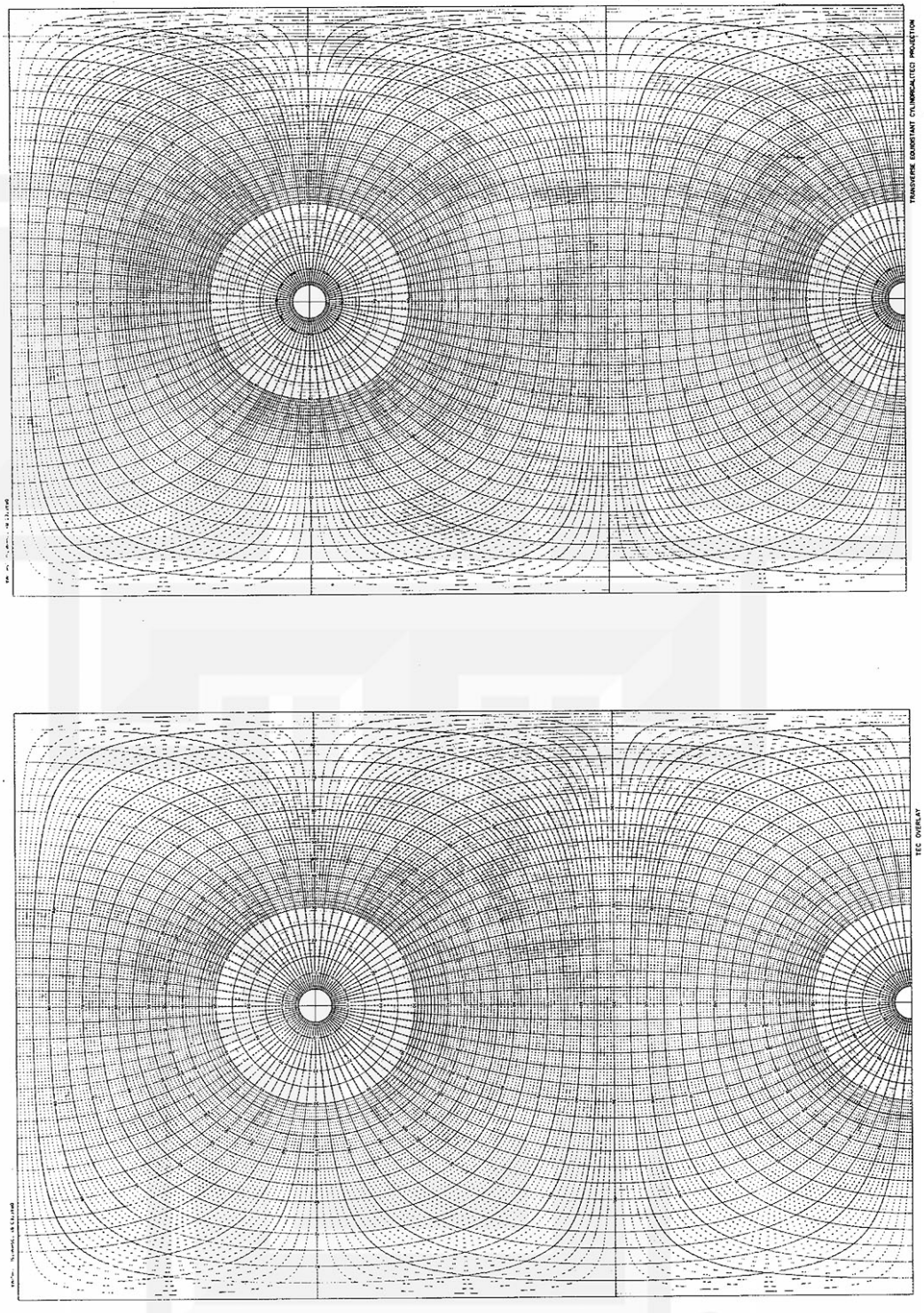

Figure 47. An example of TEC projection chart and its overlay. Above: TEC projection chart covering six quadrants. The centers of the concentric circles are poles. Both latitudes and longitudes are at one degree intervals. Below: Overlay to the TEC charts. (Drafted by T. Ushijima)

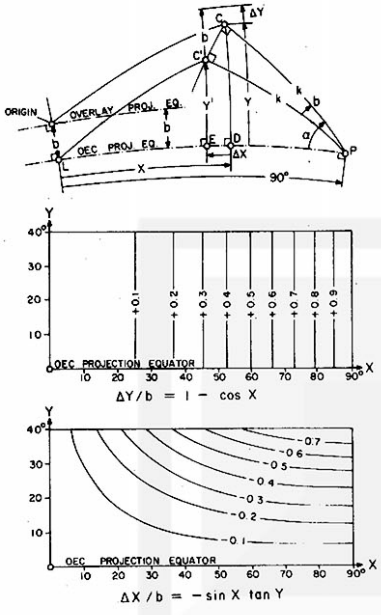

Figure 48. To evaluate the error introduced if the origin of an OEC overlay is placed at a TSP which is not located on the OEC projection equator.

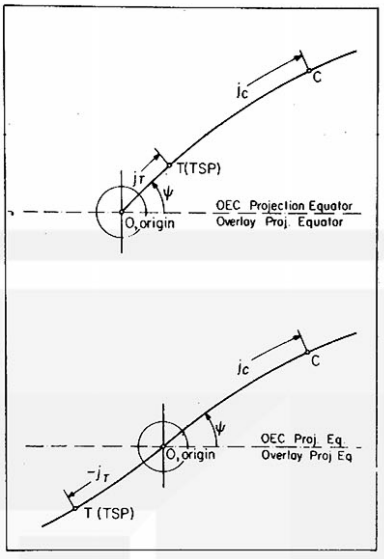

Figure 49. Proper use of an OEC overlay. For the precise measurements, the projection equator of an OEC and that of an overlay should always coincide. Only a parallel shift of the overlay is allowed in order to bring both T (TSP) and C (object) on one azimuth line on the OEC. If the TSP is within about 2 degrees from the projection equator, an approximate measurement can be made by placing the origin of the overlay to the position of the TSP. The error can be evaluated by figure 48.

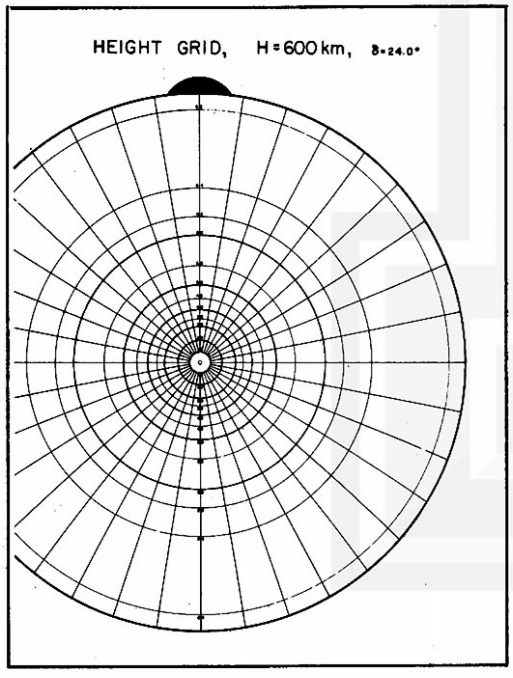

Figure 50. An OEC height grid for 600 km satellite height. The heavy line around the height grid is the apparent horizon viewed from the satellite.

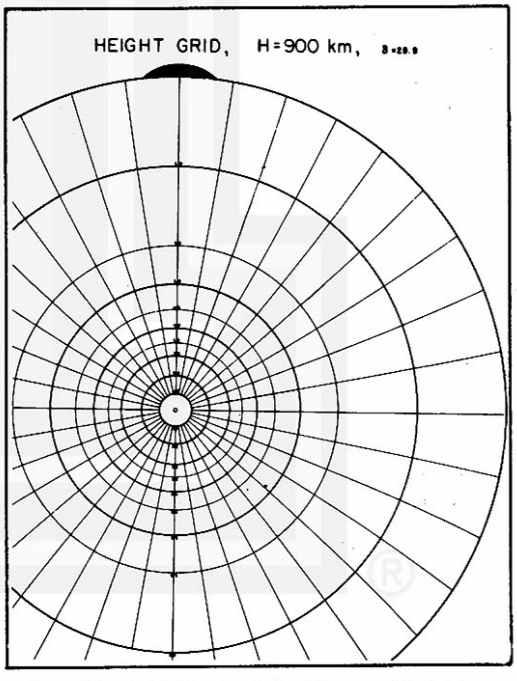

Figure 51. An OEC height grid for 900 km satellite height. The semi-disc on the apparent horizon indicate the orientation of the projection equator when the height grid is placed on an OEC chart.

4. ATTITUDE OF SATELLITE

In order to perform a high quality of rectification of satellite photographs, it is of vital importance to determine precisely the tilt of the image and the orientation of the principal plane. Because of the lack of landmarks in a majority of the TIROS photographs, we are not able to determine camera orientations using the individual image only. It necessitates, therefore, an advanced method by which a bit of photogrammetric information acquired from each photograph is pieced together into an accurate determination of a series of satellite photographs.

One of the most important parameters introduced by Glaser (5) and investigated further by Hubert (6) is the nadir angle of the satellite spin-axis. The term satellite nadir-angle (η_s) is used to designate this angle. Due to the fact that the optical axes of TIROS cameras are not exactly parallel to the spin axis, the tilts (τ) are slightly different from the satellite nadir-angle. The term tilt is applied to the nadir angle of the camera optical axis.

A. ATTITUDE RELATIVE TO THE EARTH

Although the precise motion of a TIROS spin-axis due to the nutation is not known to us, it is reasonable to assume that the orientation of the spin axis remains unchanged during the nodal period or its fraction. Figure 52 represents the positive direction of the spin axis, being from the top to the floor of TIROS. Since the cameras are mounted on the floor, the positive direction coincides with the direction in which pictures are taken.

The terrestrial spin-axis points (TSA) are the points at which the translated spin-axes intersect the earth's surface at right angles. To distinguish the intersections one from the other, the one in the positive direction viewed from the center of the earth is called the spin-axis antipode (TSA').

The plane which includes the satellite spin-axis and the local vertical through the satellite is called the primary plane. This plane does not always include the spin-axis point unless the earth is assumed to be a spheroid. Such an assumption may create an error of up to 0.2 deg of latitude; however, the relative position between TSP and TSA should not include any error if they are consistently expressed by either geodetic or geocentric latitudes. In view of the fact that the subpoint data are usually given by geodetic latitudes, the TSA will be expressed by geodetic latitude.

The following discussions are thus based upon the spheroidal approximation of the earth. The geocentric latitudes on the spheroid are labeled by the geodetic latitudes so that the landmarks with geographic grids on the maps and atlases correspond exactly to those which would appear on the surface of the spheroidal earth.

Under this assumption the primary plane includes the earth's center, TSA, TSA', TSP and the spin axis of the satellite. The point of intersection of the spin axis with the terrestrial spheroid, which is termed the terrestrial primary point (TPM) and the satellite are also in the same plane.

A three-dimensional view of a satellite, the earth, and an image plane appears in figure 53. The points, TSA, TSP, and TPM always lie on a great circle which is the intersection of the primary plane with the earth's surface. This great circle is called the primary line on the earth. As the satellite orbits around the earth, the TSP displaces on the earth's surface while the TSA remains practically at the same spot on the fixed earth during one orbit. Thus, the TPM, located on the extension of the great-circle arc connecting TSA with TSP, moves much faster than TSP forming a TPM track on the earth.

It is important to recognize that the great circle distance in degrees of TSA and TSP at any moment denotes the satellite nadir-angle. Once we know the satellite nadir-angle, the great circle distance between TSP and TPM is obtained either from Eq. (52) or figures 34 and 35 as a function of H and η_s.

On the fixed-earth coordinates projected onto a OEC chart, the primary lines connecting FSA with FSPs can be drawn with the help of an OEC overlay by superimposing it upon an OEC map so that their projection equators coincide. Figure 54 shows a schematical drawing of the primary lines. When the FSP is located closest to the FSA, the satellite nadir-angle reaches its minimum value called the minimum nadir-angle (η_s^{MIN}). If the height of the satellite remains the same, the distance between the FSP and FPM tracks also reaches a minimum value at the time of the minimum nadir-angle (t^{MIN}).

As shown in the lower diagram of figure 54, each of the primary lines on the rotating earth projected onto an OEC chart connects two moving points, TSA and TSP. In fact the change of the longitude of a TSA is obtained by Eq.(37), as

$$\theta_t^{TSA} = \Theta_t^{FSA} - (t - t_F)\,\omega_{esn} \,, \tag{77}$$

where Θ_t^{FSA} denotes the fixed-earth longitude of FSA at the time t, which may be assumed constant during any one orbit. That is to say, the longitude of a TSA decreases about 0.25 deg per minute. Exact values of the sidereal rotation rate of the earth, which are used in computing Eq.(77) appears in Table V.

B. ATTITUDE RELATIVE TO THE SUN

In order to determine the attitude of a satellite relative to the sun, it is necessary to define both local and primary sun-planes. (Figure 55)

The primary sun-plane is a plane which includes the sun and the spin axis of a

satellite. The intersection of this plane with an image plane, which is perpendicular to the spin axis, is a straight line termed image primary sun-line. This line passes through the image sun-point (ISN). Thus, the points SAT, IPM, TPM, SUN and ISN are included in the primary sun-plane. When this sun plane intersects the earth the line of intersection is a small circle unless the satellite nadir-angle is zero.

The local sun-plane is defined as a plane which includes the sun and a local vertical through any point on the earth or in space. This sun plane can be identified by adding the name of a local point included in the plane. A local TSP sun-plane is an example. It should be noted that a local sun-plane always intersects the earth with a great circle.

The point of projection of the sun onto the earth's surface using the local vertical through the sun is called the terrestrial subsolar-point (TSS). By changing the superscripts for a satellite in Eq. (29) to those for the sun, we have

$$\phi_d^{TSS} - \delta^{SUN} = \frac{R}{H+R} f_e \sin 2\phi_d^{TSS}. \tag{78}$$

Since the distance of the sun is extremely large compared with the radius of the earth, we may neglect the right side, thus

$$\phi_d^{TSS} = \delta^{SUN}. \tag{79}$$

Now we consider a local TSA sun-plane. This sun plane naturally intersects the earth with a great circle connecting TSA and TSS. Because of the large distance between the earth and the sun, the lines SUN-TPM and SUN-TSS may be considered parallel. On the other hand, the lines TPM-SAT and TSA-Earth's Center are also parallel by definition. As a result, the local TSA sun-plane and the primary sun-plane are parallel planes. It follows, therefore, that the plane of the great circle connecting TSA with TSS is always parallel to that of the small circle through the TPM. This small circle is the line of intersection between the primary sun-plane and the earth. Thus, the distance between these great and small circles on the terrestrial spheroid is equal to the distance between TPM and the great circle connecting the spin-axis with the subsolar point.

The TIROS-borne sun-angle indicator gives on each frame a sun-angle digital display as binary numbers 1/8, 1/4, 1/2, 1, 2, 4, 8, 16, 32, 64, 128, and 256. They are to be added to obtain the sun angle (γ^{SN}) which is the tangential angle of the image sun-point measured from the radial of the zero sun angle. Thus, the sun angle permits us to determine the primary sun-line on each image independently from the horizon or landmarks.

In case a well defined apparent horizon appears on an image, the orientation of a photograph can easily be determined with the help of the primary line. When the satellite nadir-angle is less than 20 deg, however, we cannot always use the primary line as an orientation reference. In such a case, the distance between the FSA sun line (great circle) and the primary sun line (small circle) on the earth is not too far apart. As a result, the primary sun lines passing through each FPM on an OEC chart

(figure 56) may be assumed parallel to the FSA sun line, the great circle connecting FSA with the FSS. In a similar manner, the primary sun lines on the rotating earth coordinates can be obtained by drawing several TSA sun lines on the earth at five or ten minute intervals.

It should be emphasized that the determination of primary sun lines on the earth becomes more accurate as the minimum nadir angle approaches zero. Thus, the attitude of a satellite relative to the sun is occasionally of vital importance.

C. SPIN-AXIS POINT IN CELESTIAL COORDINATES

The spin-axis points in terrestrial coordinates are expressed by

$$\theta^{TSA}, \phi_d^{TSA}, t \quad .$$

These coordinates are not very convenient in representing the gradual drift of the spin-axis point in the fixed space, because the longitude of TSA changes approximately 15 deg per hour.

The Eq. (30), when applied to a TSA, gives

$$\Omega^{TSA} = \Omega^{GRE} + \theta^{TSA} \tag{80}$$

where Ω^{GRE}, the right ascension of the Greenwich Meridian at the time of the longitude determination. With the use of Table XIII it is extremely easy to obtain Ω^{GRE} by adding five numbers given as Year, Day, Hour, Minute, and Second Functions. Thus, a measured θ^{TSA} can be converted into Ω^{TSA} almost immediately. At the same time the relation

$$\theta^{TSA} = \Omega^{TSA} - \Omega^{GRE} \tag{81}$$

permits us to obtain the longitude of a spin-axis point using the same table.

In view of the fact that the declination of a terrestrial point can be expressed either by

$$\phi_d^{TSA} - \delta^{TSA} = f_e \sin 2\phi_d^{TSA}$$

or

$$\delta^{TSA} = \phi_d^{TSA} - f_e \sin 2\phi_d^{TSA}, \tag{82}$$

it is preferrable not to convert the geodetic latitude of a TSA into the declination. If we do so by subtracting the second term in the right side, we have to add the same amount when the geodetic latitude is needed in order to locate a spin-axis point on a terrestrial coordinate.

Figures 57-60 give the smoothed value of the geodetic latitude (ϕ_d) vs right ascension (Ω) of the TSA of TIROS I-V. The short lines on the curves represent the time when a magnetic attitude control switch was changed. As reported by Stroud (12), TIROS

satellites were equipped with an attitude control coil wrapped around the periphery of the satellite which, when activated, alters the magnetic moment of the satellite to a large extent. With the use of these figures and Table XIII, we may assume that the TSA can be obtained for any moment we wish.

D. CHANGE OF NADIR ANGLE WITH TIME

If we assume that a satellite in a circular orbit is characterized by its minimum nadir angle η_s^{MIN}, the satellite nadir-angle at time Δt past the minimum nadir angle time is obtained by solving a right spherical triangle. The solution is

$$\cos \eta_s = \cos \eta_s^{MIN} \cos \frac{2\pi}{P_{son}} \Delta t \tag{83}$$

which can be reduced, when $\eta_s^{MIN} = 0^o$, to

$$\eta_s = \frac{2\pi}{P_{son}} \Delta t$$

and, when $\eta_s^{MIN} = 90^o$, to

$$\eta_s = 90^o.$$

The P_{son} denotes the period of a satellite in orbit through successive nodes, and is the difference between the argument of a satellite at any moment and that at the minimum nadir angle time ($u - u^{MIN}$).

The change in time of the satellite nadir-angle computed by

$$\cos \eta_s = \cos \eta_s^{MIN} \cos (u - u^{MIN}) \tag{84}$$

is shown at 30 deg intervals in figure 62. The figure gives a rough idea how the satellite nadir-angle would change with time as a satellite circles around the earth. It will be seen that the satellite nadir-angle decreases linearly when its minimum nadir angle is zero. On the other hand, η_s will stay 90 deg and never change if the minimum nadir angle is 90 deg. Between these extremes, the satellite nadir-angle varies along a sinusoidal looking curve which passes a maximum and a minimum nadir-angle point once in each orbit.

In case of an eccentric orbit, the time change of the satellite nadir-angle is not symmetric about the minimum nadir-angle time. The TIROS I-V were injected into eccentric orbits, thus, an assumption of circular orbit does not always apply. Regardless of the orbital eccentricity, the satellite nadir-angles as a function of time can easily be obtained by plotting both the TSPs and TSAs at one minute intervals and measuring the great-circle distance of the corresponding points. An OEC chart with proper inclination of the projection equator, and its overlay are normally used.

Thus, the time change of the satellite nadir-angle for any orbit can be obtained from the existing attitude data, before a particular series of pictures to be rectified

has ever been examined. Finally a graph, satellite nadir-angle vs time for a necessary period is completed for future references.

E. SATELLITE NADIR-ANGLE AND TILT

The optical axes of TIROS-borne cameras are designed to be parallel to the vehicle's spin axis. Nevertheless, the final alignment measurements revealed a few tenths of a degree deviation from the perfect parallelism. Yet the deviation is so small that we may assume that the image plane is perpendicular to the vehicle's spin axis and that the nodal spin-axis intersects the image with an oblique angle which is no less than 89.0 deg.

The distortion-free fiducial-grids of TIROS-borne 10 cameras presented in figures 17-27 are constructed in the image planes which are perpendicular to the vehicle's spin axis. The image primary-point (IPM) is located at the center of the image so that the primary tangential angle relative to the spin axis can be measured by the angular scale around the grid. The principal point (IPP) is indicated by a small open circle near the primary point which is painted black.

It will be seen that a TPP is not always located on the primary line, a great circle connecting a TSA with the corresponding TSP. On the fixed-earth spheroid as shown in figure 63, the FPP, FSP, and FOA at any instance are on a great circle, which is the intersection between the principal plane and the fixed earth. We should realize that the fixed-earth optical-axis point revolves around the FSA several times a min- making its determination extremely difficult and awkward. Unless the IPP coincides with the IPM, it is better to consider IPM being a point at the image center and let IPP move around the former.

Figure 64 represents both IPM and IPP with exaggerated χ, the angle between the optical and spin axes. Since the actual value of χ is only up to a few tenths of a degree, it is reasonable to assume that the principal line and the primary line intersect the apparent horizon at right angles. Thus, the satellite nadir-angle is measured as

$$\eta_s = 90^o - (\delta_H + \epsilon_H), \tag{85}$$

where δ_H denotes the dip angle, ϵ_H, the horizon distance. The tilt (τ) is the object angle between ISP and IPM, and can be measured by placing a proper tilt grid on the distortion-free image.

F. TRACK DISTANCES

As a satellite orbits around the earth, its terrestrial subpoint (TSP) and the terrestrial primary point (TPM) produces their track on the earth. They are called TSP track and TPM track.

A graphical representation of TSP, TPM, and TPP tracks appear in figure 65. The distance between these tracks are termed the track distance which can be expressed either by the great circle distance (d_T) or the corresponding nadir angle (η_T) viewed from the satellite. These are implicitly expressed by Eq. (52), thus

$$H = \bar{R} \left(\sin \frac{d_T}{\bar{R}} \cot \eta_T + \cos \frac{d_T}{\bar{R}} - 1 \right) \tag{86}$$

Therefore, figure 35 may conveniently be used to connect η_T to d_T or vice versa.

There is a simple way of determining the track distance by using a proper tilt grid superimposed upon a distortion-free image including the successive positions of IMPs. Figure 66 reveals the geometry of the track-distance measurement on an image plane.

In case the satellite nadir-angle is rather small, the TPM track is more or less parallel to the TSP track. The radius in the great-circle arc of a radius centered at a TSP and tangent to the TPM track thus denotes the track distance (d_T). On the distortion-free image, the circle on the earth appears as an ellipse of the nadir angle, η_T. The IPM track should always be tangent to this ellipse. Using this characteristic, the track distance in nadir angle is obtained as the nadir angle of an ellipse which is tangent to the IPM track.

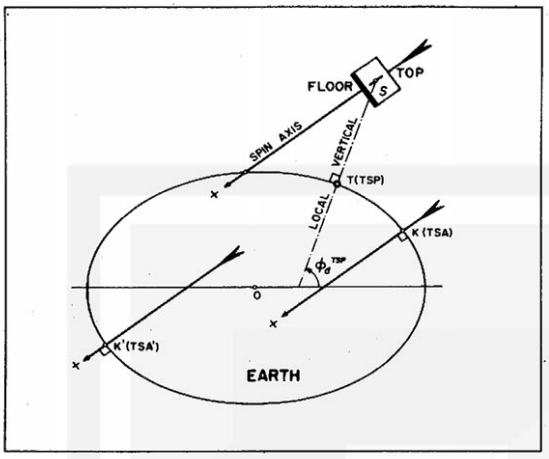

Figure 52. The terrestrial spin-axis point (TSA) and the terrestrial spin-axis antipode on a terrestrial ellipsoid.

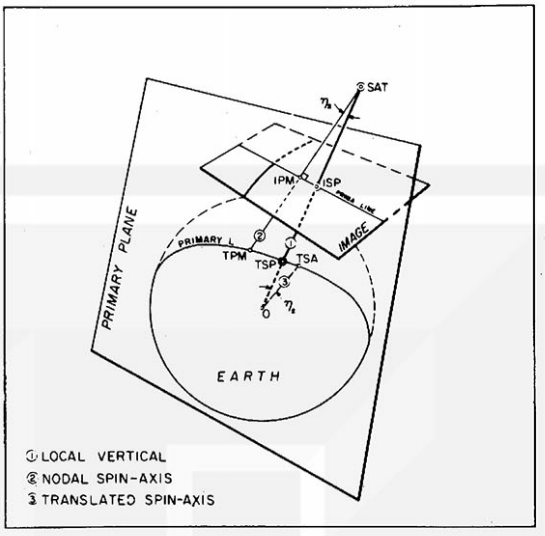

Figure 53. To define the primary plane which includes the satellite spin-axis and the local vertical through the satellite. The primary line on image and on the earth are the intersection of the primary plane with the image and the earth's surface, respectively.

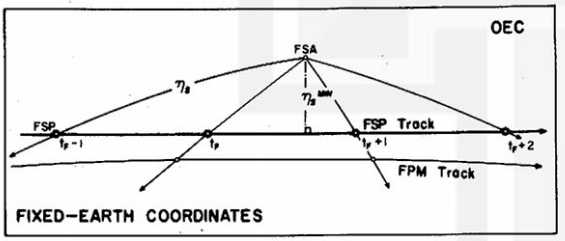

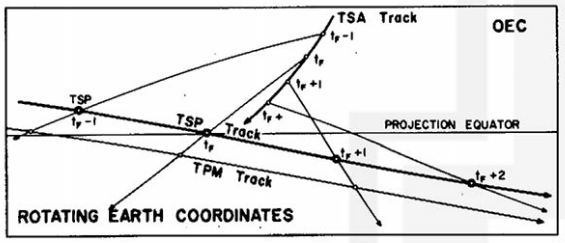

Figure 54. Subpoint and primary point tracks on the rotating and the fixed-earth coordinates. The satellite nadir angle on these coordinates are measured as the arc length connecting the spin-axis point with the subpoint.

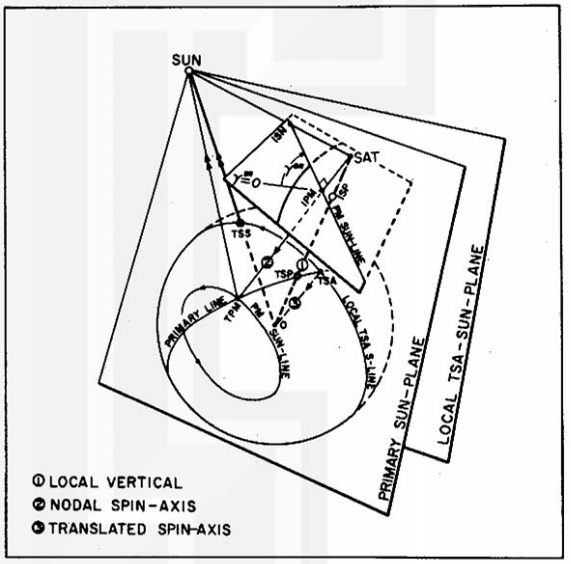

Figure 55. Showing primary and local sun-planes. The primary sun-plane includes the sun, primary point, and satellite. Its intersection with the earth forms a small circle through TPM. The local sun-plane is defined by the local vertical and the sun. This plane always intersects the spherical earth along a great circle through the local point or its subpoint.

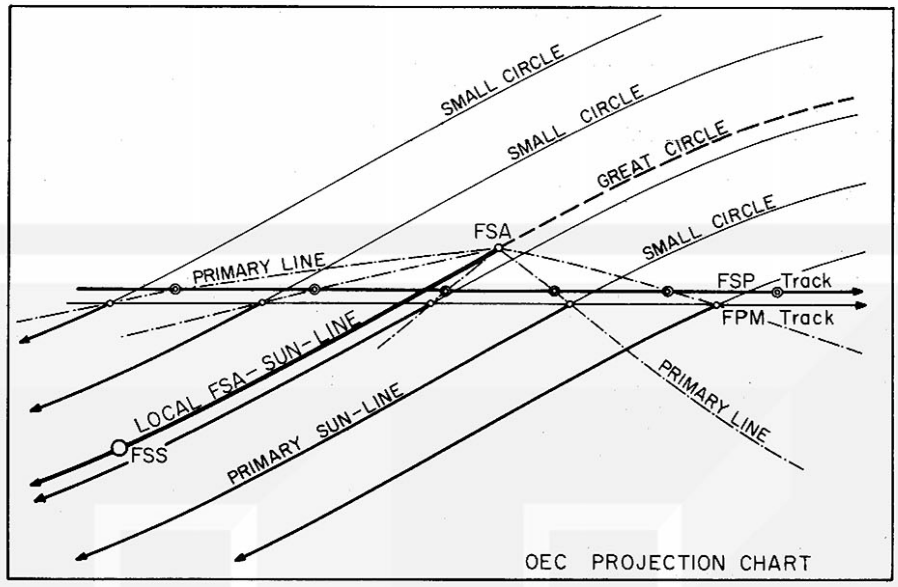

Figure 56. Showing the primary sun-lines and the local TSA-sun-line drawn on an OEC chart.

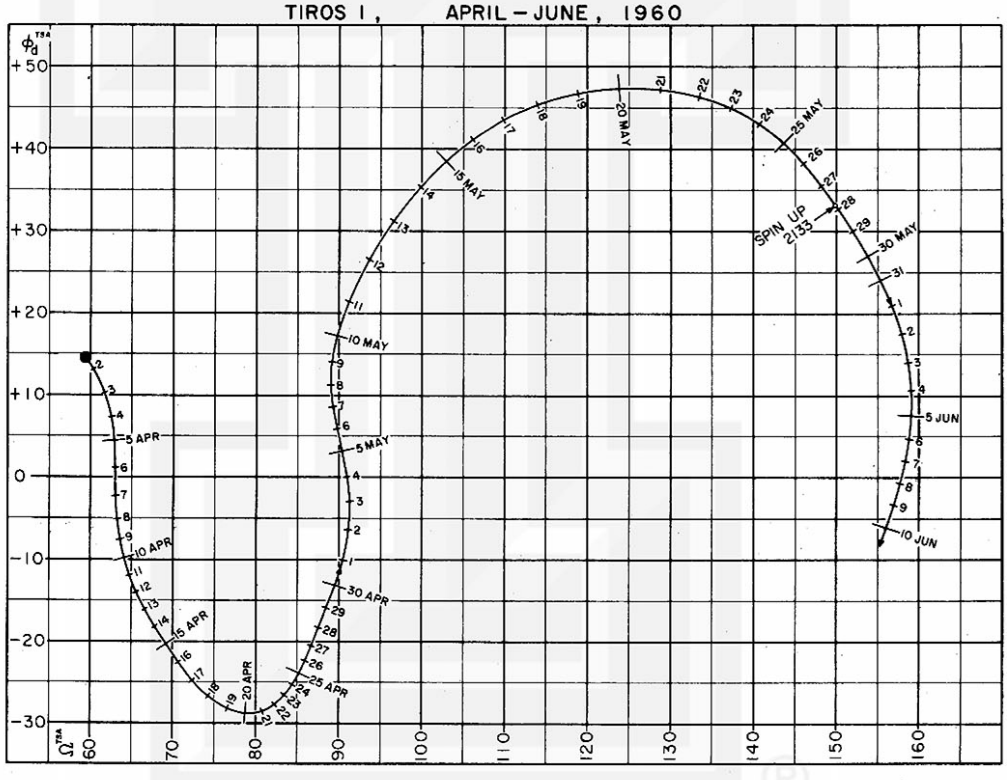

Figure 57. Movement of the terrestrial spin-axis point of TIROS I plotted on a right ascension vs geodetic latitude diagram. The lines designating the days indicate the positions of the spin-axis point at 00Z. (From L. F. Hubert, MSL Report No. 5).

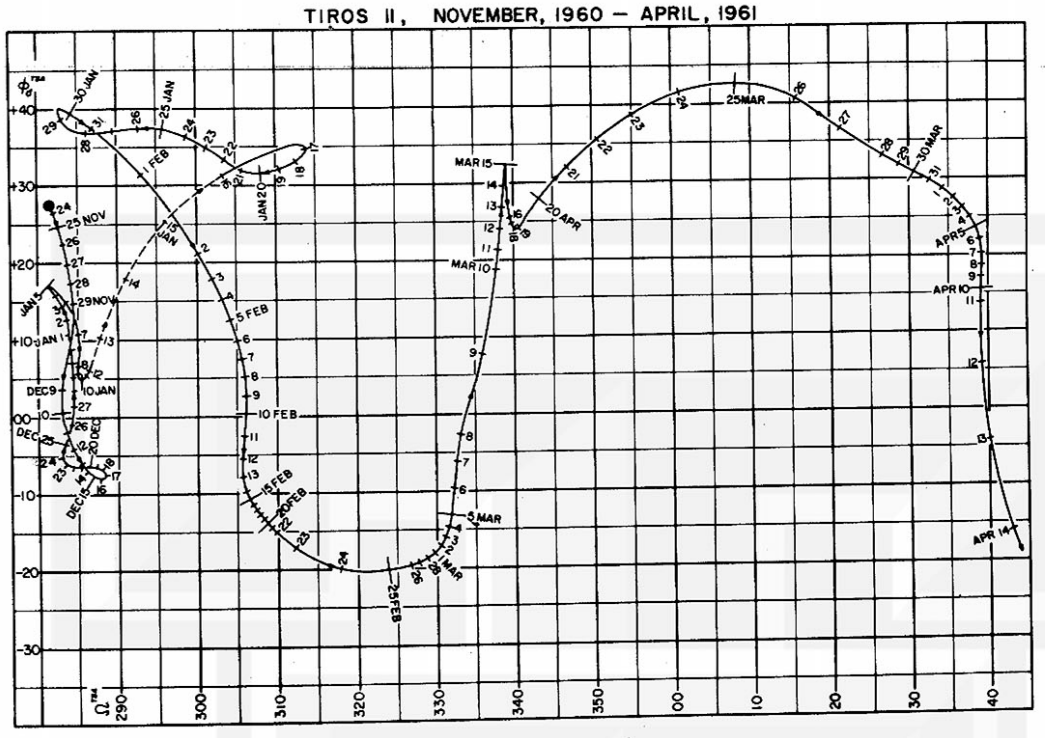

Figure 58. Movement of the terrestrial spin-axis point of TIROS II plotted on a right ascension vs geodetic latitude diagram. (Courtesy of W. R. Bandeen, NASA).

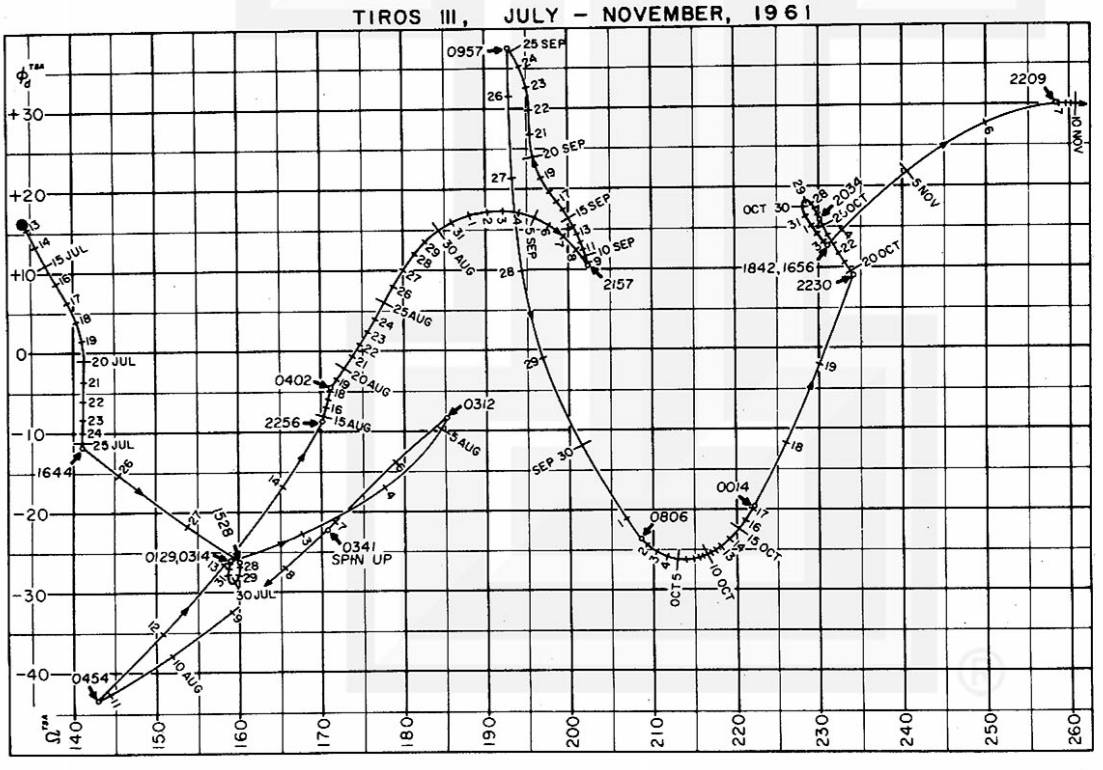

Figure 59. Movement of the terrestrial spin-axis point of TIROS III plotted on a right ascension vs geodetic latitude diagram. (From L. Goldshtak, TIROS III Attitude Data, Allied Research Associates, Inc.).

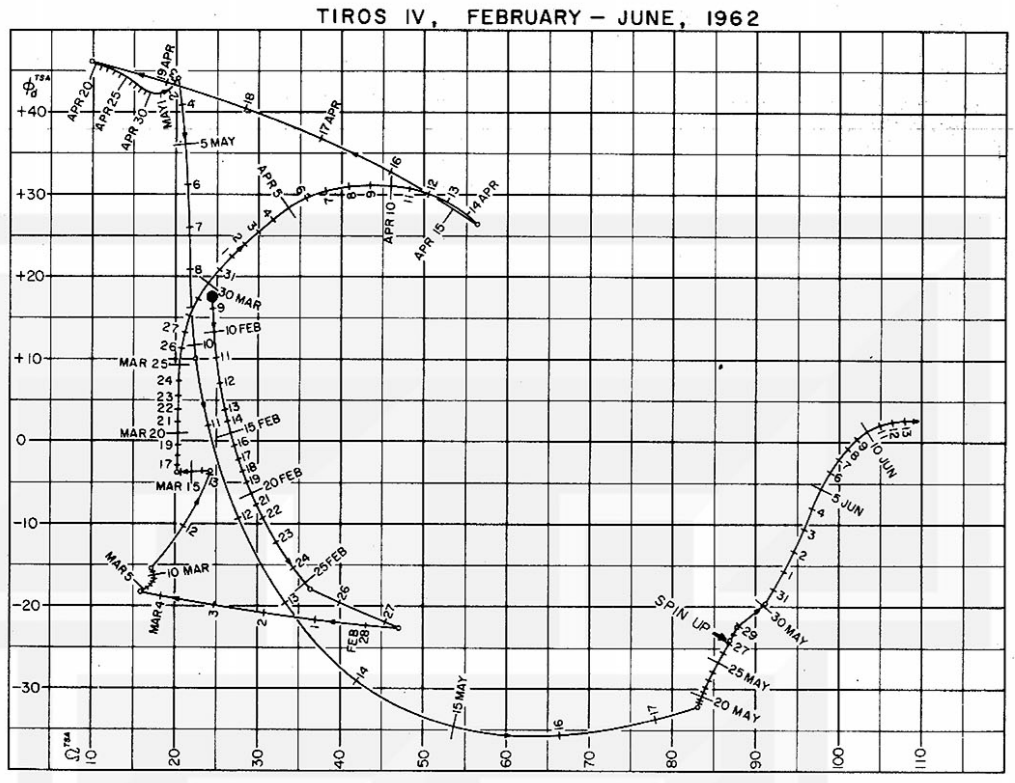

Figure 60. Movement of the terrestrial spin-axis point of TIROS IV plotted on a right ascension vs geodetic latitude diagram. Positions at OOZ each day are indicated. (Courtesy of L. Goldshlak, Allied Research Associates, Inc.).

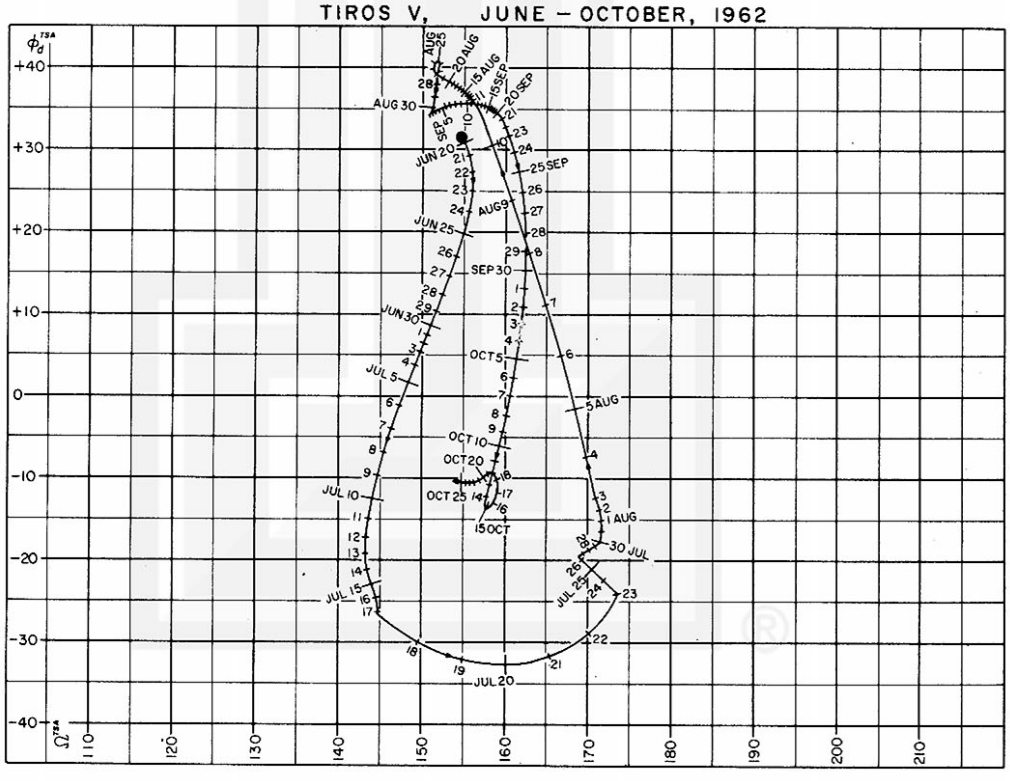

Figure 61. Movement of the terrestrial spin-axis point of TIROS V plotted on a right ascension vs geodetic latitude diagram. Positions at OOZ each day are indicated. (Courtesy of L. Goldshlak, Allied Research Associates, Inc.).

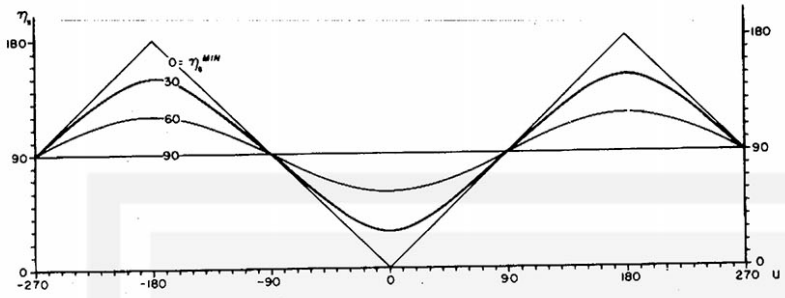

Figure 62. Change of the satellite nadir-angle as the function of the argument of satellite. The value was computed for a circular orbit.

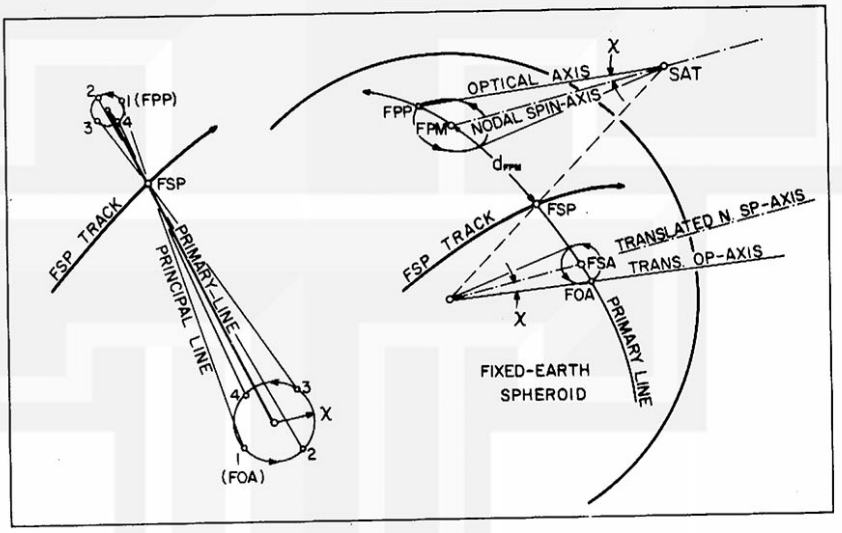

Figure 63. Motion of the principal point around the primary point caused by the satellite's spin and the small angle between optical and spin axes.

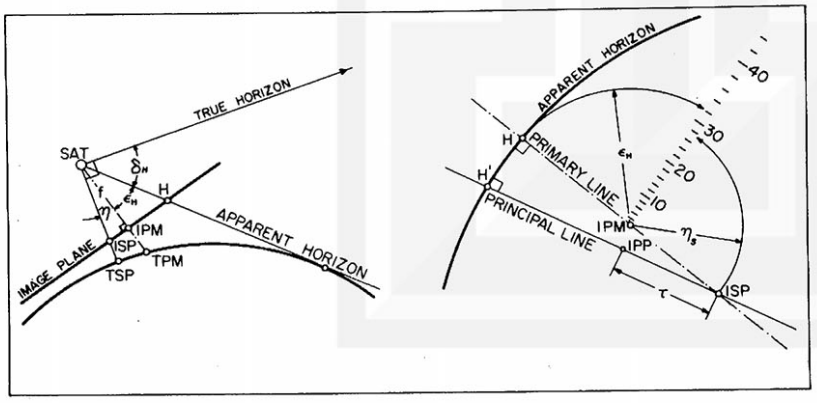

Figure 64. To define principal line and primary line on an image. The distance between IPM and IPP is usually less than one degree. Both principal and primary lines are, therefore, considered to be perpendicular to the apparent horizon on the image.

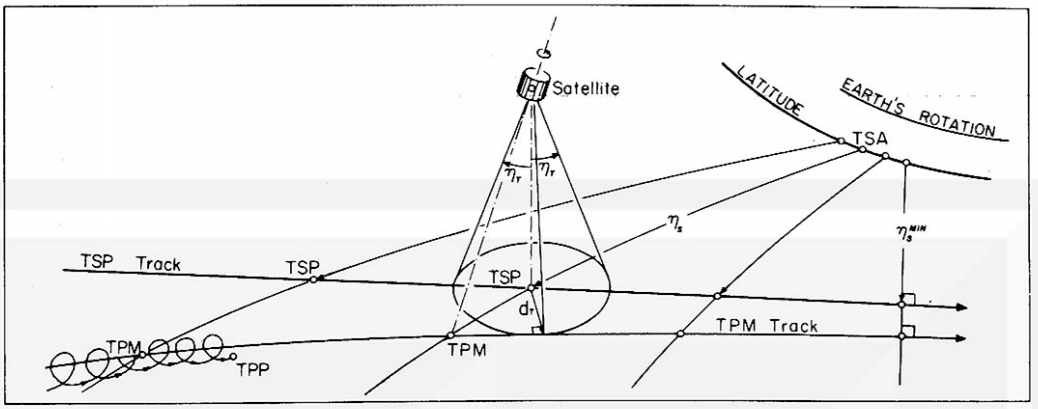

Figure 65. TSP and TPM tracks on the earth are apprxoimately parallel. The distance between these tracks, which is called the track distance, varies very gradually. It reaches a minimum value at the minimum nadir-angle time.

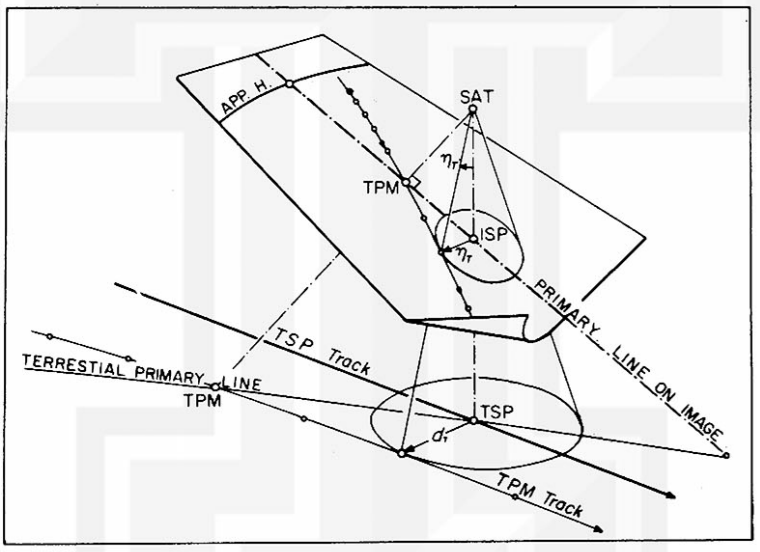

Figure 66. Geometry to obtain track distance using a proper tilt grid. The track distance is measured, first, as the nadir angle (η_T) on the image, then transformed into the great circle distance (d_T) with the use of a proper height grid.

5. RECTIFICATION OF SATELLITE PHOTOGRAPHS

The basic theories which have been discussed will lead us to proceed with the rectification of any series of satellite photographs. In addition to the photographs to be rectified, it is necessary to obtain additional data such as times, heights, subsatellite latitudes and longitudes, programmed picture start time and some spin-axis data. The spin-axis data are very useful but optional since they can be obtained from a series of photographs.

Two different but closely related methods will be introduced in this report. The one called APPROXIMATE METHOD is developed to rectify a series of photographs, none of which includes recognizable landmarks. As a result, the time determination using the attitude data obtained from other series of photographs becomes necessary. While a PRECISE METHOD does not require the attitude information at least one known landmark is needed in one of the photographs in a series to be rectified. The following table compares the processes involved in these methods.

FLOW DIAGRAM OF APPROXIMATE METHOD

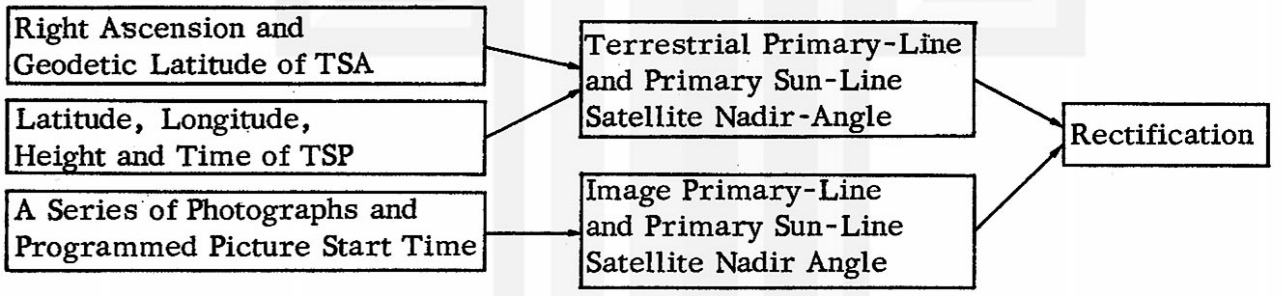

FLOW DIAGRAM OF PRECISE METHOD

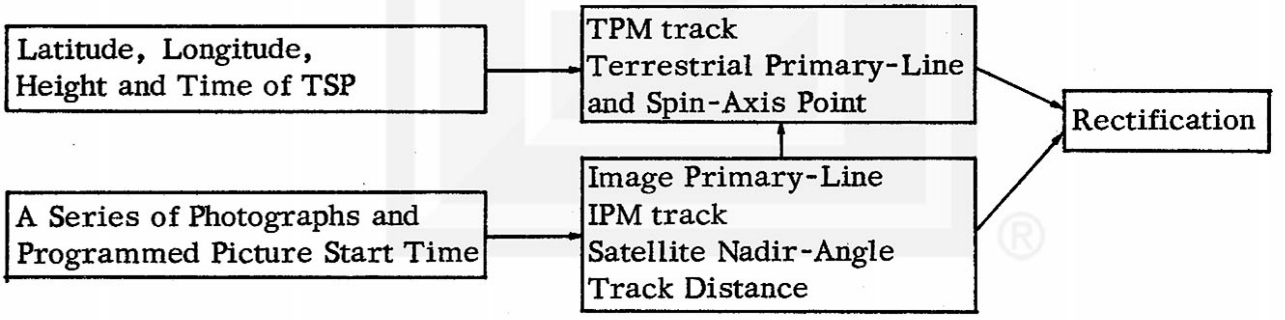

The data required to perform these rectification methods are numbered so that they can be identified when necessary. They are

(B-1) A series of tape-mode or direct-readout pictures.

(B-2) Programmed picture start time for tape-mode pictures. Actual exposure time for direct-readout pictures.

(B-3) Times, heights, subsatellite latitudes, and longitude such as appear in "Definitive AT Map" produced by NASA.

(B-4) Right ascension and declination of the spin-axis point, or minimum nadir angle and its time.

In addition to these data, it is necessary to have the copies of the following rectification grids:

(A-1) "Oblique Equidistant Cylindrical (OEC) Projection Charts," in scale 1 deg = 5 mm, with the inclination of the projection equator, 48.4° and 58.3°, are available. They are made to cover 26° on both sides of the projection equator (figures 45 and 46).

(A-2) "OEC Overlay" drawn in the scale of the OEC chart covers over 90 degrees of the projection equator (figure 47).

(A-3) "Tilt (Nadir Angle) Grids," with the principal distance of 94.7 mm, are prepared at 2 degree intervals between 0° and 130° inclusive (figure 29).

(A-4) "Height Grids" at 10 km intervals between 600 and 1,000 km of satellite altitudes. The scale of all height grids is identical to that of OEC charts and the OEC overlay.

(A-5) "Fiducial Grids" which have to be made to fit each distorted image. Experiences show that one or two kinds of fiducial grids usually match the fiducial marks on images belonging to a series of tape-mode or direct-readout pictures. The grids have to be made by those who desire to perform rectification practice.

(A-6) "Distortion-free Fiducial Grids," including both IPP and IPM are available for the 10 TIROS I-V-borne cameras (figures 17-26).

A. PRECISE METHOD OF RECTIFICATION

This rectification method permits us to rectify a series of photographs without the previous knowledge of the attitude data. The data required to perform this method are (B-1), (B-2), and (B-3). An outline of rectification procedure follows:

STEP Ia: Measurements on Image Planes
on Plastic Sheet placed on Photographs

(1a) make: fiducial grid (A-5) for all frames.
(2a) trace: apparent horizons.
(3a) transfer: image primary-points (IPM) from other frames on Distortion-free grid.
(4a) transfer apparent horizons.
(5a) obtain: primary lines, horizon distances (ϵ_H), image subpoints (ISP), and satellite nadir-angle (η_s).
(6a) transfer: a series of IPMs for other frames.
(7a) obtain: IPM track and track distance (η_T).

STEP IIa: Analysis on OEC Charts
on OEC Chart

(8a) plot: TSPs, label each with time, and draw maps including landmarks to be used.

on Translucent Sheet Placed on OEC Chart

(9a) label: each with frame number using the programmed picture start time.
(10a) draw: circles of track distance from (7a).
(11a) obtain: TPM track over the intervals for which track distances are available.
(12a) determine: TPMs for selected frames using satellite nadir-angle (η_s) from (5a) and figure 35.
(13a) obtain: TSAs for the frames used in (12a), then mean fixed-earth spin-axis point (FSA) for Frame No. Zero.
(14a) determine: TSAs for all frames.
(15a) draw: terrestrial primary lines for all frames.
(16a) measure: satellite nadir-angle (η_s) for all frames.

STEP IIIa: Final Rectification
on the Same Translucent Sheet

(17a) transfer: landmarks on (B-1) using (A-5), (A-3), and (A-6).
(18a) slide: translucent sheet keeping exposure points on TSP track.
(19a) stop: the sheet when landmarks fit the topography on OEC Chart.
(20a) measure: the amount of shift. If the shift is over three minutes change the programmed picture start time and repeat from (9a).
(21a) transfer: latitudes and longitudes from OEC to the image using (A-4), (A-3), (A-5), (A-6) and (B-1).

STEP Ia: Measurements on Image Planes

Readout images are distorted appreciably due to both electronic and optical distortions. The measurements of the angles between objects on these images must, therefore, be made after the distortion is elimated by transferring the objects from the image to the distortion-free plane. To avoid unnecessary efforts, it is preferable

to transfer only the objects needed for the attitude determination.

As an example, the six photographs (figure 67) of Hurricane Anna of 21 July 1961, readout on orbit 133, TIROS III are presented. Since all photographs already include the fiducial grids the Items (1a) - (3a) are already completed. If not, the fiducial grids have to be constructed using the method as shown in figure 16. It should be pointed out, however, that a series of IPMs was obtained by transcribing the IPM for each frame onto one image with the help of the cloud patterns in the vicinity of the IPM to be transcribed. Thus, the movement of the primary points is visualized on each readout image. We will find later that this IPM track plays an important role in the determination of the primary line on an image in which the apparent horizon is extremely poor or completely lacking.

Presented in figure 68 is the distortion-free image of the Frame 21T, which includes an apparent horizon, which was transferred from the distorted image in figure 67. Similar transfer should be done also for the other frames including apparent horizons.

When the transfer has been completed the principal line connecting the IPM with the point on the apparent horizon closest to the IPM shall be drawn. Experience revealed that an accurate determination of the primary line can be achieved by drawing several concentric circles C1, C2, C3....with their center at the IPM and then obtaining the mid-points of the line segments connecting the points of intersection of each circle and the apparent horizon. A straight line passing through the IPM and running through the mean of these mid-points represents the most probable primary line on the distortion-free image. In case the radial angle between IPM and IPP exceed one degree, this method is not too accurate. We must then use IPP to determine the principal line first, and the primary line should be drawn by connecting the TSP with the TPM. On the image plane of TIROS I-V cameras, this approximate method can be applied with great accuracy, since χ is no more than one degree.

The horizon distance (ϵ_H) can be measured by transferring the distance between IPM and the apparent horizon on the image primary line. The satellite nadir angle (η_s), by definition, is then computed by Eq. (85), if we know the satellite height which determines the dip angle (δ_H). Finally, the ISP is placed on the image primary line. The radial angle of the ISP is equal to the satellite nadir angle.

At this point the Items (4a) and (5a) have been completed. Now a series of IPMs for other frames are transcribed as shown in figure 68. Thus, the IPM track is completed. Next we place the distortion-free image (A-5), as an overlay, on the tilt grid labeled with an angle closest to η_s , in such a position that the primary line on the image coincides with the principal line on the tilt grid. Move IPM along the principal line until it reaches the point where the nadir angle on the grid becomes identical to the satellite nadir-angle η_s . Finally, the track distance is obtained as the smallest nadir-angle of the IPM track.

There are three short lines near the center of each tilt grid. The middle line intersects the principal line at the principal point of the labeled tilt. Two other short lines on the principal line give the principal points for the tilts one degree larger or

smaller than the labeled angle, so that the same also can be used for any tilt within that range.

Upon the completion of the measurements on the image planes, we usually obtain the satellite nadir-angles (η_s) and the track distance (η_T) for several frames. They may be tabulated for use in the next step.

STEP IIa: Analysis on OEC Chart

First of all, the proper longitude has to be labeled on an OEC chart so that a series of TSPs to be plotted stay close to the projection equator. If the plotted TSPs deviate more than a few degrees from the projection equator, some error in satellite nadir-angle may arise. Next we plot the TSPs and their times on the OEC chart usually at one minute intervals. At the same time the map positions of the landmarks seen on the photographs are entered in the OEC chart using reliable maps covering the analysis area.

A translucent sheet of paper is placed on the OEC chart and the exposure subpoints are plotted on the overlay sheet. The exposure times of direct-readout images are usually known within one second error, thus permitting us to locate the exposure subpoint immediately. The picture start time of a series of tape-mode photographs could be off up to a few minutes, whereby the best we can do, to begin with, is to assume that the first picture (actually the last one on the film series, the one with the largest frame number) was exposed at the programmed picture start time. The validity of this assumption will be determined later.

Now we come to Item (10a), which requires the drawing of circles indicating the track distance from several TSPs. Since the track distance, d_T, measured on the distortion-free image plane, is the nadir angle of the TPM track viewed from the satellite, the great circle distance (d_T) on the OEC chart can be obtained by using a height grid labeled with the height of the satellite at the exposure time. Figure 35 also serves for this purpose because it is a nomogram to obtain the great circle distance from the satellite height and the object nadir angle.

Before we draw the IPM track, a smooth line tangent to these track-distance circles as shown in figure 69, we must know on which side of the TPM track the TSP is located. The easiest way of determining this is to refer to the image plane with TPM track on it (figure 68). It will be found in the figure that the ISP is located to the left of the IPM track facing toward the direction of the IPM movement. The TSPs in figure 69 should, therefore, be located on the same side. Theoretically, a TPM track never crosses the corresponding TPM track. With this precaution a smooth line of TPM track is finally drawn on the OEC chart.

It is only at the time of the minimum nadir angle that the track distance in nadir angle (η_T) and the satellite nadir-angle (η_s) are identical. In other positions of a satellite, η_s is always larger than η_T. Therefore, the exact position of the TPM can be obtained by placing the center of a proper height grid at a TSP and selecting a point on the TPM track whose nadir angle coincides with η_s, the satellite nadir-angle. We may

again use figure 35 to determine the distance between TPM and TSP on the OEC chart.

Figure 70 demonstrates how the TSA is determined by extending the great circle connecting the TPM with the TSP with the help of an OEC overlay. In drawing the great circle, especially when a TSP is off from the OEC projection equator, the method described in figure 49 should be observed carefully. By doing so, theoretically, no error in the position of TSA will be introduced. The great circle distance between a TSP and the corresponding TSA is always equal to η_s, the satellite nadir-angle.

When a number of TSAs are determined from the frames including an apparent horizon and a subpoint, they are converted into the FSAs. The exposure time of an imaginary Frame No. Zero is taken as t_F, the time of fix. Equation (37) reveals that the fixed-earth longitude of a FSA is expressed by

$$\Theta_t^{FSA} = \theta_t^{TSA} + (t - t_F) \omega_{esn} \tag{87}$$

where ω_{esn} denotes the rotation rate of the earth with respect to the nodes. This rate is almost identical to the sidereal rotation rate (ω_{esf}) which appears in Table V. The table shows that a rate, 0.25 deg per min, can be used with great accuracy, as long as the total period analysis is limited to that of one orbit or a fraction thereof. Thus we use

$$\Theta_t^{FSA} = \theta_t^{TSA} + \frac{1}{4} \Delta t \tag{88}$$

where Δt is the difference, $(t - t_F)$ and is expressed in minutes.

As shown in figure 70, FSAs for Frame No. Zero is plotted on the same OEC on which the determination of TSAs has been made. It is usual to see a scatter of FSAs caused by the experimental error. The most probably position of the FSA should, therefore, be obtained by guess to a certain extent.

After the determination of the most probable position of the FSA, the positions of TSAs at the exposure times are determined by computing their longitudes usine Eq. (88) which is solved as

$$\theta_t^{TSA} = \Theta_t^{FSA} - \frac{1}{4} \Delta t . \tag{89}$$

The latitudes of the TSAs are, of course, considered to be constant during such a short period. Thus, we finally line up TSAs as shown in figure 71.

The last item of this step is to draw primary lines by connecting each TSA with the corresponding TSP by using OEC overlays. The proper use of the OEC overlay figure 49 should always be observed to obtain the best result. It is the usual practice to measure the satellite nadir-angle for each frame before the OEC overlay is removed.

The satellite nadir-angle and the height of satellite for each frame permit us to determine the exact position of TPM either by using a proper height grid or figure 35. The TPMs thus plotted are connected into a TPM track.

STEP IIIa: Final Rectification

We have, so far, accomplished our analysis under the assumption that the first tape-mode picture is taken at the programmed picture start time. This assumption can now be evaluated through the preliminary rectification. First we place, as shown in figure 72, the center of the proper height grid exactly at the TSP of the frame to be rectified. Then rotate the grid a few degrees until the primary line coincides with one of the azimuth lines on the height grid. The center line of the height grid, indicated by a semi-disc, must be kept, as much as possible, parallel to the OEC projection equator.

Next, the proper tilt grid is placed on the distortion-free fiducial grid including the objects of a frame to be rectified. Keep the IPM on both grids together; rotate one of the grids until the positions of all IPMs relative to the tilt grid fit best with those of the IPM with respect to the height grid placed properly on the OEC chart. When the best fit is reached, we stop the rotation of the grid in order to draw the primary line on the distortion-free grid. It should be emphasized that this method enables us to determine primary lines for pictures which do not include horizons. In case a distinct horizon is available, the primary line on the distortion-free grid can be used in orienting the principal line on a proper grid.

The landmark(s), which had been transcribed from the readout image to the distortion-free fiducial grid with the use of a fiducial grid can now be transferred to the translucent sheet on the OEC. If there exists more than one recognizable landmark in several photographs, we may as well proceed to transfer as many as possible (figure 72).

Untape the translucent paper to see how much translational shift is required until all landmarks reach the best fit positions. The shift is usually made in such a manner that the exposure subpoints remain, as much as possible, on the TSP track. Because the satellite tracking is so accurate, we may reasonably assume that exposures were made somewhere above the subpoint track. The distance of the shift, divided by that of the one-minute movement of TSP, is the difference between our assumed time of exposure and actual exposure times. In most cases, the amount of the shift is determined as accurate as 0.1° of arc, while a satellite travels about 3.5° per minute. This method, therefore, permits us to determine the exposure time with an accuracy of about 2 sec.

In case the time difference computed from the amount of shift is more than two minutes, we might have to repeat step II after the completion of the time correction. Because of the height change, which resulted from the subpoint shift, analysis would require the use of different height grids.

It will be seen in the section of "Approximate Method" that the estimated position of the spin-axis point permits us to estimate the satellite nadir-angle as a function of time. Using the programmed picture start time, the satellite nadir-angles for selected frames can be computed to find out if they are not too far off from those measured from the photographs with the same frame numbers. Since the TIROS meteorological satellite travels at the rate of 3.5° per min, we may assume that the one minute error

in picture start time could cause up to 3.5° of satellite nadir-angle. We usually correct the programmed picture start in 3°. This precaution will assume that the shifting process in the preliminary rectification can be performed with great accuracy.

After the completion of the final TSP shift, we should have exact TSPs and the corresponding primary line and the satellite nadir-angles (η_s) for all frames. Place the center of a proper height grid at the TSP of the frame to be rectified and rotate the grid in the manner described before. Then place the distortion-free fiducial grid over a proper tilt grid, using the above mentioned method.

Now we are ready to transcribe the 5° latitude and longitude intersections (figure 73). This transcription is made first onto the distortion-free fiducial grid with the aid of a tilt grid underneath, then finally to the fiducial grid. The geographic grid may be drawn on a plastic or translucent paper overlay placed over the cloud picture.

If required a supplementary grid with either one degree or even one-half degree intervals may be added to the basic 5° grid. An example of the geographic grid placed on a photograph appears in figure 74. After the completion of the geographic grid on several frames it is usual to see that the positions of clouds relative to the grid lines are fairly close to each other. When the same cloud on two or more pictures with geographic grids is seen within 50° of nadir angle, it is expected that its images appear on practically the same location relative to the grid lines.

After this brief check, the cloud patterns may be transcribed onto a map of any projection. Or, if desired, the geographical features, and meteorological information such as winds, isobars, etc., are transcribed onto the photographs with the geographic grids.

B. APPROXIMATE METHOD OF RECTIFICATION

To summarize this method of rectification, an outline of rectification procedure follows:

STEP Ib: Measurements on Image Planes
on Plastic Sheet Placed on Photographs

(1b) make: fiducial grid (A-5) for all frames.
(2b) trace: apparent horizons.

on Distortion-free (Fiducial) Grid

(3b) transfer: apparent horizons.
(4b) obtain: primary lines, horizon distances (ϵ_H), image subpoints (ISP), and satellite nadir-angles (η_s).

on Graph Paper

(5b) plot: the satellite nadir-angles (η_s) as a function of time.

STEP IIb: Analysis on an OEC Chart
on an OEC Chart

(6b) plot: terrestrial subpoints (TSP), label each with time.
(7b) obtain: longitude and latitude of the spin-axis point (TSA).
(8b) plot: the TSAs for the necessary period.
(9b) draw: primary lines at one minute intervals.
(10b) obtain: the satellite nadir-angles (η_s) at one minute intervals.

on Graph Paper

(11b) plot: the satellite nadir-angles (η_s) as a function of time.

STEP IIIb: Final Rectification

(12b) compare: the graphs of satellite nadir-angles using (5b) and (11b).
(13b) obtain: the exposure times of photographs.
(14b) place: a translucent sheet on the OEC chart.
(15b) draw: primary lines for each photograph.
(16b) place: a proper height grid on a primary line.
(17b) transfer: latitudes and longitudes from OEC to the image using (A-4), (A-3), (A-6), and (A-5).

SPECIAL STEP: Rectification of Photographs using Sun Angles

(18b) calculate: sun angle by adding the binary numbers.
(19b) draw: primary sun-line on the distortion-free grid.
(20b) plot: terrestrial subsun point (TSS) on the OEC chart.
(21b) draw: a great circle passing through the TSS and TSA.
(22b) draw: a primary sun-line through each primary point.
(23b) place: a proper nadir-angle grid (tilt grid) on the distortion free grid from (19b).
(24b) place: a proper height grid to fit the orientation of image primary sun-line.
(25b) transfer: latitudes and longitudes from OEC to the image using (A-4), (A-3), (A-6), and (A-5).

Explanation of each step

STEP Ib: Measurements on Image Planes

The measurements on image planes required to perform this approximate method of rectification is almost the same as the precise method. The same items used are (1b) = (1a), (2b) = (2a), (3b) = (4a), and (4b) = (5a). After the completion of a fiducial grid for the frames to be rectified, the primary lines are drawn on the distortion-free images to obtain the image subpoints (TSPs) and the satellite nadir-angles (η_s).

This approximate method does not require the IPM track if the sun angle for each frame is known. In case the sun angle is not available, the Items (3a) and (6a) have to

be added in order to orient the photographs which do not include apparent horizons.

Additional work needed to determine the exposure time in this method is to prepare a graph showing the satellite nadir-angle as a function of time. The graph is made from the result of Item (46).

STEP IIb: Analysis on OEC Chart

First the terrestrial subpoints (TSPs) are plotted. Then they are labeled with time at one minute intervals.

The right ascension and the geodetic latitude of TIROS satellite are obtained from figures 57-61 which includes their values at OOZ. Equation (81) is then used to obtain the longitude of TSA by subtracting the right ascension of Greenwich from that of TSA, thus

$$\theta^{TSA} = \Omega^{TSA} - \Omega^{GRE}$$

The right ascension of Greenwich is a function of time which can be obtained from Table XIII.

EXAMPLE: To obtain the longitude of a spin-axis point with right ascension 250.5 deg at time 15h23m13s Greenwich time on 25 July 1963.

ANSWER: First the right ascension of Greenwich is obtained by adding the time functions

Year Function--------1963	-2.21
Day Function---------July 25	+124.19
Hour Function---------15h	+45.62
Minute Function------23m	+5.77
Second Function------13s	+0.05
R.A. of Greenwich--Total	+173.42

The longitude of the spin-axis point (TSA) is, therefore,

$$250.5 - 173.4 = 77.1.$$

The latitude of TSA in Item (7b) is read off directly from figures 57-61. In view of the movement of TSA along a latitude circle at the rate of 0.25 deg per min and the availability of the subpoint data at one minute intervals, it is easier first to obtain the TSA on the minute. Then it is moved 0.25 deg of longitude per minute.

After the end of Item (9b) when all primary lines at one minute intervals are completed, the satellite nadir-angles at one minute intervals are measured by superimposing an OEC overlay upon the chart which would appear much as in figure 75. The measured satellite nadir-angles are then plotted on the same kind of graph paper as used in Item (5b).

STEP III: Final Rectification

Finally, the graphs completed in Items (5b) and (11b) are superimposed to permit the determination of the time of a series of photographs. This method can be applied to any series of photographs if some of them include a well-defined apparent horizon.

After the determination of the exposure times of photographs, their TSPs and TSAs are plotted on a translucent sheet placed on the OEC chart used for the determination of the satellite nadir-angle. In fact, it is not necessary to draw the primary lines at one minute intervals in order to measure the satellite nadir-angles at the same intervals. They can be measured on the OEC overlay without drawing primary lines which connect the corresponding TSPs with TSAs. We may, therefore, draw the primary lines for each photograph after their time of exposure has been determined in Item (13b).

In the same manner as shown in figure 73, the center of a proper height grid is placed on the TSP for an exposure so that the latitudes and longitudes on the OEC chart are transcribed onto the image coordinate using the same method as used in the precise method.

SPECIAL STEP: Rectification of Photographs using Sun Angles

The approximate method is not capable of orienting the image primary line unless a well-defined horizon is visible on the photographs.

One solution to such a case is obtained by plotting the primary-point tracks (IPM tracks and TPM tracks) as used in Items (6a) and (11a) of precise method. These two tracks are then used in transcribing the terrestrial primary line onto the image plane without using the apparent horizon as a reference.

Another solution is the use of sun angle which is obtained by adding the binary numbers on digital monitor display. The binary numbers appear as 1/8, 1/4, 1/2, 1, 2, 4, 8, 16, 32, 64, 128, 256. So far these binary numbers have not been represented properly, and appreciable errors were reported. It is recommended that the sun angles be checked carefully before they are used in the determination of primary lines.

The baseplate angle of the direction with sun angle zero for TIROS I-V is designed consistently as 340 degrees. On the other hand, the baseplate angle of the radial angle zero for cameras 1 and 2 are, respectively, 110 deg and 350 deg (figure 9). Therefore, the tangential angles of the sun angle zero are

230 degrees for camera 1

and 350 degrees for camera 2

Thus, the tangential angle of the primary sun-line on an image is obtained by adding the above tangential angle to the sun angle on the monitor display. Next, the primary sun-line is drawn on the image.

In order to draw the primary sun-line on the OEC chart, it is necessary to use the

sun-line geometry shown in figures 55 and 56. They reveal that the primary sun-lines on the earth are small circles parallel to the great circle connecting the TSA with the terrestrial subsun point (TSS). Now the TSS is obtained from Table XIV and XV which, respectively, gives the longitude and the latitude of the subsun point as a function of time in day, hour, and minute. The annual change in TSS is so small that no year function is used.

After the completion of Item (21b), a primary sun-line is drawn through each primary point in such a manner that the primary sun-line is parallel to the great circle, TSS--TSA, at the time of each primary point. Figure 76 schematically represents such primary sun-lines on the OEC chart.

To perform the final transcript of the geographic grid, the center of a proper height grid is placed at the TSP of a photograph to be rectified. Rotate the grid until the primary line coincides with one of the azimuth lines on the grid. The center line of the height grid, indicated by a semi-disc, must be kept, as much as possible, parallel to the OEC projection equator.

Next, the proper tilt grid is placed on the distortion-free fiducial grid including the primary sun-line. While putting the principal point of the tilt grid on the primary point on the distortion-free grid, rotate the tilt grid until the primary sun-lines on both image and the OEC chart cut across the azimuth and nadir-angle lines in the same manner relative to each other.

Upon completion of the orientation adjustment, we may proceed with the transfer of geographic grid as described in (21a) and (17b).

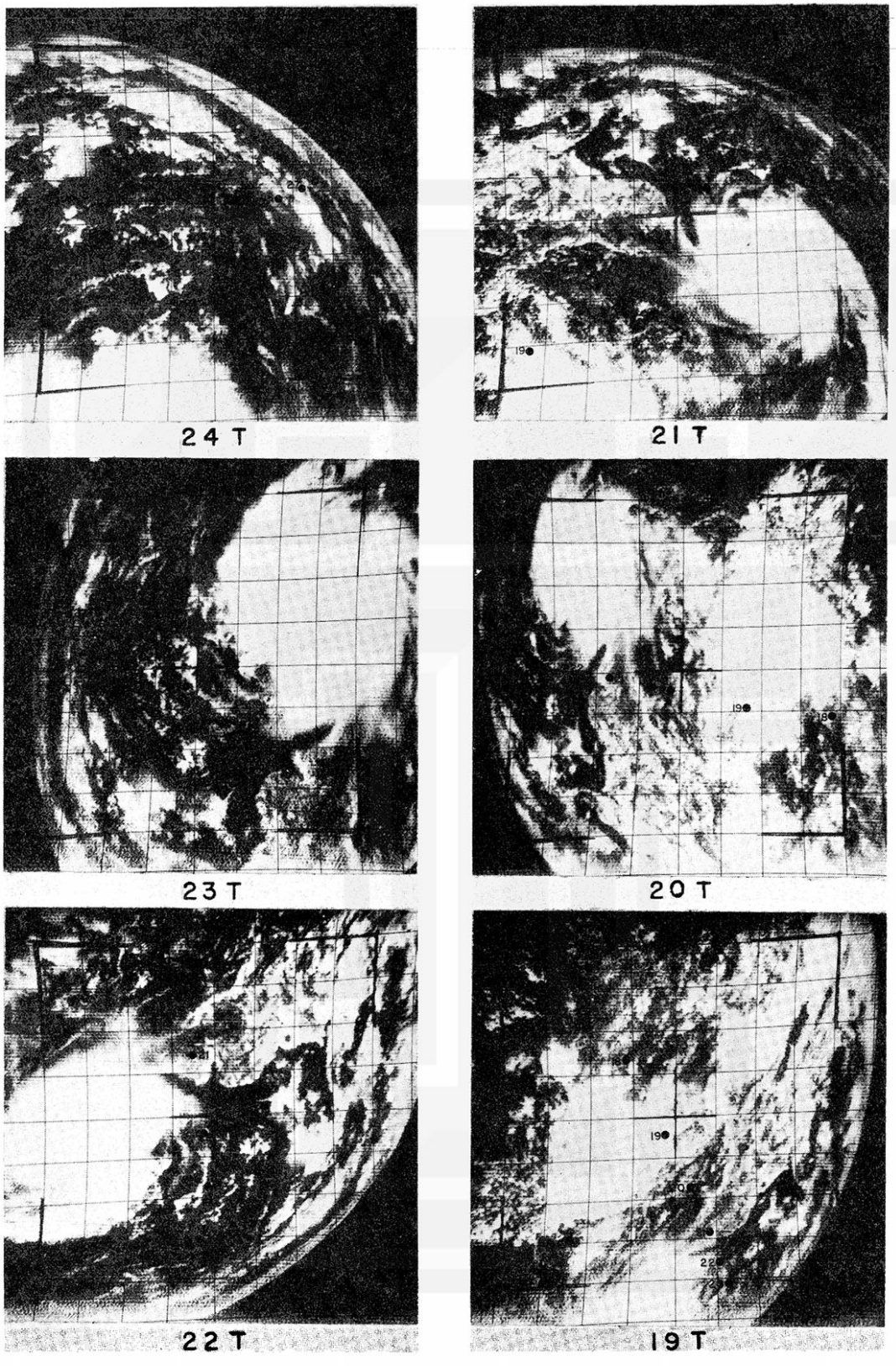

Figure 67. Fiducial grids and the primary points placed on six frames of tape-mode photographs taken during the orbit 132, TIROS III, 21 July 1961.

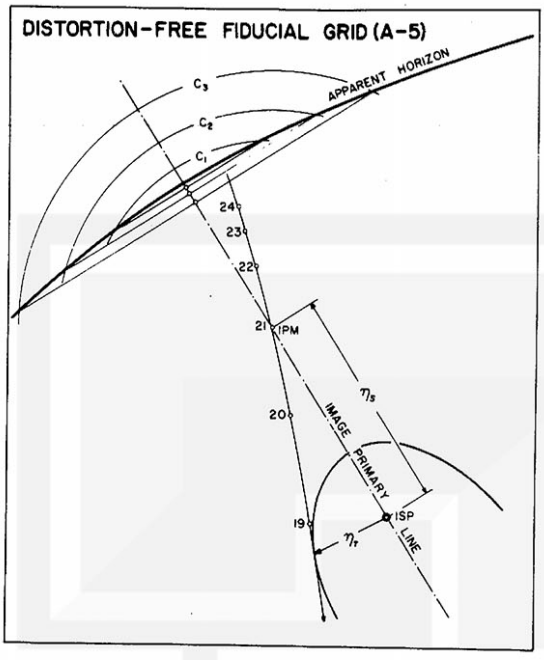

Figure 68. A method of determining the primary line of an image with an apparent horizon, and the track distance in nadir angle measured on a distortion free image.

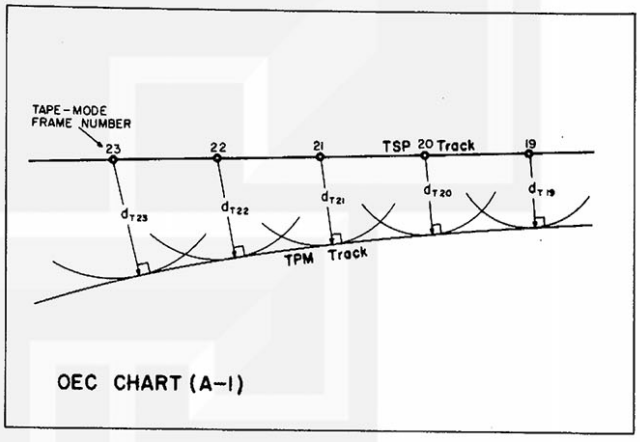

Figure 69. Process of drawing the primary point track on the earth after knowing a number of track distances.

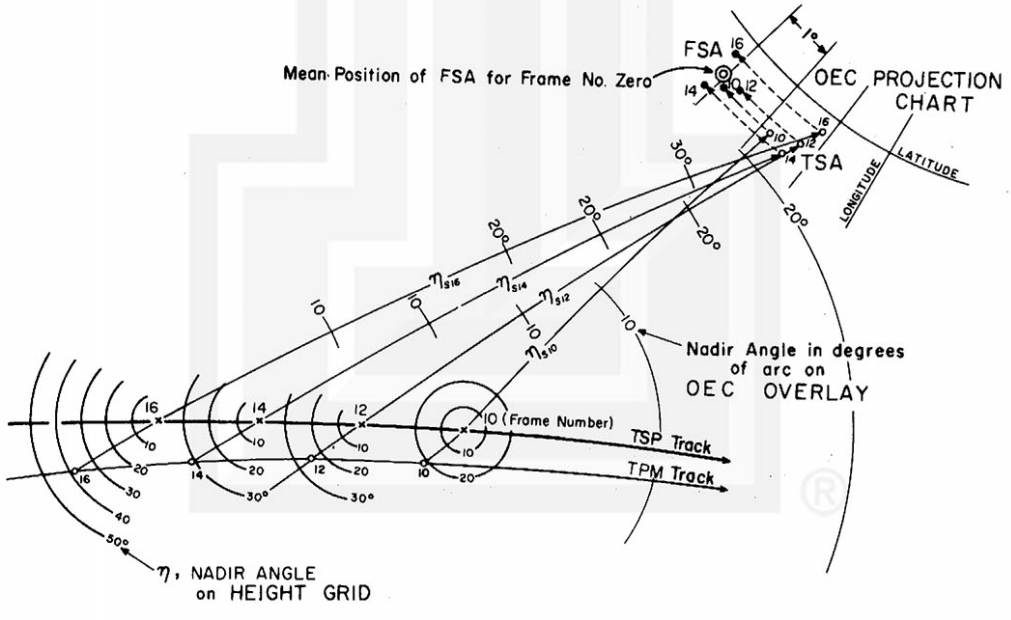

Figure 70. Determination of the TSA for each frame. After several TSAs are obtained, they are moved along each latitude to obtain the FSA for frame zero.

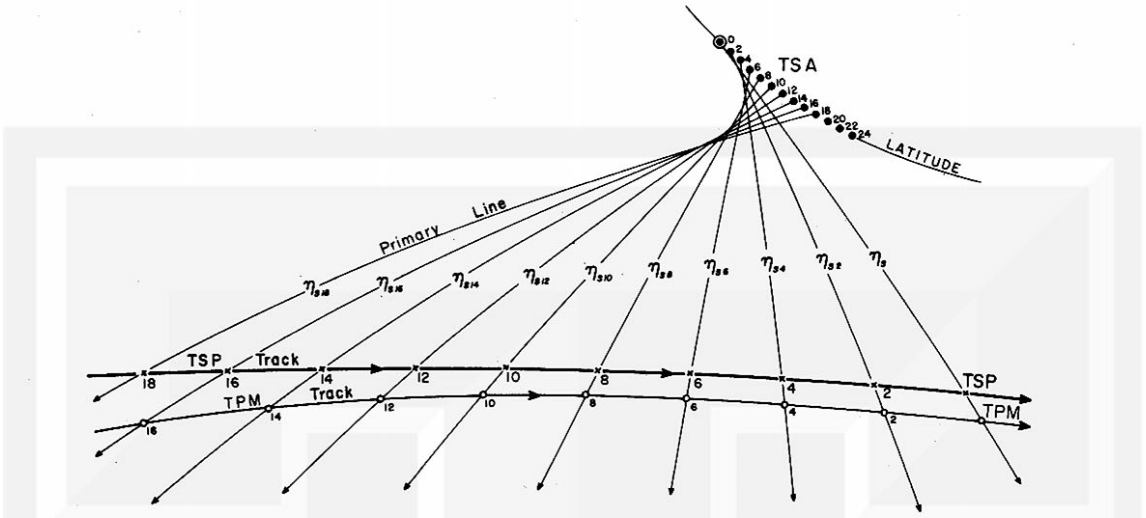

Figure 71. To determine the primary lines for each exposure point.

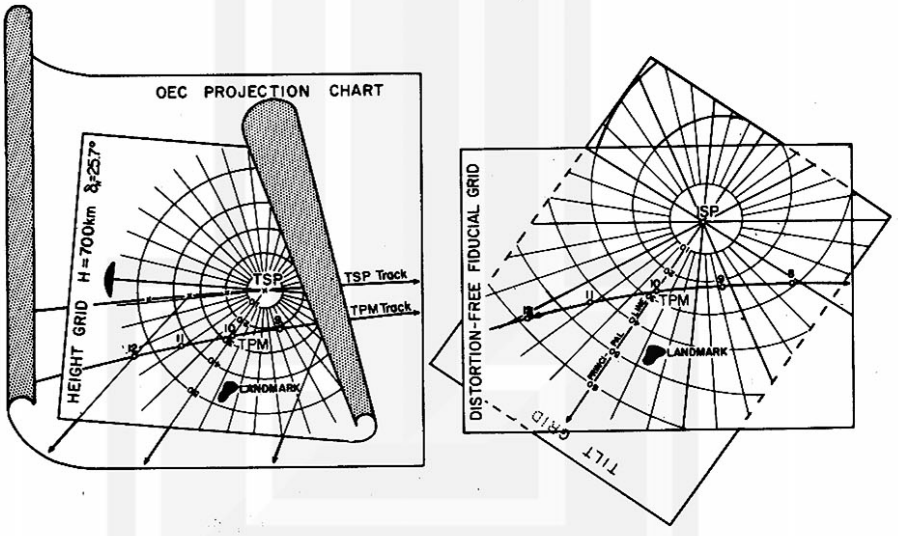

Figure 72. Time and position determination through a preliminary rectification. The right figure shows how the primary line is determined on an image without horizon. It can be done by rotating the distortion-free fiducial grid around the primary point until IPM and TPM tracks match.

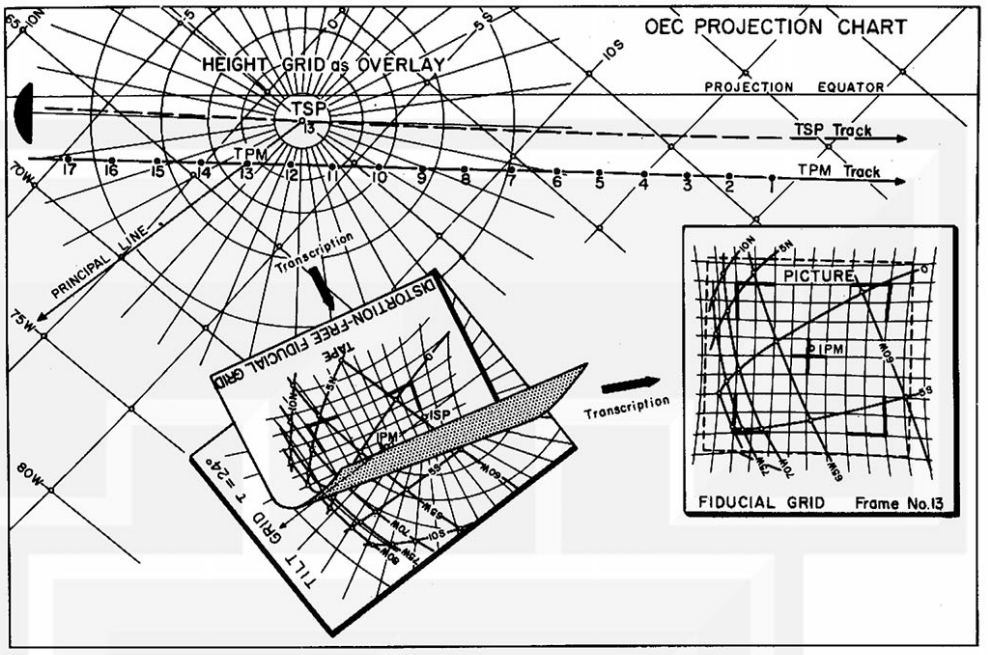

Figure 73. Processes of obtaining the latitude and longitude grid on a distorted image.

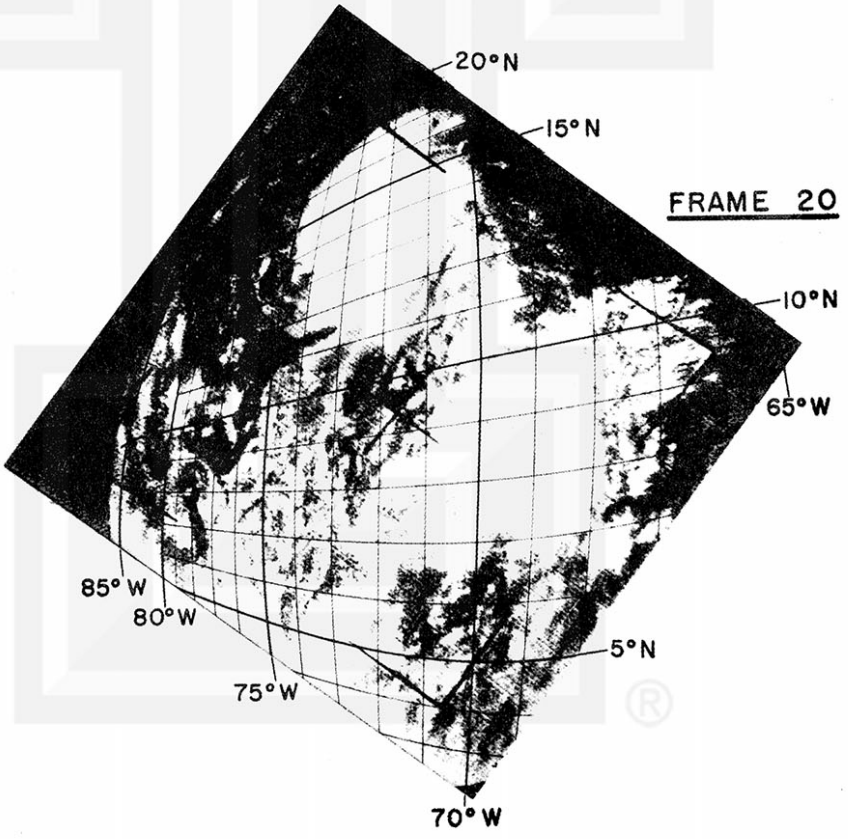

Figure 74. An example of the latitude and longitude grid drawn on a photographs.

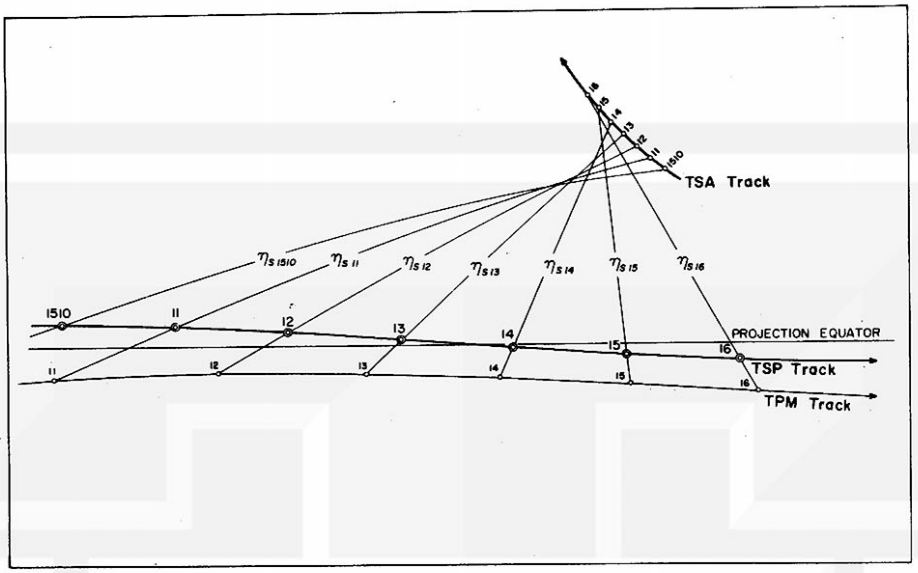

Figure 75. The primary lines at one minute intervals obtained from subpoint and attitude data. No satellite photographs are needed to obtain the primary lines as a function of time.

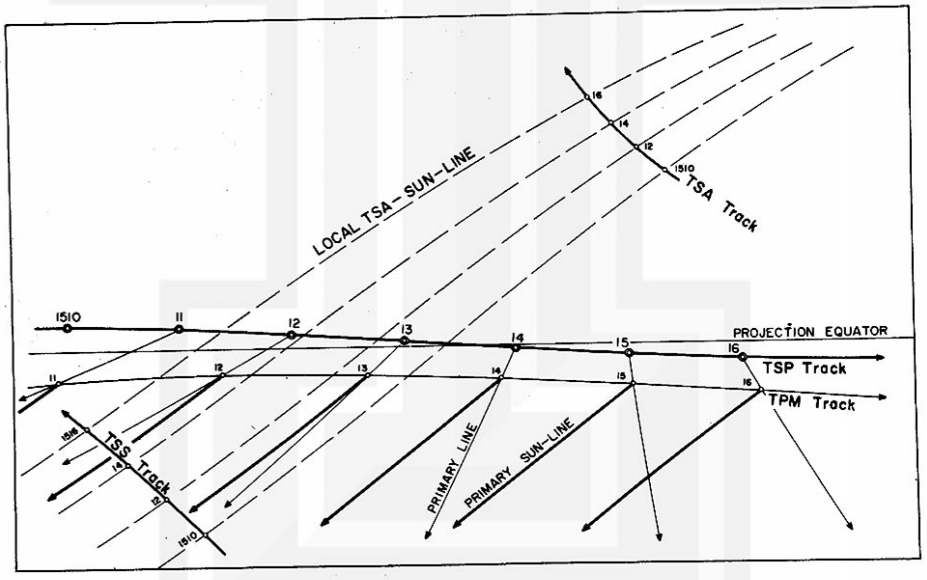

Figure 76. The primary sun-lines on the rotating earth.

	TIROS I	TIROS II	TIROS III	TIROS IV	TIROS V
Orbital Inclination, ι deg	48.40	48.57	47.90	48.30	58.10
Precession, $\dot{\Omega}^{AN}$ deg/day	-4.54	-4.63	-4.66	-4.44	-3.52
Perigee Rate, $\dot{w}$ deg/day	+4.12	+4.16	+4.15	+4.04	+1.32
Semimajor Axis, a km	7100	7054	7156	7155	7159
Eccentricity, e	0.0044	0.0095	0.0058	0.0093	0.0266
Nodal Period, P min	99.15	98.18	100.49	100.47	100.55
Perigee Height, H_P km	690	608	736	710	590
Apogee Height, H_A km	753	742	820	844	971

Table I Orbital elements and derived parameters of TIROS I-V meteorological satellites. Height of satellite represents orbital radius less semimajor axis of the earth.

Date	Days after Injection	ι deg	Ω^{AN} deg	w deg	a km	e
April 1	0	48.30	256.0	117.0	7100.0	0.0029
April 4	3	48.36	241.0	128.8	7100.1	0.0045
May 5	34	48.41	103.3	253.8	7100.4	0.0045
May 16	45	48.39	54.3	294.8	7099.8	0.0022
June 2	62	48.41	334.8	10.0	7100.3	0.0045
June 15	75	48.39	277.9	71.3	7099.4	0.0045
July 18	108	48.41	123.8	201.3	7100.2	0.0045
August 6	128	48.41	40.9	276.4	7100.1	0.0044
September 1	153	48.41	282.4	24.2	7100.1	0.0044
September 20	172	48.41	194.2	103.5	7100.0	0.0044
October 9	191	48.39	112.2	173.2	7099.7	0.0036
November 1	223	48.39	319.6	316.3	7099.7	0.0044

Table II Change in orbital parameters of TIROS I satellite. ι .... inclination, Ω^{AN} ....right ascension of the ascending node, w....argument of perigee, a....semimajor axis, and e....eccentricity.

ϕ_d	R km	R-Rp km	$\phi_d - \phi_c$ deg	$\phi_d - \phi_c$ min	ϕ_d	R km	R-Rp km	$\phi_d - \phi_c$ deg	$\phi_d - \phi_c$ min	ϕ_d	R km	R-Rp km	$\phi_d - \phi_c$ deg	$\phi_d - \phi_c$ min
0	6378.4	21.46	0.00	0.0	30	6373.0	16.10	0.17	10.0	60	6362.3	5.36	0.17	10.0
1	6378.4	21.45	0.01	0.4	31	6372.7	15.77	0.17	10.2	61	6362.0	5.04	0.16	9.8
2	6378.4	21.43	0.01	0.8	32	6372.4	15.43	0.17	10.4	62	6361.7	4.73	0.16	9.6
3	6378.3	21.40	0.02	1.2	33	6372.0	15.09	0.18	10.6	63	6361.4	4.42	0.16	9.4
4	6378.3	21.36	0.03	1.6	34	6371.7	14.75	0.18	10.8	64	6361.1	4.12	0.15	9.1
5	6378.2	21.30	0.03	2.0	35	6371.3	14.40	0.18	10.9	65	6360.8	3.83	0.15	8.9
6	6378.2	21.23	0.04	2.4	36	6371.0	14.05	0.18	11.0	66	6360.5	3.55	0.14	8.6
7	6378.1	21.14	0.05	2.8	37	6370.6	13.69	0.19	11.1	67	6360.2	3.28	0.14	8.3
8	6378.0	21.04	0.05	3.2	38	6370.3	13.33	0.19	11.3	68	6360.0	3.01	0.13	8.1
9	6377.9	20.93	0.06	3.6	39	6369.9	12.96	0.19	11.3	69	6359.7	2.76	0.13	7.8
10	6377.8	20.81	0.07	4.0	40	6369.5	12.59	0.19	11.4	70	6359.5	2.51	0.12	7.5
11	6377.6	20.68	0.07	4.3	41	6369.2	12.22	0.19	11.5	71	6359.2	2.27	0.12	7.1
12	6377.5	20.53	0.08	4.7	42	6368.8	11.85	0.19	11.5	72	6359.0	2.05	0.11	6.8
13	6377.3	20.37	0.08	5.1	43	6368.4	11.48	0.19	11.6	73	6358.8	1.83	0.11	6.5
14	6377.1	20.20	0.09	5.4	44	6368.0	11.10	0.19	11.6	74	6358.6	1.63	0.10	6.1
15	6377.0	20.02	0.10	5.8	45	6367.7	10.73	0.19	11.6	75	6358.4	1.44	0.10	5.8
16	6376.8	19.83	0.10	6.1	46	6367.3	10.36	0.19	11.6	76	6358.2	1.26	0.09	5.4
17	6376.6	19.63	0.11	6.5	47	6366.9	9.98	0.19	11.6	77	6358.0	1.09	0.08	5.1
18	6376.4	19.41	0.11	6.8	48	6366.6	9.61	0.19	11.5	78	6357.9	0.93	0.08	4.7
19	6376.1	19.19	0.12	7.1	49	6366.2	9.24	0.19	11.5	79	6357.7	0.78	0.07	4.3
20	6375.9	18.95	0.12	7.5	50	6365.8	8.87	0.19	11.4	80	6357.6	0.65	0.07	4.0
21	6375.6	18.70	0.13	7.8	51	6365.4	8.50	0.19	11.3	81	6357.5	0.53	0.06	3.6
22	6375.4	18.45	0.13	8.1	52	6365.1	8.13	0.19	11.3	82	6357.4	0.42	0.05	3.2
23	6375.1	18.18	0.14	8.3	53	6364.7	7.77	0.19	11.1	83	6357.3	0.32	0.05	2.8
24	6374.9	17.91	0.14	8.6	54	6364.4	7.41	0.18	11.0	84	6357.2	0.23	0.04	2.4
25	6374.6	17.63	0.15	8.9	55	6364.0	7.06	0.18	10.9	85	6357.1	0.16	0.03	2.0
26	6374.3	17.34	0.15	9.1	56	6363.7	6.71	0.18	10.8	86	6357.0	0.10	0.03	1.6
27	6374.0	17.04	0.16	9.4	57	6363.3	6.37	0.18	10.6	87	6357.0	0.06	0.02	1.2
28	6373.7	16.73	0.16	9.6	58	6363.0	6.03	0.17	10.4	88	6357.0	0.03	0.01	0.8
29	6373.4	16.42	0.16	9.8	59	6362.6	5.69	0.17	10.2	89	6357.0	0.01	0.01	0.4
										90	6356.9	0.00	0.00	0.0

Table III The radius, the excess radius, and the difference between the geodetic and geocentric latitudes of the earth tabulated as a function of latitudes.

TIROS	I				II				III				IV				V			
Camera No.	1		2		1		2		1		2		1		2		1		2	
Optical Axis Deviation (χ)	0.73^o		0.45^o		0.52^o		0.47^o		0.37^o		0.53^o		0.53^o		0.34^o		0.62^o		0.64^o	
Principal Tangential Angle of IPM (γ^{**})					290^o		251^o		232^o		235^o		227^o		264^o		264^o		256^o	
Baseplate Angle of Opt. Axis (ϕ_s)	290^o		170^o		289.5^o		169.5^o		289.8^o		169.8^o		289.8^o		169.8^o		289.7^o		169.5^o	
Focal Length of Lens (f)	40.0 mm		5.3 mm		40.0 mm		5.3 mm		5.3 mm		5.3 mm		5.0 mm		5.7 mm		5.0 mm		5.7 mm	
Distance of Test Target	204.5"		18.95"		600.4"		62.45"		63.63"		62.82"		65.89"		66.65"		63.63"		62.82"	
Line Width of Test Target	0.321"		0.200"		0.948"		0.704"		0.352"		0.352"		0.352"		0.352"		0.352"		0.352"	
Radial Angle (ϵ_T) and Mean Radial Distortion ($\bar{E}$)	ϵ_T deg	$\bar{E}$	ϵ_T deg	$\bar{E}$	ϵ_T deg	$\bar{E}$	ϵ_T deg	$\bar{E}$	ϵ_T deg	$\bar{E}$	ϵ_T deg	$\bar{E}$	ϵ_T deg	$\bar{E}$	ϵ_T deg	$\bar{E}$	ϵ_T deg	$\bar{E}$	ϵ_T deg	$\bar{E}$
	0.50	1.00	2.68	0.99	2.00	1.00	9.83	0.99	9.50	0.99	9.62	1.00	9.18	0.99	9.08	1.01	10.52	0.99	10.25	1.00
	1.00	0.99	5.67	1.01	4.00	1.00	19.31	0.96	18.83	0.97	19.07	0.97	18.23	0.97	18.05	1.03	20.73	0.95	20.23	1.00
	1.50	0.98	8.98	1.00	6.00	1.02	-----	----	-----	----	-----	----	22.82	0.95	22.58	1.04	25.83	0.92	25.22	1.00
	2.00	0.97	13.52	1.00			28.90	0.91	28.33	0.92	28.63	0.92	27.50	0.93	27.23	1.06	30.88	0.90	30.22	1.01
	2.50	0.97	18.08	0.99			-----	----	33.15	0.88	33.48	0.88	32.24	0.89	31.95	1.08	35.95	0.85	35.20	1.03
	3.00	0.99	22.70	0.97			38.63	0.84	38.02	0.84	38.38	0.83	37.05	0.86			40.96	0.81		
	3.50	0.98	27.38	0.94			43.58	0.72	42.97	0.80	43.33	0.79	41.97	0.81						
	3.98	0.97	32.13	0.90					47.98	0.74	48.35	0.74	46.98	0.78						
	4.48	0.97																		
	4.98	0.97																		

Table IV Characteristics of TIROS-borne cameras.

SIDEREAL ROTATION ANGLE OF THE EARTH

Hour / Minute	0	1	2	3	4	5	6	7	8	9	10	11	12	13	14	15	16	17	18	19	20	21	22	23	Hour / Min
0	0.0	15.0	30.1	45.1	60.2	75.2	90.2	105.3	120.3	135.4	150.4	165.5	180.5	195.5	210.6	225.6	240.7	255.7	270.7	285.8	300.8	315.9	330.9	345.9	0
1	0.3	15.3	30.3	45.4	60.4	75.5	90.5	105.5	120.6	135.6	150.7	165.7	180.7	195.8	210.8	225.9	240.9	255.9	271.0	286.0	301.1	316.1	331.2	346.2	1
2	0.5	15.5	30.6	45.6	60.7	75.7	90.7	105.8	120.8	135.9	150.9	166.0	181.0	196.0	211.1	226.1	241.2	256.2	271.2	286.3	301.3	316.4	331.4	346.4	2
3	0.8	15.8	30.8	45.9	60.9	76.0	91.0	106.0	121.1	136.1	151.2	166.2	181.2	196.3	211.3	226.4	241.4	256.4	271.5	286.5	301.6	316.6	331.7	346.7	3
4	1.0	16.0	31.1	46.1	61.2	76.2	91.2	106.3	121.3	136.4	151.4	166.5	181.5	196.5	211.6	226.6	241.7	256.7	271.7	286.8	301.8	316.9	331.9	346.9	4
5	1.3	16.3	31.3	46.4	61.4	76.5	91.5	106.5	121.6	136.6	151.7	166.7	181.7	196.8	211.8	226.9	241.9	256.9	272.0	287.0	302.1	317.1	332.2	347.2	5
6	1.5	16.5	31.6	46.6	61.7	76.7	91.7	106.8	121.8	136.9	151.9	167.0	182.0	197.0	212.1	227.1	242.2	257.2	272.2	287.3	302.3	317.4	332.4	347.4	6
7	1.8	16.8	31.8	46.9	61.9	77.0	92.0	107.0	122.1	137.1	152.2	167.2	182.2	197.3	212.3	227.4	242.4	257.4	272.5	287.5	302.6	317.6	332.7	347.7	7
8	2.0	17.0	32.1	47.1	62.2	77.2	92.2	107.3	122.3	137.4	152.4	167.5	182.5	197.5	212.6	227.6	242.7	257.7	272.7	287.8	302.8	317.9	332.9	347.9	8
9	2.3	17.3	32.3	47.4	62.4	77.5	92.5	107.5	122.6	137.6	152.7	167.7	182.7	197.8	212.8	227.9	242.9	257.9	273.0	288.0	303.1	318.1	333.2	348.2	9
10	2.5	17.5	32.6	47.6	62.7	77.7	92.7	107.8	122.8	137.9	152.9	168.0	183.0	198.0	213.1	228.1	243.2	258.2	273.2	288.3	303.3	318.4	333.4	348.4	10
11	2.8	17.8	32.8	47.9	62.9	78.0	93.0	108.0	123.1	138.1	153.2	168.2	183.2	198.3	213.3	228.4	243.4	258.4	273.5	288.5	303.6	318.6	333.7	348.7	11
12	3.0	18.0	33.1	48.1	63.2	78.2	93.2	108.3	123.3	138.4	153.4	168.5	183.5	198.5	213.6	228.6	243.7	258.7	273.7	288.8	303.8	318.9	333.9	348.9	12
13	3.3	18.3	33.3	48.4	63.4	78.5	93.5	108.5	123.6	138.6	153.7	168.7	183.7	198.8	213.8	228.9	243.9	258.9	274.0	289.0	304.1	319.1	334.2	349.2	13
14	3.5	18.5	33.6	48.6	63.7	78.7	93.7	108.8	123.8	138.9	153.9	169.0	184.0	199.0	214.1	229.1	244.2	259.2	274.2	289.3	304.3	319.4	334.4	349.4	14
15	3.8	18.8	33.8	48.9	63.9	79.0	94.0	109.0	124.1	139.1	154.2	169.2	184.3	199.3	214.3	229.4	244.4	259.5	274.5	289.5	304.6	319.6	334.7	349.7	15
16	4.0	19.1	34.1	49.1	64.2	79.2	94.3	109.3	124.3	139.4	154.4	169.5	184.5	199.5	214.6	229.6	244.7	259.7	274.7	289.8	304.8	319.9	334.9	350.0	16
17	4.3	19.3	34.3	49.4	64.4	79.5	94.5	109.5	124.6	139.6	154.7	169.7	184.8	199.8	214.8	229.9	244.9	260.0	275.0	290.0	305.1	320.1	335.2	350.2	17
18	4.5	19.6	34.6	49.6	64.7	79.7	94.8	109.8	124.8	139.9	154.9	170.0	185.0	200.0	215.1	230.1	245.2	260.2	275.2	290.3	305.3	320.4	335.4	350.5	18
19	4.8	19.8	34.8	49.9	64.9	80.0	95.0	110.0	125.1	140.1	155.2	170.2	185.3	200.3	215.3	230.4	245.4	260.5	275.5	290.5	305.6	320.6	335.7	350.7	19
20	5.0	20.1	35.1	50.1	65.2	80.2	95.3	110.3	125.3	140.4	155.4	170.5	185.5	200.5	215.6	230.6	245.7	260.7	275.7	290.8	305.8	320.9	335.9	351.0	20
21	5.3	20.3	35.3	50.4	65.4	80.5	95.5	110.5	125.6	140.6	155.7	170.7	185.8	200.8	215.8	230.9	245.9	261.0	276.0	291.0	306.1	321.1	336.2	351.2	21
22	5.5	20.6	35.6	50.6	65.7	80.7	95.8	110.8	125.8	140.9	155.9	171.0	186.0	201.0	216.1	231.1	246.2	261.2	276.2	291.3	306.3	321.4	336.4	351.5	22
23	5.8	20.8	35.8	50.9	65.9	81.0	96.0	111.0	126.1	141.1	156.2	171.2	186.3	201.3	216.3	231.4	246.4	261.5	276.5	291.5	306.6	321.6	336.7	351.7	23
24	6.0	21.1	36.1	51.1	66.2	81.2	96.3	111.3	126.3	141.4	156.4	171.5	186.5	201.5	216.6	231.6	246.7	261.7	276.7	291.8	306.8	321.9	336.9	352.0	24
25	6.3	21.3	36.3	51.4	66.4	81.5	96.5	111.5	126.6	141.6	156.7	171.7	186.8	201.8	216.8	231.9	246.9	262.0	277.0	292.0	307.1	322.1	337.2	352.2	25
26	6.5	21.6	36.6	51.6	66.7	81.7	96.8	111.8	126.8	141.9	156.9	172.0	187.0	202.0	217.1	232.1	247.2	262.2	277.2	292.3	307.3	322.4	337.4	352.5	26
27	6.8	21.8	36.8	51.9	66.9	82.0	97.0	112.0	127.1	142.1	157.2	172.2	187.3	202.3	217.3	232.4	247.4	262.5	277.5	292.5	307.6	322.6	337.7	352.7	27
28	7.0	22.1	37.1	52.1	67.2	82.2	97.3	112.3	127.3	142.4	157.4	172.5	187.5	202.5	217.6	232.6	247.7	262.7	277.7	292.8	307.8	322.9	337.9	353.0	28
29	7.3	22.3	37.3	52.4	67.4	82.5	97.5	112.5	127.6	142.6	157.7	172.7	187.8	202.8	217.8	232.9	247.9	263.0	278.0	293.0	308.1	323.1	338.2	353.2	29
30	7.5	22.6	37.6	52.6	67.7	82.7	97.8	112.8	127.9	142.9	157.9	173.0	188.0	203.1	218.1	233.1	248.2	263.2	278.3	293.3	308.3	323.4	338.4	353.5	30
31	7.8	22.8	37.9	52.9	67.9	83.0	98.0	113.1	128.1	143.1	158.2	173.2	188.3	203.3	218.3	233.4	248.4	263.5	278.5	293.6	308.6	323.6	338.7	353.7	31
32	8.0	23.1	38.1	53.1	68.2	83.2	98.3	113.3	128.4	143.4	158.4	173.5	188.6	203.6	218.6	233.6	248.7	263.7	278.8	293.8	308.8	323.9	338.9	354.0	32
33	8.3	23.3	38.4	53.4	68.4	83.5	98.5	113.6	128.6	143.6	158.7	173.7	188.8	203.8	218.8	233.9	248.9	264.0	279.0	294.1	309.1	324.1	339.2	354.2	33
34	8.5	23.6	38.6	53.6	68.7	83.7	98.8	113.8	128.9	143.9	158.9	174.0	189.0	204.1	219.1	234.1	249.2	264.2	279.3	294.3	309.3	324.4	339.4	354.5	34
35	8.8	23.8	38.9	53.9	68.9	84.0	99.0	114.1	129.1	144.1	159.2	174.2	189.3	204.3	219.3	234.4	249.4	264.5	279.5	294.6	309.6	324.6	339.7	354.7	35
36	9.0	24.1	39.1	54.1	69.2	84.2	99.3	114.3	129.4	144.4	159.4	174.5	189.5	204.6	219.6	234.6	249.7	264.7	279.8	294.8	309.8	324.9	339.9	355.0	36
37	9.3	24.3	39.4	54.4	69.4	84.5	99.5	114.6	129.6	144.6	159.7	174.7	189.8	204.8	219.8	234.9	249.9	265.0	280.0	295.1	310.1	325.1	340.2	355.2	37
38	9.5	24.6	39.6	54.6	69.7	84.7	99.8	114.8	129.9	144.9	159.9	175.0	190.0	205.1	220.1	235.1	250.2	265.2	280.3	295.3	310.3	325.4	340.4	355.5	38
39	9.8	24.8	39.9	54.9	69.9	85.0	100.0	115.1	130.1	145.1	160.2	175.2	190.3	205.3	220.3	235.4	250.4	265.5	280.5	295.6	310.6	325.6	340.7	355.7	39
40	10.0	25.1	40.1	55.1	70.2	85.2	100.3	115.3	130.4	145.4	160.4	175.5	190.5	205.6	220.6	235.6	250.7	265.7	280.8	295.8	310.8	325.9	340.9	356.0	40
41	10.3	25.3	40.4	55.4	70.4	85.5	100.5	115.6	130.6	145.6	160.7	175.7	190.8	205.8	220.8	235.9	250.9	266.0	281.0	296.1	311.1	326.1	341.2	356.2	41
42	10.5	25.6	40.6	55.6	70.7	85.7	100.8	115.8	130.9	145.9	160.9	176.0	191.0	206.1	221.1	236.1	251.2	266.2	281.3	296.3	311.3	326.4	341.4	356.5	42
43	10.8	25.8	40.9	55.9	70.9	86.0	101.0	116.1	131.1	146.1	161.2	176.2	191.3	206.3	221.3	236.4	251.4	266.5	281.5	296.6	311.6	326.6	341.7	356.7	43
44	11.0	26.1	41.1	56.2	71.2	86.2	101.3	116.3	131.4	146.4	161.4	176.5	191.5	206.6	221.6	236.6	251.7	266.7	281.8	296.8	311.9	326.9	341.9	357.0	44
45	11.3	26.3	41.4	56.4	71.4	86.5	101.5	116.6	131.6	146.7	161.7	176.7	191.8	206.8	221.9	236.9	251.9	267.0	282.0	297.1	312.1	327.1	342.2	357.2	45
46	11.5	26.6	41.6	56.7	71.7	86.7	101.8	116.8	131.9	146.9	161.9	177.0	192.0	207.1	222.1	237.1	252.2	267.2	282.3	297.3	312.4	327.4	342.4	357.5	46
47	11.8	26.8	41.9	56.9	71.9	87.0	102.0	117.1	132.1	147.2	162.2	177.2	192.3	207.3	222.4	237.4	252.4	267.5	282.5	297.6	312.6	327.6	342.7	357.7	47
48	12.0	27.1	42.1	57.2	72.2	87.2	102.3	117.3	132.4	147.4	162.4	177.5	192.5	207.6	222.6	237.6	252.7	267.7	282.8	297.8	312.9	327.9	342.9	358.0	48
49	12.3	27.3	42.4	57.4	72.4	87.5	102.5	117.6	132.6	147.7	162.7	177.7	192.8	207.8	222.9	237.9	252.9	268.0	283.0	298.1	313.1	328.1	343.2	358.2	49
50	12.5	27.6	42.6	57.7	72.7	87.7	102.8	117.8	132.9	147.9	162.9	178.0	193.0	208.1	223.1	238.1	253.2	268.2	283.3	298.3	313.4	328.4	343.4	358.5	50
51	12.8	27.8	42.9	57.9	72.9	88.0	103.0	118.1	133.1	148.2	163.2	178.2	193.3	208.3	223.4	238.4	253.4	268.5	283.5	298.6	313.6	328.6	343.7	358.7	51
52	13.0	28.1	43.1	58.2	73.2	88.2	103.3	118.3	133.4	148.4	163.4	178.5	193.5	208.6	223.6	238.6	253.7	268.7	283.8	298.8	313.9	328.9	343.9	359.0	52
53	13.3	28.3	43.4	58.4	73.4	88.5	103.5	118.6	133.6	148.7	163.7	178.7	193.8	208.8	223.9	238.9	253.9	269.0	284.0	299.1	314.1	329.1	344.2	359.2	53
54	13.5	28.6	43.6	58.7	73.7	88.7	103.8	118.8	133.9	148.9	163.9	179.0	194.0	209.1	224.1	239.1	254.2	269.2	284.3	299.3	314.4	329.4	344.4	359.5	54
55	13.8	28.8	43.9	58.9	73.9	89.0	104.0	119.1	134.1	149.2	164.2	179.2	194.3	209.3	224.4	239.4	254.4	269.5	284.5	299.6	314.6	329.6	344.7	359.7	55
56	14.0	29.1	44.1	59.2	74.2	89.2	104.3	119.3	134.4	149.4	164.4	179.5	194.5	209.6	224.6	239.6	254.7	269.7	284.8	299.8	314.9	329.9	344.9	360.0	56
57	14.3	29.3	44.4	59.4	74.4	89.5	104.5	119.6	134.6	149.7	164.7	179.7	194.8	209.8	224.9	239.9	254.9	270.0	285.0	300.1	315.1	330.1	345.2	360.2	57
58	14.5	29.6	44.6	59.7	74.7	89.7	104.8	119.8	134.9	149.9	164.9	180.0	195.0	210.1	225.1	240.1	255.2	270.2	285.3	300.3	315.4	330.4	345.4	360.5	58
59	14.8	29.8	44.9	59.9	74.9	90.0	105.0	120.1	135.1	150.2	165.2	180.2	195.3	210.3	225.4	240.4	255.4	270.5	285.5	300.6	315.6	330.6	345.7	360.7	59
60	15.0	30.1	45.1	60.2	75.2	90.2	105.3	120.3	135.4	150.4	165.5	180.5	195.5	210.6	225.6	240.7	255.7	270.7	285.8	300.8	315.9	330.9	345.9	361.0	60
Min / Hour	0	1	2	3	4	5	6	7	8	9	10	11	12	13	14	15	16	17	18	19	20	21	22	23	Min / Hour

Table V Sidereal rotation angle of the earth as a function of hours and minutes. The rotation angle in degrees can be obtained by reading off the number at the intersection of hour column and minute row. The top and bottom numbers denote the hours, and the side numbers, the minutes.

IMAGE HORIZONTAL ANGLES

τ \ ψ	0	10	20	30	40	50	60	70	80
0	0.00	10.00	20.00	30.00	40.00	50.00	60.00	70.00	80.00
1	0.00	10.00	20.00	30.00	40.00	50.00	60.00	70.00	80.00
2	0.00	10.00	19.98	29.98	39.98	49.98	59.98	69.98	80.00
3	0.00	9.98	19.97	29.97	39.97	49.97	59.97	69.97	79.98
4	0.00	9.98	19.95	29.93	39.93	49.93	59.93	69.95	79.98
5	0.00	9.97	19.93	29.90	39.90	49.90	59.90	69.93	79.97
6	0.00	9.95	19.90	29.87	39.85	49.85	59.87	69.90	79.95
7	0.00	9.93	19.87	29.82	39.78	49.78	59.82	69.87	79.93
8	0.00	9.90	19.82	29.75	39.72	49.72	59.75	69.82	79.90
9	0.00	9.88	19.77	29.70	39.65	49.65	59.70	69.77	79.88
10	0.00	9.85	19.72	29.62	39.57	49.57	59.62	69.72	79.85
11	0.00	9.82	19.67	29.55	39.48	49.48	59.53	69.65	79.82
12	0.00	9.78	19.60	29.45	39.38	49.38	59.45	69.58	79.78
13	0.00	9.75	19.53	29.37	39.27	49.27	59.35	69.52	79.75
14	0.00	9.72	19.45	29.25	39.15	49.15	59.25	69.43	79.70
15	0.00	9.67	19.37	29.15	39.02	49.02	59.13	69.35	79.65
16	0.00	9.62	19.28	29.03	38.88	48.88	59.02	69.27	79.60
17	0.00	9.57	19.18	28.90	38.75	48.73	58.88	69.17	79.55
18	0.00	9.52	19.10	28.77	38.58	48.58	58.73	69.05	79.50
19	0.00	9.47	18.98	28.63	38.43	48.42	58.58	68.95	79.43
20	0.00	9.40	18.88	28.48	38.25	48.23	58.43	68.83	79.37
21	0.00	9.35	18.77	28.32	38.07	48.05	58.27	68.70	79.30
22	0.00	9.28	18.65	28.17	37.88	47.85	58.08	68.57	79.23
23	0.00	9.22	18.52	27.98	37.68	47.65	57.90	68.43	79.15
24	0.00	9.15	18.40	27.82	37.47	47.43	57.72	68.28	79.08
25	0.00	9.08	18.25	27.62	37.25	47.20	57.50	68.12	78.98
26	0.00	9.00	18.12	27.43	37.02	46.97	57.28	67.95	78.90
27	0.00	8.93	17.97	27.22	36.78	46.72	57.05	67.78	78.80
28	0.00	8.85	17.82	27.02	36.53	46.47	56.82	67.60	78.70
29	0.00	8.77	17.65	26.80	36.27	46.18	56.57	67.40	78.60
30	0.00	8.68	17.50	26.57	36.00	45.90	56.32	67.20	78.50
31	0.00	8.60	17.33	26.33	35.73	45.62	56.03	67.00	78.38
32	0.00	8.50	17.15	26.08	35.43	45.30	55.75	66.77	78.25
33	0.00	8.42	16.97	25.83	35.13	44.98	55.45	66.53	78.13
34	0.00	8.32	16.78	25.58	34.82	44.65	55.15	66.30	78.00
35	0.00	8.22	16.60	25.32	34.50	44.32	54.82	66.05	77.85
36	0.00	8.12	16.40	25.03	34.17	43.95	54.48	65.78	77.70
37	0.00	8.02	16.20	24.75	33.83	43.58	54.13	65.50	77.55
38	0.00	7.92	16.00	24.47	33.47	43.20	53.77	65.22	77.38
39	0.00	7.80	15.80	24.17	33.12	42.80	53.40	64.90	77.22
40	0.00	7.70	15.58	23.85	32.73	42.40	53.00	64.58	77.03
41	0.00	7.58	15.37	23.55	32.35	41.97	52.58	64.25	76.85
42	0.00	7.47	15.13	23.22	31.95	41.53	52.15	63.90	76.65
43	0.00	7.35	14.90	22.88	31.53	41.08	51.72	63.55	76.45
44	0.00	7.23	14.67	22.55	31.12	40.60	51.25	63.17	76.23

τ \ ψ	0	10	20	30	40	50	60	70	80
45	0.00	7.10	14.43	22.20	30.68	40.12	50.77	62.77	76.00
46	0.00	6.98	14.18	21.85	30.23	39.62	50.27	62.35	75.75
47	0.00	6.85	13.93	21.50	29.78	39.10	49.75	61.92	75.50
48	0.00	6.73	13.68	21.12	29.32	38.57	49.22	61.45	75.23
49	0.00	6.60	13.43	20.75	28.83	38.02	48.65	60.98	74.95
50	0.00	6.47	13.17	20.37	28.33	37.45	48.07	60.48	74.67
51	0.00	6.33	12.90	19.97	27.83	36.87	47.47	59.95	74.35
52	0.00	6.20	12.63	19.57	27.32	36.27	46.83	59.42	74.02
53	0.00	6.05	12.35	19.17	26.80	35.65	46.18	58.83	73.67
54	0.00	5.92	12.08	18.75	26.25	35.02	45.52	58.23	73.30
55	0.00	5.78	11.80	18.32	25.70	34.35	44.82	57.60	72.92
56	0.00	5.63	11.50	17.90	25.13	33.68	44.08	56.95	72.50
57	0.00	5.48	11.22	17.45	24.57	32.98	43.33	56.25	72.07
58	0.00	5.33	10.92	17.02	23.97	32.27	42.55	55.52	71.60
59	0.00	5.18	10.62	16.57	23.37	31.55	41.73	54.75	71.10
60	0.00	5.03	10.32	16.10	22.77	30.78	40.90	53.95	70.57
61	0.00	4.88	10.00	15.63	22.13	30.02	40.02	53.10	70.02
62	0.00	4.73	9.70	15.17	21.50	29.23	39.12	52.22	69.42
63	0.00	4.58	9.38	14.68	20.85	28.42	38.18	51.28	68.77
64	0.00	4.42	9.07	14.20	20.20	27.58	37.22	50.30	68.08
65	0.00	4.27	8.75	13.72	19.53	26.73	36.20	49.27	67.35
66	0.00	4.10	8.42	13.22	18.85	25.87	35.17	48.18	66.57
67	0.00	3.93	8.10	12.72	18.15	24.97	34.08	47.03	65.72
68	0.00	3.78	7.77	12.20	17.45	24.07	32.98	45.83	64.80
69	0.00	3.62	7.43	11.68	16.73	23.13	31.83	44.55	63.80
70	0.00	3.45	7.10	11.17	16.02	22.18	30.65	43.22	62.73
71	0.00	3.28	6.75	10.65	15.28	21.20	29.42	41.82	61.57
72	0.00	3.12	6.42	10.12	14.53	20.22	28.15	40.33	60.28
73	0.00	2.95	6.07	9.58	13.78	19.22	26.85	38.77	58.90
74	0.00	2.78	5.73	9.05	13.02	18.18	25.52	37.13	57.40
75	0.00	2.62	5.38	8.50	12.25	17.15	24.15	35.42	55.73
76	0.00	2.45	5.03	7.95	11.48	16.08	22.73	33.62	53.92
77	0.00	2.27	4.68	7.40	10.68	15.00	21.28	31.72	51.92
78	0.00	2.10	4.33	6.85	9.90	13.92	19.80	29.73	49.70
79	0.00	1.93	3.97	6.28	9.10	12.82	18.28	27.67	47.25
80	0.00	1.75	3.62	5.73	8.28	11.70	16.73	25.50	44.57
81	0.00	1.58	3.27	5.17	7.48	10.57	15.17	23.25	41.58
82	0.00	1.40	2.90	4.60	6.67	9.42	13.55	20.93	38.28
83	0.00	1.23	2.53	4.02	5.83	8.27	11.92	18.52	34.65
84	0.00	1.05	2.18	3.45	5.02	7.10	10.27	16.02	30.67
85	0.00	0.88	1.82	2.88	4.18	5.93	8.58	13.47	26.30
86	0.00	0.70	1.45	2.30	3.35	4.75	6.88	10.85	21.58
87	0.00	0.53	1.08	1.73	2.52	3.57	5.18	8.18	16.53
88	0.00	0.35	0.73	1.15	1.68	2.38	3.47	5.48	11.20
89	0.00	0.18	0.37	0.58	0.83	1.18	1.73	2.75	5.65
90	0.00	0.00	0.00	0.00	0.00	0.00	0.00	0.00	0.00

Table VI Image horizontal angles (ψ_i) given as a function of the horizontal angles (ψ) and the tilts (τ). The horizontal angles in degrees are computed from Equation (49).

VERTICAL ANGLES

η \ ψ	0	10	20	30	40	50	60	70	80
0	0.00	0.00	0.00	0.00	0.00	0.00	0.00	0.00	0.00
10	10.00	9.85	9.40	8.68	7.70	6.47	5.03	3.45	1.75
20	20.00	19.72	18.88	17.50	15.58	13.17	10.32	7.10	3.62
30	30.00	29.62	28.48	26.57	23.85	20.37	16.10	11.17	5.73
35	35.00	34.58	33.35	31.23	28.22	24.23	19.30	13.47	6.93
40	40.00	39.57	38.25	36.00	32.73	28.33	22.77	16.02	8.28
45	45.00	44.57	43.22	40.90	37.45	32.73	26.57	18.88	9.85
50	50.00	49.57	48.23	45.90	42.40	37.45	30.78	22.18	11.70
55	55.00	54.58	53.30	51.05	47.57	42.55	35.53	26.03	13.93
60	60.00	59.62	58.43	56.32	53.00	48.07	40.90	30.65	16.73
62	62.00	61.63	60.50	58.45	55.23	50.40	43.23	32.75	18.08
64	64.00	63.65	62.57	60.62	57.52	52.82	45.72	35.03	19.60
66	66.00	65.67	64.65	62.80	59.83	55.28	48.32	37.53	21.30
68	68.00	67.70	66.73	64.98	62.20	57.85	51.07	40.25	23.25
70	70.00	69.72	68.83	67.20	64.58	60.48	53.95	43.22	25.50
72	72.00	71.73	70.93	69.43	67.02	63.18	56.98	46.47	28.12
74	74.00	73.77	73.03	71.68	69.48	65.97	60.17	50.02	31.20
76	76.00	75.80	75.13	73.93	71.97	68.80	63.50	53.92	34.85
78	78.00	77.82	77.25	76.22	74.50	71.70	66.97	58.13	39.25
80	80.00	79.85	79.37	78.50	77.03	74.67	70.57	62.73	44.57
82	82.00	81.88	81.50	80.78	79.60	77.67	74.30	67.67	51.02
84	84.00	83.90	83.62	83.08	82.18	80.72	78.13	72.92	58.82
86	86.00	85.93	85.75	85.38	84.78	83.78	82.03	78.45	68.07
88	88.00	87.97	87.87	87.68	87.38	86.88	86.00	84.17	78.63
90	90.00	90.00	90.00	90.00	90.00	90.00	90.00	90.00	90.00

Table VII Vertical angles (ζ) given as a function of the nadir angles (η) and the horizontal angles (ψ). The vertical angles in degrees are computed from Equation (50). This table may be used in making tilt grid for any tilt.

48.4° OEC PROJECTION DATA

ϕ \ θ	-25	-20	-15	-10	-5	0	5	10	15	20	25	30	35	40	45	50	55	60	65	70	75	80	85	90	θ \ ϕ
75															77.75 30.28	78.97 29.53	80.25 28.87	81.55 28.27	82.90 27.77	84.28 27.35	85.70 27.02	87.10 26.78	88.55 26.65	90.00 26.60	75
70												70.05 29.73	71.42 28.50	72.85 27.35	74.35 26.30	75.92 25.33	77.55 24.48	79.23 23.72	80.95 23.08	82.72 22.55	84.52 22.13	86.33 21.85	88.17 21.65	90.00 21.60	70
65										62.83 29.57	64.32 27.92	65.90 26.35	67.57 24.87	69.33 23.50	71.17 22.23	73.07 21.08	75.03 20.05	77.07 19.15	79.15 18.37	81.27 17.73	83.42 17.25	85.62 16.88	87.78 16.67	90.00 16.60	65
60								55.07 30.67	56.63 28.57	58.32 26.57	60.10 24.63	61.97 22.83	63.95 21.13	66.02 19.55	68.17 18.10	70.38 16.77	72.68 15.58	75.03 14.55	77.43 13.67	79.88 12.92	82.38 12.35	84.90 11.93	87.45 11.68	90.00 11.60	60
55							48.50 30.42	50.22 27.98	52.07 25.65	54.03 23.40	56.10 21.27	58.27 19.23	60.50 17.33	62.87 15.55	65.30 13.92	67.82 12.43	70.40 11.10	73.07 9.93	75.78 8.92	78.57 8.08	81.40 7.45	84.23 6.98	87.12 6.68	90.00 6.60	55
50						41.70 30.57	43.62 27.82	45.63 25.17	47.73 22.60	49.95 20.13	52.28 17.80	54.70 15.55	57.22 13.47	59.83 11.52	62.53 9.72	65.33 8.07	68.22 6.60	71.17 5.30	74.18 4.18	77.28 3.27	80.40 2.55	83.60 2.02	86.78 1.70	90.00 1.60	50
45					34.70 31.03	36.78 28.00	38.97 25.05	41.23 22.18	43.58 19.42	46.07 16.78	48.62 14.23	51.27 11.83	54.02 9.57	56.88 7.45	59.85 5.48	62.90 3.70	66.05 2.08	69.30 0.65	72.62 -0.55	76.00 -1.57	79.43 -2.37	82.93 -2.95	86.47 -3.28	90.00 -3.40	45
40				27.48 31.77	29.77 28.48	32.10 25.27	34.53 22.13	37.03 19.10	39.60 16.17	42.30 13.35	45.07 10.63	47.92 8.07	50.92 5.63	54.00 3.37	57.20 1.25	60.50 -0.70	63.90 -2.43	67.43 -3.97	71.03 -5.30	74.72 -6.40	78.47 -7.27	82.28 -7.90	86.13 -8.28	90.00 -8.40	40
35				22.52 29.15	25.07 25.73	27.63 22.38	30.28 19.12	32.97 15.92	35.75 12.85	38.62 9.87	41.58 7.00	44.65 4.27	47.83 1.70	51.13 -0.73	54.55 -3.00	58.10 -5.07	61.73 -6.95	65.52 -8.62	69.42 -10.05	73.40 -11.23	77.48 -12.18	81.60 -12.85	85.78 -13.27	90.00 -13.40	35
30			15.07 29.98	17.82 26.38	20.58 22.87	23.35 19.38	26.18 16.00	29.05 12.68	32.00 9.47	35.03 6.33	38.17 3.35	41.42 0.47	44.77 -2.27	48.25 -4.83	51.87 -7.23	55.63 -9.45	59.55 -11.45	63.58 -13.23	67.77 -14.77	72.05 -16.05	76.45 -17.07	80.92 -17.80	85.43 -18.25	90.00 -18.40	30
25		7.37 30.82	10.37 27.13	13.33 23.47	16.28 19.85	19.22 16.30	22.20 12.80	25.22 9.38	28.32 6.03	31.90 2.78	34.78 -0.33	38.17 -3.35	41.68 -6.20	45.35 -8.92	49.17 -11.47	53.13 -13.80	57.28 -15.93	61.57 -17.83	66.03 -19.48	70.63 -20.87	75.35 -21.97	80.18 -22.77	85.07 -23.23	80.00 -23.40	25
20	-0.53 31.60	2.75 27.85	5.93 24.13	9.05 20.43	12.15 16.77	15.23 13.13	18.33 9.55	21.47 6.03	24.68 2.58	27.97 -0.77	31.37 -4.02	34.90 -7.13	38.57 -10.13	42.38 -12.98	46.37 -15.65	50.53 -18.13	54.90 -20.40	59.47 -22.42	64.18 -24.18	69.03 -25.68	73.95 -26.85	79.38 -27.70	84.67 -28.23	90.00 -28.40	20
15	-5.05 28.50	-1.62 24.77	1.70 21.02	4.93 17.30	8.15 13.58	11.33 9.90	14.53 6.25	17.78 2.67	21.07 -0.87	24.47 -4.32	27.95 -7.67	31.58 -10.92	35.35 -14.03	39.30 -17.00	43.45 -19.82	47.80 -22.42	52.37 -24.82	57.18 -26.97	62.20 -28.87	67.47 -30.47	72.90 -31.73				15
10	-9.32 25.25	-5.78 21.53	-2.37 17.82	0.97 14.07	4.25 10.33	7.52 6.62	10.78 2.93	14.08 -0.72	17.40 -4.32	20.90 -7.85	24.47 -11.30	28.17 -14.65	32.03 -17.88	36.10 -20.98	40.38 -23.92	44.90 -26.67	49.67 -29.20	54.73 -31.50							10
5			-6.28 14.52	-2.90 10.78	0.43 7.05	3.75 3.32	7.05 -0.40	10.40 -4.10	13.80 -7.75	17.30 -11.37	20.90 -14.88	27.33 -18.33	28.58 -21.68	32.73 -24.90	37.10 -27.97	41.77 -30.85									5
0				-6.68 7.47	-3.32 3.73	0.00 0.00	3.32 -3.73	6.68 -7.47	10.08 -11.17	13.58 -14.82	17.20 -18.42	20.97 -21.95	24.93 -25.40	29.12 -28.73	33.58 -31.92										0
-5					-7.05 0.40	-3.75 -3.32	-0.43 -7.05	2.90 -10.78	6.28 -14.52	9.77 -18.23	13.35 -21.88	17.10 -25.50	21.07 -29.03	25.27 -32.47											-5
-10						-7.52 -6.62	-4.25 -10.33	-0.97 -14.07	2.37 -17.82	5.78 -21.53	9.32 -25.25	13.00 -28.92	16.90 -32.52												-10
-15							-8.15 -13.58	-4.93 -17.30	-1.70 -21.02	1.62 -24.77	5.05 -28.50	8.65 -32.22													-15
-20								-9.05 -20.43	-5.93 -24.13	-2.75 -27.85	0.53 -31.60														-20
ϕ \ θ	-25	-20	-15	-10	-5	0	5	10	15	20	25	30	35	40	45	50	55	60	65	70	75	80	85	90	θ \ ϕ

Table VIII OEC projection data for the inclination, 48.4 degrees of the projection equator. The table gives both x (upper number) and y (lower number) in degrees of the great-circle arc as a function of ϕ, the earth latitude, and θ, the earth longitude measured eastward from the intersection between the earth and projection equators. The table includes one quarter of the zone within about 30 degrees from the projection equator. The values are computed from Equations (69) and (70).

58.3° OEC PROJECTION DATA

φ \ θ	-25	-20	-15	-10	-5	0	5	10	15	20	25	30	35	40	45	50	55	60	65	70	75	80	85	90	θ \ φ
85										84.58 29.87	84.78 29.48	85.03 29.12	85.32 28.75	85.63 28.42	86.00 28.10	86.37 27.82	86.77 27.57	87.18 27.35	87.62 27.15	88.10 26.95	88.55 26.87	89.03 26.78	89.52 26.72	90.00 26.70	85
80									78.98 28.63	79.37 27.83	79.83 27.07	80.33 26.33	80.92 25.63	81.55 25.00	82.25 24.38	83.00 23.85	83.77 23.37	84.58 22.92	85.45 22.55	86.33 22.25	87.22 22.02	88.13 21.83	89.07 21.73	90.00 21.70	80
75								73.22 27.98	73.73 26.78	74.35 25.62	75.07 24.50	75.87 23.42	76.75 22.42	77.70 21.48	78.72 20.60	79.80 19.80	80.97 19.10	82.17 18.48	83.40 17.93	84.67 17.50	85.98 17.15	87.30 16.90	88.65 16.75	90.00 16.70	75
70							67.32 27.93	67.93 26.32	68.68 24.73	69.52 23.23	70.52 21.78	71.58 20.38	72.77 19.07	74.05 17.87	75.37 16.73	76.80 15.72	78.28 14.80	79.85 14.00	81.45 13.28	83.12 12.73	84.80 12.28	86.52 11.95	88.27 11.77	90.00 11.70	70
65						61.27 28.43	61.97 26.42	62.78 24.43	63.78 22.53	64.88 20.70	66.12 18.92	67.47 17.23	68.93 15.65	70.50 14.18	72.15 12.83	73.90 11.57	75.72 10.47	77.63 9.50	79.60 8.63	81.60 7.95	83.67 7.42	85.77 7.02	87.87 6.78	90.00 6.70	65
60						55.83 27.07	56.77 24.70	57.82 22.42	59.03 20.18	60.40 18.03	61.87 15.97	63.48 14.03	65.22 12.17	67.08 10.47	69.03 8.87	71.08 7.42	73.23 6.12	75.47 4.98	77.77 3.97	80.13 3.17	82.57 2.53	85.02 2.07	87.50 1.78	90.00 1.70	60
55					49.57 28.23	50.55 25.50	51.68 22.82	52.98 20.22	54.43 17.72	56.03 15.28	57.77 12.95	59.63 10.73	61.62 8.65	63.73 6.70	65.97 4.88	68.33 3.23	70.77 1.77	73.33 0.45	75.97 -0.68	78.68 -1.62	81.47 -2.33	84.28 -2.87	87.13 -3.20	90.00 -3.30	55
50				43.15 29.83	44.18 26.75	45.40 23.73	46.77 20.78	48.30 17.92	49.97 15.13	51.78 12.43	53.75 9.87	55.83 7.43	58.10 5.10	60.45 2.93	62.97 0.90	65.60 -0.93	68.35 -2.60	71.20 -4.07	74.17 -5.35	77.22 -6.38	80.33 -7.22	83.53 -7.82	86.75 -8.18	90.00 -8.30	50
45				37.65 28.43	38.93 25.08	40.38 21.82	41.98 18.62	43.73 15.50	45.60 12.47	47.65 9.55	49.82 6.75	52.12 4.07	54.58 1.52	57.20 -0.87	59.95 -3.08	62.85 -5.12	65.88 -6.95	69.05 -8.60	72.33 -10.00	75.72 -11.17	79.20 -12.08	82.77 -12.77	86.37 -13.17	90.00 -13.30	45
40			30.90 30.43	32.32 26.80	33.85 23.25	35.52 19.73	37.33 16.32	39.27 12.98	41.35 9.75	43.57 6.58	45.93 3.57	48.45 0.68	51.10 -2.08	53.93 -4.65	56.92 -7.08	60.07 -9.30	63.38 -11.27	66.85 -13.10	70.45 -14.67	74.20 -15.93	78.03 -16.97	81.97 -17.70	85.97 -18.13	90.00 -18.30	40
35			25.45 28.80	27.12 24.98	28.88 21.23	30.78 17.53	32.77 13.92	34.90 10.38	37.15 6.95	39.53 3.62	42.07 0.38	44.75 -2.70	47.60 -5.63	50.63 -8.43	53.83 -11.03	57.23 -13.45	60.78 -15.63	64.55 -17.60	68.48 -19.28	72.58 -20.70	76.80 -21.83	81.13 -22.63	85.53 -23.13	90.00 -23.30	35
30		18.35 30.98	20.20 26.97	22.12 23.00	24.10 19.08	26.17 15.23	28.33 11.45	30.62 7.75	33.00 4.13	35.53 0.62	38.22 -2.78	41.05 -6.07	44.07 -9.20	47.27 -12.17	50.65 -14.97	54.27 -17.57	58.10 -19.92	62.15 -22.03	66.40 -23.92	70.85 -25.45	75.47 -26.68	80.23 -27.57	85.08 -28.12	90.00 -28.30	30
25		13.00 29.05	15.10 24.97	17.23 20.87	19.42 16.82	21.63 12.83	23.95 8.92	26.37 5.05	28.87 1.28	31.52 -2.38	34.33 -5.95	37.30 -9.42	40.45 -12.72	43.80 -15.87	47.38 -18.87	51.18 -21.63	55.27 -24.18	59.58 -26.47	64.17 -28.48	69.00 -30.18	74.03 -31.52				25
20	5.52 31.17	7.87 26.93	10.20 22.75	12.50 18.57	14.85 14.45	17.20 10.35	19.65 6.32	22.15 2.35	24.77 -1.57	27.50 -5.38	30.40 -9.10	33.47 -12.70	36.72 -16.18	40.22 -19.52	43.93 -22.68	47.93 -25.63	52.22 -28.38	56.83 -30.83							20
15	0.38 28.90	2.95 24.65	5.45 20.42	7.92 16.18	10.37 11.98	12.85 7.82	15.37 3.70	17.97 -0.38	20.65 -4.40	23.45 -8.33	26.40 -12.20	29.55 -15.95	32.87 -19.60	36.45 -23.10	40.30 -26.42	44.45 -29.57	48.93 -32.48								15
10	-4.55 26.45	-1.82 22.20	0.83 17.95	3.42 13.70	5.97 9.45	8.53 5.23	11.12 1.03	13.78 -3.12	16.50 -7.22	19.33 -11.27	22.33 -15.25	25.50 -19.13	28.85 -22.92	32.48 -26.58	36.42 -30.08										10
5	-9.25 23.83	-6.38 19.62	-3.65 15.38	-0.98 11.12	1.65 6.87	4.25 2.63	6.88 -1.60	9.55 -5.82	12.30 -10.00	15.15 -14.13	18.12 -18.20	21.28 -22.22	24.63 -26.12	28.28 -29.93											5
0			-8.02 12.72	-5.30 8.50	-2.63 4.25	0.00 0.00	2.63 -4.25	5.30 -8.50	8.02 -12.72	10.83 -16.92	13.77 -21.07	16.88 -25.18	20.20 -29.22												0
-5					-6.88 1.60	-4.25 -2.63	-1.65 -6.87	0.98 -11.12	3.65 -15.38	6.38 -19.62	9.25 -23.83	12.27 -28.02	15.48 -32.13												-5
-10						-8.53 -5.23	-5.97 -9.45	-3.42 -13.70	-0.83 -17.95	1.82 -22.20	4.55 -26.45	7.42 -30.68													-10
-15								-7.92 -16.18	-5.45 -20.42	-2.95 -24.65	-0.38 -28.90														-15
φ \ θ	-25	-20	-15	-10	-5	0	5	10	15	20	25	30	35	40	45	50	55	60	65	70	75	80	85	90	θ \ φ

Table IX OEC projection data for the inclination, 58.3 degrees of the projection equator. The table gives both x (upper number) and y (lower number) in degrees of the great-circle arc as a function of ϕ, the earth latitude, and θ, the earth longitude measured eastward from the intersection between the earth and projection equators. The table includes one quarter of the zone within about 30 degrees from the projection equator. The values are computed from Equations (69) and (70).

TEC PROJECTION DATA

ϕ \ θ	0	5	10	15	20	25	30	35	40	45	50	55	60	65	70	75	80	85	90	θ \ ϕ
0	0.00	0.00	0.00	0.00	0.00	0.00	0.00	0.00	0.00	0.00	0.00	0.00	0.00	0.00	0.00	0.00	0.00	0.00	0.00	0
	0.00	5.00	10.00	15.00	20.00	25.00	30.00	35.00	40.00	45.00	50.00	55.00	60.00	65.00	70.00	75.00	80.00	85.00	90.00	
5	5.00	5.02	5.07	5.18	5.32	5.52	5.78	6.10	6.52	7.05	7.75	8.68	9.93	11.70	14.35	18.72	26.80	45.08	90.00	5
	0.00	4.98	9.97	14.95	19.93	24.90	29.88	34.85	39.83	44.78	49.75	54.68	59.63	64.53	69.42	74.22	78.83	82.93	85.00	
10	10.00	10.03	10.15	10.35	10.62	11.00	11.52	12.13	12.97	14.00	15.35	17.08	19.43	22.65	27.28	34.28	45.43	63.72	90.00	10
	0.00	4.92	9.85	14.77	19.68	24.58	29.48	34.38	39.28	44.13	48.98	53.77	58.52	63.18	67.73	72.03	75.90	78.83	80.00	
15	15.00	15.07	15.22	15.50	15.92	16.47	17.20	18.12	19.28	20.75	22.63	25.03	28.20	32.37	38.08	45.53	57.07	71.97	90.00	15
	0.00	4.83	9.65	14.47	19.28	24.08	28.88	33.65	38.37	43.08	47.72	52.30	56.77	61.10	65.18	68.92	72.05	74.20	75.00	
20	20.00	20.08	20.28	20.65	21.17	21.87	22.80	23.95	25.42	27.23	29.52	32.38	36.07	40.73	46.77	54.60	64.52	76.52	90.00	20
	0.00	4.70	9.38	14.08	18.75	23.40	28.03	32.62	37.17	41.65	46.03	50.33	54.47	58.38	62.02	65.18	67.73	69.42	70.00	
25	25.00	25.08	25.33	25.77	26.38	27.23	28.30	29.65	31.33	33.40	35.97	39.12	43.00	47.83	53.77	60.97	69.58	79.40	90.00	25
	0.00	4.53	9.05	13.57	18.05	22.52	26.95	31.32	35.63	39.87	43.97	47.93	51.70	55.22	58.38	61.10	63.20	64.53	65.00	
30	30.00	30.10	30.37	30.87	31.57	32.50	33.70	35.18	37.00	39.23	41.92	45.20	49.10	53.80	59.35	65.85	73.27	81.40	90.00	30
	0.00	4.33	8.65	12.95	17.23	21.47	25.67	29.78	33.82	37.75	41.57	45.18	48.58	51.72	54.47	56.78	58.52	59.62	60.00	
35	35.00	35.12	35.40	35.93	36.68	37.70	38.97	40.52	42.43	44.72	47.45	50.67	54.47	58.88	63.98	69.72	76.07	82.90	90.00	35
	0.00	4.10	8.18	12.23	16.27	20.25	24.18	28.02	31.77	35.40	38.87	42.15	45.18	47.95	50.33	52.30	53.77	54.70	55.00	
40	40.00	40.12	40.43	40.97	41.77	42.80	44.08	45.70	47.60	49.88	52.55	55.63	59.22	63.28	67.83	72.87	78.30	84.07	90.00	40
	0.00	3.83	7.65	11.43	15.20	18.88	22.52	26.07	29.50	32.80	35.93	38.87	41.57	43.97	46.03	47.72	48.97	49.75	50.00	
45	45.00	45.10	45.45	45.98	46.78	47.82	49.10	50.67	52.55	54.73	57.27	60.15	63.43	67.10	71.12	75.48	80.15	85.02	90.00	45
	0.00	3.53	7.05	10.55	14.00	17.40	20.70	23.92	27.03	30.00	32.80	35.38	37.77	39.85	41.63	43.07	44.13	44.78	45.00	
50	50.00	50.10	50.43	50.97	51.73	52.75	53.98	55.50	57.27	59.32	61.67	64.30	67.23	70.47	73.98	77.73	81.72	85.82	90.00	50
	0.00	3.22	6.40	9.57	12.70	15.75	18.75	21.63	24.40	27.03	29.50	31.77	33.82	35.63	37.15	38.37	39.27	39.82	40.00	
55	55.00	55.10	55.40	55.92	56.65	57.60	58.77	60.15	61.78	63.65	65.77	68.12	70.70	73.52	76.53	79.73	83.07	86.50	90.00	55
	0.00	2.87	5.72	8.53	11.32	14.03	16.67	19.20	21.63	23.93	26.07	28.02	29.78	31.32	32.62	33.63	34.38	34.85	35.00	
60	60.00	60.10	60.38	60.85	61.53	62.37	63.43	64.68	66.15	67.80	69.63	71.68	73.88	76.28	78.83	81.50	84.27	87.12	90.00	60
	0.00	2.50	4.97	7.43	9.85	12.20	14.47	16.67	18.75	20.70	22.53	24.18	25.67	26.95	28.03	28.88	29.50	29.87	30.00	
65	65.00	65.08	65.33	65.77	66.33	67.10	68.02	69.10	70.35	71.75	73.32	75.02	76.88	78.85	80.93	83.12	85.38	87.67	90.00	65
	0.00	2.12	4.22	6.28	8.32	10.28	12.20	14.02	15.77	17.38	18.88	20.25	21.47	22.53	23.40	24.10	24.60	24.90	25.00	
70	70.00	70.07	70.28	70.63	71.12	71.75	72.50	73.40	74.43	75.57	76.83	78.20	79.68	81.25	82.90	84.62	86.38	88.20	90.00	70
	0.00	1.70	3.40	5.08	6.72	8.32	9.85	11.32	12.70	14.00	15.20	16.27	17.23	18.05	18.75	19.28	19.68	19.92	20.00	
75	75.00	75.07	75.22	75.48	75.87	76.35	76.93	77.63	78.40	79.27	80.22	81.27	82.37	83.53	84.77	86.03	87.33	88.65	90.00	75
	0.00	1.28	2.58	3.83	5.08	6.28	7.43	8.53	9.57	10.55	11.43	12.25	12.95	13.57	14.08	14.48	14.77	14.95	15.00	
80	80.00	80.03	80.15	80.33	80.60	80.93	81.32	81.78	82.30	82.90	83.55	84.22	84.97	85.75	86.55	87.38	88.23	89.12	90.00	80
	0.00	0.87	1.73	2.58	3.40	4.22	4.98	5.72	6.42	7.05	7.65	8.18	8.65	9.07	9.38	9.65	9.85	9.97	10.00	
85	85.00	85.02	85.08	85.17	85.30	85.47	85.67	85.90	86.17	86.47	86.78	87.13	87.50	87.88	88.30	88.70	89.13	89.57	90.00	85
	0.00	0.43	0.87	1.30	1.72	2.12	2.50	2.87	3.22	3.53	3.83	4.10	4.33	4.53	4.70	4.83	4.92	4.98	5.00	
90	90.00	90.00	90.00	90.00	90.00	90.00	90.00	90.00	90.00	90.00	90.00	90.00	90.00	90.00	90.00	90.00	90.00	90.00	90.00	90
	0.00	0.00	0.00	0.00	0.00	0.00	0.00	0.00	0.00	0.00	0.00	0.00	0.00	0.00	0.00	0.00	0.00	0.00	0.00	
ϕ \ θ	0	5	10	15	20	25	30	35	40	45	50	55	60	65	70	75	80	85	90	θ \ ϕ

Table X TEC projection data. The numbers in the table denote both x (lower numbers) and y (upper numbers) in degrees computed from Equation (70). To produce TEC table, i, the inclination of the projection equator is chosen as 90.0 degrees. ϕ ....the earth latitude, θ ....the earth longitude measured from the intersection of the TEC projection equator and the earth equator.

$\Delta\rho$ \ d (km)	0	200	400	600	800	1000	1200	1400	1600	1800	2000	2200	2400	2600	2800	3000
0	0.0	0.0	0.0	0.0	0.0	0.0	0.0	0.0	0.0	0.0	0.0	0.0	0.0	0.0	0.0	0.0
10	0.0	0.0	0.0	0.0	0.1	0.1	0.2	0.2	0.3	0.4	0.5	0.6	0.7	0.8	1.0	1.1
20	0.0	0.0	0.0	0.1	0.2	0.2	0.4	0.5	0.6	0.8	1.0	1.2	1.4	1.7	1.9	2.2
30	0.0	0.0	0.0	0.1	0.2	0.4	0.5	0.7	0.9	1.2	1.5	1.8	2.1	2.5	2.9	3.3
32.2 km	0.0	0.0	0.0	0.1	0.2	0.4	0.6	0.8	1.0	1.3	1.6	1.9	2.3	2.7	3.1	3.5

Table XI Height of the earth's surface above the spheroid with mean radius of the earth, which is tangent to the terrestrial ellipsoid at the subsatellite point (TSP). $\Delta\rho$ ....the excess radius of curvature of the earth. d ....the distance between an object on the earth and the TSP. The numbers in the table are the heights in km computed from Equation (61).

η \ d	1	2	3	4	5	6	8	10	12	14	16	18	20	22	24	26	28	30	32	34	36	38	40
0																							
1	6365																						
2	3181	6360	9533																				
3	2119	4237	6349	8460																			
4	1588	3174	4756	6337	7913	9484																	
5	1269	2536	3799	5062	6319	7573																	
6	1056	2110	3161	4211	5256	6298	8369																
7	904	1806	2704	3602	4496	5386	7155	8909															
8	790	1577	2361	3145	3925	4701	6244	7771	9281														
9	701	1399	2094	2789	3480	4168	5533	6885	8220	9537													
10	629	1256	1880	2504	3123	3740	4964	6174	7369	8547	9707												
11	571	1139	1704	2270	2831	3389	4497	5592	6672	7736	8783	9812											
12	522	1042	1558	2074	2587	3097	4107	5105	6089	7058	8011	8946	9862										
13	480	959	1433	1909	2380	2848	3777	4693	5595	6484	7356	8211	9050	9868									
14	445	887	1326	1766	2202	2635	3492	4338	5171	5989	6793	7580	8351	9104	9838								
15	414	826	1233	1642	2047	2449	3245	4030	4802	5560	6304	7032	7744	8439	9116	9773							
16	387	771	1152	1534	1911	2286	3029	3759	4478	5183	5874	6551	7211	7855	8482	9090	9680						
17	363	723	1080	1437	1791	2142	2837	3520	4191	4850	5494	6125	6739	7339	7921	8486	9033	9561					
18	341	680	1015	1352	1684	2014	2665	3306	3935	4552	5155	5744	6319	6878	7421	7947	8455	8945	9417	9870			
19	322	642	958	1275	1588	1898	2512	3115	3706	4285	4851	5403	5941	6464	6972	7462	7936	8393	8832	9252	9654		
20	304	607	905	1205	1501	1794	2373	2941	3498	4043	4576	5095	5600	6090	6565	7025	7468	7895	8304	8695	9068	9421	9756
21	289	575	858	1142	1422	1699	2247	2784	3310	3824	4326	4815	5290	5750	6197	6627	7042	7441	7823	8187	8535	8863	9173
22	274	546	814	1084	1349	1613	2131	2640	3138	3624	4098	4559	5006	5440	5860	6264	6654	7028	7384	7725	8048	8353	8641
23	261	520	775	1031	1283	1533	2026	2508	2980	3440	3888	4324	4747	5156	5551	5932	6297	6648	6982	7300	7602	7886	8153
24	249	495	738	982	1222	1460	1928	2387	2834	3271	3695	4108	4507	4894	5267	5625	5969	6298	6611	6909	7190	7455	7703
25	237	473	704	937	1166	1392	1838	2275	2700	3114	3517	3908	4286	4652	5004	5342	5666	5974	6269	6547	6810	7057	7288
26	227	452	673	895	1114	1330	1755	2170	2575	2969	3352	3723	4081	4381	4760	5079	5384	5675	5951	6212	6458	6688	6902
27	217	432	644	856	1065	1271	1677	2073	2459	2834	3198	3550	3890	4218	4533	4834	5122	5396	5655	5900	6130	6344	6543
28	208	414	616	820	1020	1217	1605	1983	2351	2708	3054	3389	3712	4023	4321	4605	4877	5135	5379	5608	5823	6023	6208
29	199	397	591	786	977	1166	1537	1898	2249	2590	2920	3238	3545	3840	4122	4391	4648	4891	5120	5335	5536	5723	5894
30	192	381	567	754	937	1118	1473	1819	2154	2479	2793	3097	3388	3668	3936	4190	4433	4662	4877	5079	5267	5441	5600
31	184	366	544	724	899	1073	1413	1744	2064	2375	2674	2963	3241	3506	3760	4001	4230	4446	4648	4838	5013	5174	5322
32	177	352	523	695	864	1030	1356	1673	1980	2276	2562	2837	3101	3354	3594	3823	4039	4242	4432	4610	4774	4924	5061
33	170	338	503	668	830	990	1303	1606	1900	2183	2456	2718	2970	3210	3438	3654	3858	4050	4229	4395	4548	4687	4813
34	164	326	484	643	799	952	1252	1543	1824	2095	2356	2606	2845	3073	3289	3494	3687	3867	4035	4191	4333	4462	4579
35	158	313	466	619	768	916	1204	1482	1752	2011	2260	2498	2726	2943	3148	3342	3524	3694	3851	3996	4129	4249	4356
36	152	302	448	596	740	881	1158	1425	1683	1931	2169	2397	2614	2820	3014	3198	3369	3529	3677	3812	3936	4046	4144
37	147	291	432	574	712	848	1114	1371	1618	1855	2082	2300	2506	2702	2886	3060	3222	3372	3510	3637	3751	3852	3942
38	141	281	416	553	686	817	1072	1318	1555	1782	2000	2207	2403	2589	2764	2928	3081	3222	3351	3469	3574	3668	3749
39	136	271	401	533	661	787	1032	1269	1496	1713	1921	2118	2305	2482	2648	2803	2946	3079	3199	3309	3406	3491	3565
40	131	261	387	514	637	758	994	1221	1439	1647	1845	2034	2212	2379	2536	2682	2817	2941	3054	3155	3245	3322	3388
41	127	252	373	495	614	731	958	1175	1384	1583	1772	1952	2121	2280	2429	2567	2694	2810	2914	3008	3090	3160	3219
42	122	243	360	478	592	704	922	1131	1331	1522	1703	1874	2035	2186	2326	2456	2575	2683	2780	2866	2941	3004	3056
43	118	234	347	461	571	679	888	1089	1281	1463	1636	1799	1951	2094	2227	2349	2461	2561	2651	2730	2798	2854	2900
44	114	226	335	444	550	654	856	1048	1232	1406	1571	1726	1871	2006	2131	2246	2350	2444	2527	2599	2660	2710	2749
45	110	218	323	429	531	631	824	1009	1185	1351	1508	1656	1794	1922	2039	2147	2244	2331	2407	2472	2527	2570	2603
46	106	211	311	413	512	608	794	971	1139	1298	1448	1589	1719	1840	1951	2051	2142	2221	2291	2350	2398	2436	2463
47	103	203	300	399	493	586	764	934	1095	1247	1390	1523	1647	1761	1865	1959	2042	2116	2179	2232	2274	2306	2327
48	99	196	290	384	475	564	736	899	1053	1198	1334	1460	1577	1684	1782	1869	1946	2014	2071	2117	2154	2180	2196.
49	96	189	279	371	458	544	708	864	1012	1150	1279	1399	1509	1610	1701	1782	1853	1915	1966	2007	2038	2058	2068
50	92	183	269	357	441	524	682	831	972	1104	1226	1339	1443	1538	1623	1698	1763	1818	1864	1899	1924	1940	1945
51	89	176	259	344	425	504	656	799	933	1058	1175	1282	1380	1468	1547	1616	1675	1725	1765	1795	1815	1825	1825
52	86	170	250	331	409	485	630	767	895	1014	1125	1226	1318	1400	1473	1536	1590	1634	1669	1693	1708	1713	1708
53	83	164	241	319	394	467	606	736	858	972	1076	1171	1257	1334	1401	1459	1507	1546	1575	1595	1604	1604	1595
54	80	158	232	307	379	449	582	707	823	930	1029	1118	1198	1269	1882	1384	1427	1460	1484	1498	1503	1498	1484
55	77	152	223	296	364	431	559	678	788	889	982	1066	1141	1207	1263	1310	1348	1376	1395	1405	1405	1395	1376
56	74	146	214	284	350	414	536	649	754	850	937	1016	1085	1145	1196	1238	1271	1294	1308	1313	1308	1294	1271
57	71	140	206	273	336	397	514	621	721	811	893	966	1030	1085	1131	1168	1196	1215	1224	1224	1215	1196	1168
58	68	135	198	262	323	381	492	594	688	773	850	918	977	1027	1068	1100	1123	1136	1141	1136	1123	1100	1068
59	66	130	190	251	309	365	471	568	656	736	808	871	925	970	1006	1033	1051	1060	1060	1051	1033	1006	970
60	63	124	182	241	296	349	450	542	625	700	767	824	873	914	945	967	981	985	981	967	945	914	873
61	61	119	174	231	283	334	429	516	595	665	726	779	823	859	885	903	912	912	903	885	859	823	779
62	58	114	167	221	271	319	409	491	565	630	687	735	774	805	827	840	844	840	827	805	774	735	687
63	56	109	159	211	259	304	390	467	535	596	648	691	726	752	769	778	778	769	752	726	691	648	596
64	53	104	152	201	246	290	370	443	507	562	609	648	678	700	713	717	713	700	678	648	609	562	507
65	51	100	145	192	235	275	351	419	478	529	572	606	632	649	657	657	649	632	606	572	529	478	419
66	49	95	138	182	223	261	333	396	450	497	535	564	586	598	603	598	586	564	535	497	450	396	333
67	46	90	131	173	211	248	314	373	423	465	498	524	540	549	549	540	524	498	465	423	373	314	248
68	44	86	124	164	200	234	296	350	396	433	462	483	496	500	496	483	462	433	396	350	296	234	164
69	42	81	117	155	189	221	278	328	369	402	427	444	452	452	444	427	402	369	328	278	221	155	81
70	39	77	111	146	178	207	261	306	343	372	392	405	409	405	392	372	343	306	261	207	146	77	0
71	37	73	104	137	167	194	243	284	317	341	358	366	366	358	341	317	284	243	194	137	73	0	
72	35	68	98	129	156	181	226	263	291	311	324	328	324	311	291	263	226	181	129	68	0		
73	33	64	91	120	145	169	209	241	266	282	290	290	282	266	241	209	169	120	64	0			
74	31	60	85	112	135	156	192	220	241	253	257	253	241	220	192	156	112	60	0				
75	29	56	79	103	124	143	175	200	216	224	224	216	200	175	143	103	56	0					
76	27	52	73	95	114	131	159	179	191	195	191	179	159	131	95	52	0						
77	25	47	66	87	104	119	143	159	167	167	159	143	119	87	47	0							
78	23	43	60	79	94	107	126	138	142	138	126	107	79	43	0								
79	21	39	54	71	84	94	110	118	118	110	94	71	39	0									
80	19	35	48	63	74	82	94	98	94	82	63	35	0										
81	17	31	42	55	64	71	78	78	71	55	31	0											
82	15	27	36	47	54	59	63	59	47	27	0												
83	13	23	31	39	44	47	47	39	23	0													
84	11	19	25	31	34	35	31	19	0														
85	9	16	19	23	24	23	16	0															
86	7	12	13	16	15	12	0																
87	5	8	7	8	5	0																	
88	3	4	1	0																			
89	1	0																					
90																							

Table XII Height of satellite as a function of the nadir angle (η) of an object at the distance (d) in degrees of arc from the sub-satellite point. The numbers to the left denote the nadir angle at one degree increments, and those at the top denote the distance from the subpoint in degrees of great-circle arc. The numbers in the table are the heights of the satellite in km. Computed from Equation (52).

RIGHT ASCENSION OF GREENWICH

YEAR FUNCTION

1960	1961	1962	1963	1964	1965	1966	1967	1968	1969	1970
-2.48	-1.73	-1.97	-2.21	-2.45	-1.70	-1.94	-2.18	-2.42	-1.68	-1.91

DAY FUNCTION (* is for leap year)

DAY	MAR	APR	MAY	JUN	JUL	AUG	SEPT	OCT	NOV	DEC	JAN	FEB	MAR	MAR*
1		10.84	40.41	70.96	100.53	131.08	161.64	191.21	221.76	251.33	281.88	312.44	340.03	341.02
2		11.83	41.39	71.95	101.52	132.07	162.62	192.19	222.75	252.31	282.87	313.42	341.02	342.00
3		12.81	42.38	72.93	102.50	133.06	163.60	193.18	223.73	253.30	283.85	314.41	342.00	342.99
4		13.80	43.37	73.92	103.49	134.04	164.60	194.16	224.72	254.28	284.84	315.39	342.99	343.97
5		14.78	44.35	74.91	104.47	135.03	165.58	195.15	225.70	255.27	285.82	316.38	343.97	344.96
6		15.77	45.34	75.89	105.46	136.01	166.57	196.13	226.69	256.26	286.81	317.36	344.96	345.95
7		16.76	46.32	76.88	106.44	137.00	167.55	197.12	227.67	257.24	287.80	318.35	345.95	346.93
8		17.74	47.30	77.86	107.43	137.98	168.54	198.11	228.66	258.23	288.78	319.33	346.93	347.92
9		18.73	48.29	78.85	108.42	138.97	169.52	199.09	229.64	259.21	289.77	320.32	347.92	348.90
10		19.71	49.28	79.83	109.40	139.96	170.51	200.08	230.63	260.20	290.75	321.31	348.90	349.89
11		20.70	50.26	80.82	110.39	140.94	171.49	201.06	231.62	261.18	291.74	322.29	349.89	350.87
12		21.68	51.25	81.80	111.37	141.93	172.48	202.05	232.60	262.17	292.72	323.28	350.87	351.86
13		22.67	52.24	82.79	112.36	142.91	173.46	203.03	233.59	263.16	293.71	324.26	351.86	352.84
14		23.65	53.22	83.78	113.34	143.90	174.45	204.02	234.57	264.14	294.69	325.25	352.84	353.83
15		24.64	54.21	84.76	114.33	144.88	175.44	205.00	235.56	265.13	295.68	326.23	353.83	354.82
16		25.63	55.19	85.75	115.32	145.87	176.42	205.99	236.54	266.11	296.67	327.22	354.82	355.80
17		26.61	56.18	86.73	116.30	146.85	177.41	206.98	237.53	267.10	297.65	328.20	355.80	356.79
18		27.60	57.16	87.72	117.29	147.84	178.39	207.96	238.52	268.08	298.64	329.19	356.79	357.77
19		28.58	58.15	88.70	118.27	148.83	179.38	208.95	239.50	269.07	299.62	330.18	357.77	358.76
20		29.57	59.14	89.69	119.26	149.81	180.36	209.93	240.49	270.05	300.61	331.16	358.76	359.74
21	0.00	30.55	60.12	90.68	120.24	150.80	181.35	210.92	241.47	271.04	301.59	332.15		
22	0.99	31.53	61.11	91.66	121.23	151.78	182.34	211.90	242.46	272.03	302.58	333.13		
23	1.97	32.52	62.09	92.65	122.21	152.77	183.32	212.89	243.44	273.01	303.56	334.12		
24	2.96	33.51	63.08	93.63	123.20	153.75	184.31	213.88	244.43	274.00	304.55	335.10		
25	3.94	34.50	64.06	94.62	124.19	154.74	185.29	214.86	245.41	274.98	305.54	336.09		
26	4.93	35.48	65.05	95.60	125.17	155.72	186.28	215.85	246.40	275.97	306.52	337.08		
27	5.91	36.47	66.04	96.59	126.16	156.71	187.26	216.83	247.39	276.95	307.51	338.06		
28	6.90	37.45	67.02	97.57	127.14	157.70	188.25	217.82	248.37	277.94	308.49	339.05		
29	7.88	38.44	68.01	98.56	128.13	158.68	189.24	218.80	249.36	278.92	309.48	340.03		
30	8.87	39.42	68.99	99.55	129.11	159.67	190.22	219.79	250.34	279.91	310.46			
31	9.85		69.97		130.10	160.65		220.77		280.90	311.45			

HOUR FUNCTION (hours in Greenwich time)

0	1	2	3	4	5	6	7	8	9	10	11
-180.00	+164.96	-149.92	-134.88	-119.84	-104.79	-89.75	-74.71	-59.67	-44.63	-29.59	-14.55
12	13	14	15	16	17	18	19	20	21	22	23
00.49	15.53	30.58	45.62	60.66	75.70	90.74	105.78	120.82	135.86	150.90	165.94

MINUTE FUNCTION

0	1	2	3	4	5	6	7	8	9	10	11	12	13	14	15	16	17	18	19
0.00	0.25	0.50	0.75	1.00	1.25	1.50	1.75	2.01	2.26	2.51	2.76	3.01	3.26	3.51	3.76	4.01	4.26	4.51	4.76
20	21	22	23	24	25	26	27	28	29	30	31	32	33	34	35	36	37	38	39
5.01	5.26	5.51	5.77	6.02	6.27	6.52	6.77	7.02	7.27	7.52	7.77	8.02	8.27	8.52	8.77	9.02	9.28	9.53	9.78
40	41	42	43	44	45	46	47	48	49	50	51	52	53	54	55	56	57	58	59
10.03	10.28	10.53	10.78	11.03	11.28	11.53	11.78	12.03	12.28	12.53	12.78	13.04	13.29	13.54	13.79	14.04	14.29	14.54	14.79

SECOND FUNCTION

0	2	4	6	8	10	12	14	16	18	20	22	24	26	28	30	32	34	36	38	40	42	44	46	48	50	52	54	56	58	60
0.00	0.01	0.02	0.03	0.04	0.04	0.05	0.06	0.07	0.08	0.08	0.09	0.10	0.11	0.12	0.13	0.13	0.14	0.15	0.16	0.17	0.18	0.18	0.19	0.20	0.21	0.22	0.23	0.23	0.24	0.25

Table XIII Right ascension of Greenwich. The right ascension in degrees at a given moment is obtained by adding the numbers in Year, Day, Hour, Minute, and Second Functions. Equation (33) gives the breakdown of the right ascension into five functions. The year in the Year Function table begins at 0000Z, March 21 and ends 2400Z March 20 of the following year.

GEODETIC LATITUDE OF SUBSOLAR POINT

DAY FUNCTION

DAY	JAN	FEB	DAY	MAR	APR	MAY	JUN	JUL	AUG	SEP	OCT	NOV	DEC
*			1	-7.9	+4.3	+14.9	+22.0	+23.2	+18.2	+8.5	-2.9	-14.2	-21.7
1	-23.1	-17.3	2	-7.5	+4.7	+15.2	+22.1	+23.1	+17.9	+8.2	-3.3	-14.5	-21.9
2	-23.0	-17.0	3	-7.1	+5.0	+15.5	+22.2	+23.0	+17.7	+7.8	-3.7	-14.9	-22.0
3	-22.9	-16.7	4	-6.7	+5.4	+15.8	+22.4	+22.9	+17.4	+7.5	4.1	-15.2	-22.1
4	-22.8	-16.4	5	-6.3	+5.8	+16.0	+22.5	+22.9	+17.2	+7.0	4.5	-15.5	-22.3
5	-22.7	-16.1	6	-5.9	+6.2	+16.3	+22.6	+22.8	+16.9	+6.7	5.9	-15.8	-22.4
6	-22.6	-15.8	7	-5.6	+6.6	+16.6	+22.7	+22.7	+16.6	+6.3	5.2	-16.1	-22.5
7	-22.5	-15.5	8	-5.2	+6.9	+16.9	+22.8	+22.6	+16.4	+6.0	5.6	-16.4	-22.7
8	-22.3	-15.2	9	-4.8	+7.3	+17.2	+22.9	+22.5	+16.1	+5.6	6.0	-16.7	-22.8
9	-22.2	-14.9	10	-4.4	+7.7	+17.4	+23.0	+22.3	+15.8	+5.2	6.4	-17.0	-22.9
10	-22.0	-14.6	11	-4.0	+8.0	+17.7	+23.0	+22.2	+15.5	+4.8	6.8	-17.2	-22.9
11	-21.9	-14.3	12	-3.6	+8.4	+18.0	+23.1	+22.1	+15.2	+4.5	7.1	-17.5	-23.0
12	-21.8	-13.9	13	-3.2	+8.8	+18.2	+23.2	+21.9	+14.9	+4.0	-7.5	-17.8	-23.1
13	-21.6	-13.6	14	-2.8	+9.2	+18.5	+23.2	+21.8	+14.6	+3.7	-7.9	-18.0	-23.2
14	-21.4	-13.3	15	-2.4	+9.5	+18.7	+23.3	+21.6	+14.3	+3.3	-8.3	-18.3	-23.2
15	-21.3	-12.9	16	-2.0	+9.9	+18.9	+23.3	+21.5	+14.0	+2.9	-8.6	-18.6	-23.3
16	-21.1	-12.6	17	-1.6	+10.2	+19.2	+23.4	+21.3	+13.7	+2.5	-9.0	-18.8	-23.3
17	-20.9	-12.2	18	-1.2	+10.6	+19.4	+23.4	+21.2	+13.3	+2.2	-9.4	-19.0	-23.4
18	-20.7	-11.9	19	-0.8	+10.9	+19.6	+23.4	+21.0	+13.0	+1.8	-9.7	-19.3	-23.4
19	-20.5	-11.5	20	-0.4	+11.3	+19.8	+23.4	+20.8	+12.7	+1.4	-10.1	-19.5	-23.4
20	-20.3	-11.2	21	0.0	+11.6	+20.0	+23.4	+20.6	+12.4	+1.0	-10.5	-19.8	-23.4
21	-20.1	-10.8	22	+0.4	+12.0	+20.3	+23.5	+20.4	+12.0	+0.6	-10.8	-20.0	-23.5
22	-19.8	-10.5	23	+0.8	+12.3	+20.5	+23.4	+20.2	+11.7	+0.2	-11.2	-20.2	-23.4
23	-19.6	-10.1	24	+1.2	+12.6	+20.6	+23.4	+20.0	+11.4	-0.2	-11.5	-20.4	-23.4
24	-19.4	-9.7	25	+1.5	+13.0	+20.8	+23.4	+19.8	+11.0	-0.6	-11.9	-20.6	-23.4
25	-19.1	-9.4	26	+1.9	+13.3	+21.0	+23.4	+19.6	+10.7	-1.0	-12.2	-20.8	-23.4
26	-18.9	-9.0	27	+2.3	+13.6	+21.2	+23.4	+19.4	+10.3	-1.4	-12.6	-21.0	-23.4
27	-18.6	-8.6	28	+2.7	+13.9	+21.4	+23.3	+19.2	+10.0	-1.8	-12.9	-21.2	-23.3
28	-18.4	-8.2	29	+3.1	+14.3	+21.5	+23.3	+18.9	+9.6	-2.1	-13.2	-21.4	-23.3
29	-18.1	-7.9	30	+3.5	+14.6	+21.7	+23.2	+18.7	+9.3	-2.5	-13.5	-21.5	-23.2
30	-17.8		31	+3.9	+14.9	+21.8	+23.2	+18.5	+8.9	-2.9	-13.9	-21.7	-23.2
31	-17.6			+4.3		+22.0		+18.2	+8.5		-14.2		-23.1

* is for leap year months after March 1

YEAR AND HOUR FUNCTION

YEAR			HOUR																					
1960	1964	1968	0	2	4	6	8	10	12	14	16	18	20	22	24									
1961	1965	1969										0	2	4	6	8	10	12	14	16	18	20	22	24
1962	1966	1970							0	2	4	6	8	10	12	14	16	18	20	22	24			
1963	1967	1971				0	2	4	6	8	10	12	14	16	18	20	22	24						
Absolute value of Geodetic Latitude from DAY FUNCTION		0-12	-0.2	-0.2	-0.2	-0.1	-0.1	0.0	0.0	0.0	0.1	0.1	0.1	0.2	0.2	0.2	0.3	0.3	0.3	0.4	0.4	0.4	0.5	0.5
		12-20	-0.2	-0.1	-0.1	-0.1	-0.1	0.0	0.0	0.0	0.1	0.1	0.1	0.1	0.2	0.2	0.2	0.2	0.3	0.3	0.3	0.3	0.4	0.4
		20-22	-0.1	-0.1	-0.1	-0.1	0.0	0.0	0.0	0.0	0.0	0.1	0.1	0.1	0.1	0.1	0.1	0.2	0.2	0.2	0.2	0.2	0.2	0.3
		22-23	-0.1	0.0	0.0	0.0	0.0	0.0	0.0	0.0	0.0	0.0	0.0	0.0	0.1	0.1	0.1	0.1	0.1	0.1	0.1	0.1	0.1	0.1
		23-	0.0	0.0	0.0	0.0	0.0	0.0	0.0	0.0	0.0	0.0	0.0	0.0	0.0	0.0	0.0	0.0	0.0	0.0	0.0	0.0	0.0	0.0

Table XIV Geodetic latitude of Subsolar point at any given time is obtained from this table by simply adding the angles in degrees tabulated as the Day Function and the Year and Hour Function. The Day Function is obtained by selecting the angle at the intersection of the month and the day, tabulated in the column between Feb. and March, except for the 12 month period following leap year, March 1, for which the days given in the first column are used.

The Year and Hour Function is determined as a function of the hour, which varies according to the year, and the absolute value of the Geodetic latitude from the particular day. It is required to change the sign of the Hour Function when the Day Function is decreasing with time. (Hours in Greenwich Time)

LONGITUDE OF SUBSOLAR POINT

DAY FUNCTION

DAY	JAN	FEB	DAY	MAR	APR	MAY	JUN	JUL	AUG	SEP	OCT	NOV	DEC
*			1	+3.2	1.0	-0.7	-0.6	+0.9	+1.6	+0.1	-2.5	-4.1	-2.8
1	+0.8	+3.4	2	+3.0	1.0	-0.7	-0.6	+0.9	+1.6	0.0	-2.6	-4.1	-2.7
2	+0.9	+3.4	3	+3.0	0.9	-0.8	-0.5	+1.0	+1.5	-0.1	-2.7	-4.1	-2.6
3	+1.0	+3.5	4	+3.0	0.8	-0.8	-0.5	+1.0	+1.5	-0.2	-2.7	-4.1	-2.5
4	+1.2	+3.5	5	+2.9	0.7	-0.8	-0.4	+1.1	+1.5	-0.3	-2.8	-4.1	-2.4
5	+1.3	+3.5	6	+2.9	0.7	-0.8	-0.4	+1.1	+1.5	-0.3	-2.9	-4.1	-2.3
6	+1.4	+3.5	7	+2.8	0.6	-0.9	-0.4	+1.2	+1.4	-0.4	-2.9	-4.1	-2.2
7	+1.5	+3.5	8	+2.8	0.5	-0.9	-0.3	+1.2	+1.4	-0.5	-3.0	-4.1	-2.1
8	+1.6	+3.6	9	+2.7	0.5	-0.9	-0.3	+1.2	+1.4	-0.6	-3.1	-4.1	-2.0
9	+1.7	+3.6	10	+2.6	0.4	-0.9	-0.2	+1.3	+1.4	-0.7	-3.2	-4.0	-1.9
10	+1.8	+3.6	11	+2.6	0.3	-0.9	-0.2	+1.3	+1.3	-0.8	-3.3	-4.0	-1.8
11	+1.9	+3.6	12	+2.5	0.3	-0.9	-0.1	+1.4	+1.3	-0.9	-3.3	-4.0	-1.7
12	+2.0	+3.6	13	+2.4	0.2	-0.9	-0.1	+1.4	+1.2	-0.9	-3.4	-3.9	-1.5
13	+2.1	+3.6	14	+2.4	0.1	-0.9	-0.0	+1.4	+1.2	-1.0	-3.4	-3.9	-1.4
14	+2.2	+3.6	15	+2.3	0.1	-0.9	+0.0	+1.4	+1.1	-1.1	-3.5	-3.9	-1.3
15	+2.3	+3.6	16	+2.2	0.0	-0.9	+0.1	+1.5	+1.1	-1.2	-3.6	-3.8	-1.2
16	+2.4	+3.5	17	+2.2	-0.1	-0.9	+0.1	+1.5	+1.0	-1.3	-3.6	-3.8	-1.1
17	+2.5	+3.5	18	+2.1	-0.1	-0.9	+0.2	+1.5	+1.0	-1.4	-3.7	-3.7	-1.0
18	+2.6	+3.5	19	+2.0	-0.2	-0.9	+0.3	+1.5	+0.9	-1.5	-3.7	-3.7	-0.8
19	+2.6	+3.5	20	+1.9	-0.2	-0.9	+0.3	+1.6	+0.9	-1.6	-3.8	-3.6	-0.7
20	+2.7	+3.5	21	+1.9	-0.3	-0.9	+0.4	+1.6	+0.8	-1.7	-3.8	-3.6	-0.6
21	+2.8	+3.4	22	+1.8	-0.3	-0.9	+0.4	+1.6	+0.8	-1.7	-3.8	-3.5	-0.4
22	+2.9	+3.4	23	+1.7	-0.4	-0.9	+0.5	+1.6	+0.7	-1.8	-3.9	-3.4	-0.3
23	+2.9	+3.4	24	+1.6	-0.4	-0.8	+0.5	+1.6	+0.6	-1.9	-3.9	-3.4	-0.2
24	+3.0	+3.3	25	+1.6	-0.5	-0.8	+0.6	+1.6	+0.6	-2.0	-3.9	-3.3	-0.1
25	+3.1	+3.3	26	+1.5	-0.5	-0.8	+0.6	+1.6	+0.5	-2.1	-4.0	-3.2	0.0
26	+3.1	+3.2	27	+1.4	-0.6	-0.8	+0.7	+1.6	+0.4	-2.2	-4.0	-3.2	+0.2
27	+3.2	+3.2	28	+1.3	-0.6	-0.7	+0.7	+1.6	+0.4	-2.3	-4.0	-3.1	+0.3
28	+3.2	+3.2	29	+1.3	-0.6	-0.7	+0.8	+1.6	+0.3	-2.3	-4.0	-3.0	+0.4
29	+3.3	+3.2	30	+1.2	-0.7	-0.7	+0.8	+1.6	+0.2	-2.4	-4.1	-2.9	+0.5
30	+3.3		31	+1.1	-0.7	-0.6	+0.9	+1.6	+0.1	-2.5	-4.1	-2.8	+0.7
31	+3.4			+1.0		-0.6		+1.6	+0.1		-4.1		+0.8

*is for leap year months after March 1

HOUR FUNCTION

0	1	2	3	4	5	6	7	8	9	10	11
+180	+165	+150	+135	+120	+105	+90	+75	+60	+45	+30	+15

12	13	14	15	16	17	18	19	20	21	22	23
0	-15	-30	-45	-60	-75	-90	-105	-120	-135	-150	-165

MINUTE FUNCTION

0	2	4	6	8	10	12	14	16	18	20	22	24	26	28
0.0	-0.5	-1.0	-1.5	-2.0	-2.5	-3.0	-3.5	-4.0	-4.5	-5.0	-5.5	-6.0	-6.5	-7.0

30	32	34	36	38	40	42	44	46	48	50	52	54	56	58
-7.5	-8.0	-8.5	-9.0	-9.5	-10.0	-10.5	-11.0	-11.5	-12.0	-12.5	-13.0	-13.5	-14.0	-14.5

Table XV Longitude of Subsolar point at any given time is obtained from this table by simply adding the angles tabulated as Day Function, Hour Function and Minute Function. The days in the column between Feb. and March are used except for the 12 month period following leap year, March 1, for which the days given in the first column are used. (Hours in Greenwich Time)

GLOSSARY

ANOMALISTIC PERIOD OF SATELLITE (P_{soa}): The time elapsing between successive passages of a satellite through the perigee.

APPARENT IMAGE ROTATION: The rotation of image principal line in successive frames caused by the combined effects of spinning motion of a satellite, rotation of terrestrial principal line, and the fixed intervals between pictures. The rate of apparent image rotation may be faster or slower than the spin rate of the satellite.

APPARENT SOLAR ROTATION RATE OF THE EARTH (ω_{ess}): (see Mean Solar Rotation Rate of the Earth)

APOGEE: The point in its orbit at which the satellite is farthest from the center of the earth.

APSIS: The points in an elliptic orbit at which the radius vectors reach a maximum or a minimun. (e.g. perigee and apogee of a satellite orbit). The line joining these two points is called the line of apsides.

ARGUMENT OF PERIGEE (w): The geocentric angle of the perigee measured in the orbital plane from its ascending node in the direction of motion.

ARGUMENT OF SATELLITE (u_s): The geocentric angle of a satellite measured in the orbital plane from the ascending node in the direction of motion.

ARGUMENT OF SATELLITE AT MINIMUM (MAXIMUM) NADIR ANGLE (u_s^{MIN}): (see Argument of Satellite and Nadir Angle)

ASCENDING NODE (AN): The point at the equator at which the satellite in its orbital motion crosses from the southern to the northern hemisphere. Terrestrial Ascending Node (TAN) is given in degrees longitude. Celestial Ascending Node (CAN) is given on right ascension hours, minutes, etc.

ASCENDING NODE TIME (t^{AN}): The time when the satellite passes the ascending node.

AXIS OF HOMOLOGY: The intersection of an image plane and projectively related horizontal plane.

AZIMUTH (α): A horizontal direction expressed in degrees measured clockwise from an adopted reference direction, usually true north.

BASEPLATE ANGLE (ϕ_B): The tangential angle on TIROS baseplate with respect to its center located at the intersection of the spin axis and the baseplate. The angle, viewed from the TIROS top, is measured clockwise from the zero reference line engraved on the baseplate.

BULGE OF THE EARTH ($R_E - R_P$): The difference between the equatorial and the polar radii of the earth.

CDA: Command and Data Acquisition Station (see Data Acquisition Station)

CELESTIAL (C): The prefix to designate lines or points which have been projected onto the celestial sphere by means of the radials through the center of the earth.

CELESTIAL EQUATOR: The great circle along which the plane of the earth's equator intersects the celestial sphere.

CELESTIAL SPHERE: An imaginary sphere of infinite radius with its center located at the observer or at the center of the earth. In satellite meteorology the center of the celestial sphere is at the center of the earth. Lines or points are projected onto the celestial sphere using radials through the center of the earth.

CELESTIAL SUBSATELLITE POINT (CSP): A point on the celestial sphere the declination of which is identical to the geocentric latitude of TSP and the right ascension of that of TSP.

CLOUD BAND: A broad band of clouds, from about 10 to 100 or more miles wide, and varying in length from a few tens of miles to hundreds of miles. (see Cloud Street)

CLOUD STREET: A line of clouds a few to ten miles wide, and varying in length.

COA: Celestial Optical-Axis Point. (see Optical-Axis Point)

COA': Celestial Optical-Axis Antipode. (see Optical-Axis Point)

CPM: Celestial Primary Point. (see Primary Point)

CPP: Celestial Principal Point. (see Principal Point)

CSA: Celestial Spin-Axis Point. (see Spin-Axis Point)

CSA': Celestial Spin-Axis Antipode. (see Spin-Axis Point)

CSP: Celestial Subsatellite Point. (see Subsatellite Point)

CSS: Celestial Subsun Point. (see Subsun Point)

DATA-ACQUISITION STATION (CDA): A ground station at which various functions to control satellite operations and to obtain data from the satellite are performed. The CDA transmits programming signals to the satellite, and commands transmission of data to the ground. Processing of data by electronic machine and by hand is accomplished at the CDA station. Raw and processed data are disseminated from CDA stations.

DECLINATION (δ): The angular distance of an object north (+) or south (-) from the celestial equator measured along the hour circle passing through the object.

DEGRADATION: The lessening of picture image quality because of "noise", rotation of the satellite, etc., or any optical, electronic, or mechanical distortions in the image-forming system.

DESCENDING NODE (DN): The southbound equator crossing of the satellite; given in degrees longitude, date, and time for any given orbit or pass. Terrestrial Descending Node (TDN): Celestial Descending Node (CDN).

DIP ANGLE (δ_H): The vertical angle at the exposure station between the true and apparent horizons measured on the principal plane.

DIRECT ORBIT: The orbit with inclination between 0^o and 90^o. Same as the prograde orbit.

DISTORTED PERSPECTIVE TILT GRID: (see Distorted Tilt Grid)

DISTORTED TILT GRID: Tilt grid distorted to fit to the actual distorted images. For operational purposes, one set of distorted tilt grids for one camera is sufficient. Perspective tilt grids are similarly converted into distorted tilt grids.

DISTORTION: An apparent warping and twisting of a picture image received from a satellite. This distortion has two causes: electronic and optical. "Electronic Distortion" is caused by imperfections in the circuitry, the tape recorder, the vidicon tube structure, the transmission system, or the signal characteristics. "Optical Distortion" is caused by the characteristics of the lens and optical alignment.

DISTORTION-FREE (FIDUCIAL) GRID: The image of a fiducial grid transcribed onto the plane of test target with any principal distance. There exists only one distortion-free fiducial grid for each TIROS camera. Any object angle measured on this grid represents the true angle.

ECLIPTIC: The great circle in which the plane of the earth's orbit intersects the celestial sphere.

EEC PROJECTION: Abbreviation for Equatorial Equidistant Cylindrical Projection. (see Cylindrical Projection)

EQUATION OF TIME ($\mathcal{E}$): The apparent solar-time less mean solar-time at any instance.

EQUIDISTANT CYLINDRICAL PROJECTION: A cylindrical projection in which the distance along the projection equator and the projection meridians is identical to that of the great circle arc. This projection is classified into EEC, TEC, and OEC for which the inclination of the projection equator is 0, 90, and other angles, respectively.

EXCESS RADIUS OF CURVATURE ($\Delta\rho_e$): True radius of curvature of the terrestrial ellipsoid less the mean radius of the earth. The excess radius of curvature varies between plus and minus 32.2 km.

EXCESS RADIUS OF THE EARTH ($R - R_p$): The earth's radius at any point less its polar radius.

FIDUCIAL MARKS: Index marks rigidly connected with the camera optical system so that they form images on the negative. The fiducial marks of TIROS vidicon cameras are the "L" shaped corner marks and the "+" shaped mark near the picture center, which are on the focal plane.

FIXED-EARTH (F): The prefix to designate a line or point which is projected onto the surface of a virtual earth whose rotational motion has been fixed. The time of fix may be chosen at any moment. The fixed-earth latitude is identical to the true latitude. The fixed-earth longitude of a terrestrial point increases at the rate of about 0.25 deg per minute.

FIXED-EARTH LONGITUDE (Θ): The meridional angle of a point, on the earth or in space, measured eastward from the Greenwich Meridian at the time of fix.

FIXED-SPACE ROTATION-RATE OF THE EARTH (ω_{esf}): Angular velocity of the earth's rotation with respect to fixed space. As a result of the periodic, irregular and secular variations the rate varies slightly.

FIXED-SPACE SPIN-PERIOD OF A SATELLITE (P_{ssf}): The time required for one complete rotation of a satellite with respect to fixed space.

FOA: Fixed Earth Optical-Axis Point. (see Optical-Axis Point)

FOA': Fixed Earth Optical-Axis Antipode. (see Optical-Axis Point)

FOCUS SHEET: A focus sheet is a diagram containing fiducial marks scaled to produce the correct projected image size for the scale of perspective or latitude-

longitude grids used. For convenience, the focus sheet usually also contains a small sharp vertical shaft at the principal point, about which graphs used for attitude or rectification may be rotated.

FPM: Fixed Earth Primary Point. (see Primary Point)

FPP: Fixed Earth Principal Point. (see Principal Point)

FSA: Fixed Earth Spin-Axis Point. (see Spin-Axis Point)

FSA': Fixed Earth Spin-Axis Antipode. (see Spin-Axis Point)

FSS: Fixed Earth Subsun Point. (see Subsun Point)

GAMMA: Gamma is the angle at the satellite between the satellite spin-axis and the satellite-sun line.

GEOCENTRIC LATITUDE (ϕ_c): The angle measured in the meridional plane, between the terrestrial equator and the geocentric radius-vector.

GEODETIC LATITUDE (ϕ_d): The angle measured in a meridional plane between the local vertical and the equatorial plane of the earth.

HEIGHT GRID: Groups of lines on a plane or a cylindrical surface tangent to the earth's surface at TSP. Regular height grids include isolines of horizontal and nadir angles. Perspective height grids include lines of vertical angles oriented toward the four orthogonal horizontal directions. Height grids may be constructed to fit the scale and the projection of a map.

HORIZON DISTANCE (ϵ_H): The radial angle measured on the principal line between the principal point and the apparent horizon.

HORIZONTAL ANGLE (ψ): The angle between the principal plane and a vertical plane through the satellite. The angle of these two planes measured on an image plane is the image horizontal angle.

IGL: Image Sun-Glint Point. (see Sun-Glint Point)

IMAGE (I): The prefix to designate a line or a point on an image surface.

IMAGE HORIZONTAL-ANGLE (ψ_i): (see Horizontal Angle)

IMAGE PRIMARY LINE: (see Primary Line)

IMAGE (PRIMARY) SUN-LINE: The intersection of a primary sun-plane with the image plane.

IMAGE PRINCIPAL LINE: (see Principal Line)

IMAGE RASTER LINE: One line of raster on an image plane. (see Raster)

INCLINATION (OF SATELLITE ORBIT) (ι): The angle defined by the axial vectors of the earth's and the satellite's rotation measured from the spin vector of the earth. Inclination of retrograde orbit is expressed by 180 degrees minus the prograde inclination.

INTERNATIONAL ELLIPSOID: (see Terrestrial Ellipsoid)

IPM: Image Primary Point. (see Primary Point)

IPP: Image Principal Point. (see Principal Point)

ISN: Image Sun-Point. The point of projection of the sun onto an image plane.

ISP: Image Subsatellite Point. (see Subsatellite Point)

ISS: Image Subsun Point. (see Subsun Point)

LATITUDE-LONGITUDE GRID: A latitude-longitude grid is a form of perspective grid in which the quadrilaterals are latitudes and longitudes.

LINE OF APSIDES OR NODES: (see Apsis and Node)

LOCAL RADIUS OF CURVATURE OF THE EARTH (ρ_e): The radius of curvature of a standard earth at the local point of interest. This curvature is the fuction of both latitude and the azimuth angle.

LOCAL SUN-PLANE: A plane defined by the sun and the local vertical through a point on the earth or in space. The plane is identified by adding the local point, thus: local TSP sun-plane.

LOCAL SUN-LINE: The intersection of the local sun-plane with the surface of the earth. The local sun-line passes through the local point and orients toward the direction of the sun.

LOCAL VERTICAL: A line perpendicular to the surface of a standard earth.

LOL: Teletype code for the argument of satellite at which the minimum nadir-angle occurs.

MAXIMUM SATELLITE NADIR-ANGLE (η_c^{MAX}): (see Satellite Nadir-Angle)

MEAN RADIAL DISTORTION: The ratio of the tangent of a mean radial angle on an

image and that of the corresponding radial angle in the true object space. Mean radial distortion is expressed as a function of radial angles.

MEAN SOLAR ROTATION RATE OF THE EARTH ($\bar{\omega}_{ess}$): Mean angular velocity of the earth's rotation with respect to the sun. The apparent solar rotation rate (ω_{ess}) varies from day to day mainly because of the variable speed of the earth's motion around the sun and the inclination of the ecliptic to the celestial equator. The apparent solar day may differ as much as half a minute from the mean solar day.

MINIMUM SATELLITE NADIR-ANGLE (η_s^{MIN}): (see Satellite Nadir-Angle)

MSL: Abbreviation for Meteorological Satellite Laboratory. A unit of the U.S. Weather Bureau National Weather Satellite Center.

NADIR ANGLE (η): The angle measured at the satellite between a specific axis or ray and the local vertical. The nadir angles of the satellite spin-axis and a camera optical-axis are called the "satellite nadir-angle" (η_s) and the "tilt" (τ), respectively.

NADIR POINT: The point on the celestial sphere directly beneath the satellite and directly opposite the zenith.

NASA: Abbreviation for National Aeronautics and Space Administration.

NODE: The points at the equator at which the satellite, in its orbital motion crosses the equator. The line connecting the ascending and the descending nodes is called the line of nodes.

NODAL PERIOD (P_{son}): The time elapsing between successive passages of the satellite through the ascending node.

NODAL SPIN-AXIS: An axis parallel to the satellite spin-axis through the front nodal point of the camera lens. The positive direction is from the top to the floor of a satellite.

NOISE: A voltage received through an antenna system or within the ground amplifier and other electronics that does not correspond to any intended signal. The "noise" seen on TIROS pictures is ordinarily in the form of small specks; occasionally noise appears in the form of bands or streaks along raster lines. TIROS radiation analog traces also include noise which is either regular or irregular pulsations superimposed upon the true signals.

NON: Teletype code for the minimum satellite nadir-angle.

NUTATION OF SATELLITE: A variation in the precessional motion of a satellite spin-axis.

OBJECT SPACE ANGLE: The angle between two rays in space that intersect at the front nodal point of a camera lens.

OBLIQUE MERCATOR MAP PROJECTION: An oblique mercator map projection is a mercator map projection in which the tangent cylinder is inclined to the equator. It is convenient to have the inclination approximate that of the satellite orbit inclination.

OEC OVERLAY: An overlay chart placed on an OEC chart for the purpose of measuring the great-circle distance and the azimuth between the points on the chart. The chart can be obtained by changing the longitudes and latitudes on a TEC projection chart into the great-circle distances and the azimuths.

OEC PROJECTION: Abbreviation for Oblique Equidistant Cylindrical Projection. A cylindrical projection which preserves the actual great circle distances along the projection equator and the projection meridians. The projection equator is a great circle on the terrestrial spheroid along which the cylindrical surface is tangent. The projection meridians are the great circles perpendicular to the projection equator.

OPTICAL AXIS: A straight line passing through the front and rear nodal points of a camera lens. The direction on the axis is considered positive from the rear to the front nodal points.

OPTICAL-AXIS ANTIPODE (OA'): (see Optical-Axis Point)

OPTICAL-AXIS POINT (OA): The points at which the lines parallel to the optical axis of a satellite-borne camera intersect the earth at right angles. The optical-axis antipode and the optical-axis point are located, respectively, toward the positive and negative directions of the optical axis translated to the center of the earth. Terrestrial Optical-Axis Point (TOA), Terrestrial Optical-Axis Antipode (TOA'), Fixed-Earth Optical-Axis Point (FOA), and Fixed-Earth Optical-Axis Antipode (FOA').

OPTICAL AND ELECTRONIC DISTORTIONS: (see Distortion)

ORBIT: The path which a celestial object follows in its motions through space, relative to some selected point.

ORBIT NUMBER: In satellite meteorology orbit number refers to a particular circuit beginning at the satellite ascending node. The orbit number from launch to the first ascending node is designated zero, thereafter the number increases by one at each ascending node.

PERIGEE: The point in its orbit at which the satellite is closest to the center of the earth.

PERIGEE RATE ($\dot{w}$): Rate of change of the argument of perigee. It is usually measured in degrees per day.

PERSPECTIVE GRID (TILT AND HEIGHT COMBINED): A perspective grid is a network of lines constructed for an oblique photograph, the lines representing corresponding lines of an imaginary quadrilateral on the surface of the earth. A distorted perspective grid may incorporate the effect of lens distortion in addition to perspective. The grids also have the principal point indicated, and the horizon, if present. A library of perspective grids may be prepared for discrete increments of tilt and satellite height.

PERSPECTIVE HEIGHT GRID: (see Height Grid)

PERSPECTIVE TILT GRID: Tilt grid consisting of isolines of vertical angles in the orientation of principal plane and its perpendicular.

PRECESSION RATE ($\dot{\Omega}^{AN}$): The fixed space angular motion of the orbital line of nodes; positive to the East, negative to the West.

PRIMARY LINE: A line of intersection between the primary plane and the image plane (Image Primary Line), the earth (Terrestrial Primary Line), the fixed earth (Fixed Primary Line), or the celestial sphere (Celestial Primary Line).

PRIMARY PLANE: A plane including the nodal spin-axis and the local vertical through the satellite.

PRIMARY POINT (PM): Point of intersection of nodal spin-axis with the image plane (IPM), with the earth (TPM), or with the fixed-earth (FPM).

PRIMARY SUN-LINE: The intersection of a primary sun-plane with the earth or with an image.

PRIMARY SUN-PLANE: A plane including the sun and the satellite spin-axis.

PRIMARY TANGENTIAL-ANGLE (γ'): (see Tangential Angle)

PRINCIPAL DISTANCE (f): The distance measured along the optical axis either from the nodal point or the interior perspective center to the image or target plane.

PRINCIPAL LINE: A line of intersection between the principal plane and the image plane (Image Principal Line), the earth (Terrestrial Principal-Line), or the fixed earth (Fixed-Earth Principal Line).

PRINCIPAL PLANE: The plane which includes the optical axis of a camera and the local vertical through the front nodal-point of a satellite camera lens.

PRINCIPAL POINT: The point of intersection of the optical axis of the camera with the image plane (IPP), with the earth (TPP), or with the fixed earth (FPP).

PRINCIPAL TANGENTIAL-ANGLE (γ): (see Tangential Angle)

PROGRADE ORBIT: (see Direct Orbit)

PROJECTION EQUATOR: The great circle of the earth along which the surface of a cylindrical projection contacts the earth's surface.

PROJECTION MERIDIAN: Great circles which are perpendicular to the plane of the projection equator of a cylindrical projection.

R/O: Abbreviation for readout orbit.

RADIAL ANGLE (ϵ): An angle between the optical axis and the line connecting the interior perspective center with any point on a photograph or a target.

RASTER: The pattern followed by the electron-beam exploring-element scanning the screen of a television transmitter or receiver. The scanning pattern or raster of the vidicon used in TIROS satellites is, theoretically, a series of straight parallel lines.

RASTER LINE: One scan line of a TV system.

READ-OUT STATION: (see Data Acquisition Station)

RESOLUTION: The ability of a film, a lens, a combination of both, and/or a vidicon system to render barely distinguishable a standard pattern of black and white lines. When the resolution is said to be, e.g., 10 lines per millimeter, it means that the pattern whose line-plus-space width is 0.1 mm is barely resolved, the finer patterns are not resolved, and the coarser patterns are more clearly resolved.

RETROGRADE ORBIT: (see Inclination)

RIGHT ASCENSION (Ω): The arc measured eastward along the celestial equator from the vernal equinox to the great circle passing through the celestial poles and the object projected onto the celestial sphere. This angle is frequently given in hours and minutes--24 hours equivalent to 360 degrees.

SATELLITE NADIR-ANGLE (η_s): The nadir angle of a satellite spin-axis. The angle is measured from the nadir point to the positive direction of the nodal spin-axis.

SOLAR SPIN PERIOD (P_{sss}): The time elapsed between successive primary sun-plane crossings of a particular satellite baseplate angle.

SPIN AXIS: The axis about which the satellite spins. The positive direction along the spin axis is designated from the top to the floor of the satellite.

SPIN-AXIS ANTIPODE (SA'): (see Spin-Axis Point)

SPIN-AXIS POINT (SA): The points at which the lines parallel to the spin axis of a satellite intersect the earth's surface at right angles. The spin-axis antipode and the spin-axis point are located, respectively, toward the positive and negative direction of the spin axis translated to the center of the earth. Terrestrial Spin-Axis Point (TSA), Terrestrial Spin-Axis Antipode (TSA'), Fixed-Earth Spin-Axis Point (FSA) and Fixed-Earth Spin-Axis Antipode (FSA').

SPIN PERIOD (P) AND SPIN RATE (ω): Time required for a complete rotation. The spin period varies according to a reference plane with respect to which the period is measured. The reference planes are primary plane, sun plane, equinox plane, etc.

SUBPOINT TRACK: Locus of subsatellite points on the earth (TSP Track), on image (ISP Track), or on a celestial sphere (CSP Track).

SUBSATELLITE DECLINATION: The declination of a subsatellite point.

SUBSATELLITE POINT: Intersections of the local vertical passing through the satellite with the earth's surface (TSP), with the fixed earth (FSP), with the image plane (ISP), and with the celestial sphere (CSP). The coordinates of these points are expressed either by subsatellite latitude (ϕ^{TSP}) and longitude (θ^{TSP}) or by declination (δ^{CSP}) and right ascension (Ω^{CSP}).

SUBSOLAR POINT (SS): Intersection of the local vertical through the sun with the surface of the earth (TSS), and with the fixed-earth (FSS). The image subsolar point (ISS) denotes the projection of TSS onto an image plane.

SUN-GLINT POINT (GL): A point on the earth where the line connecting the satellite with the image of the sun formed by the earth's surface as a convective mirror intersects the earth's surface.

SUN PLANE: A plane defined by the sun and another straight line. The local sun-plane includes the local vertical. The spin-axis sun-plane includes the spin axis of a satellite.

TANGENTIAL ANGLE: The angle of a radial on image measured clockwise from the reference radial through IPP (Principal Tangential-Angle) or (Primary Tangential-Angle).

TEC PROJECTION: Abbreviation for Transverse Equidistant Cylindrical Projection. (see OEC Projection)

TERRESTRIAL (T): The term to designate a line or a point on the earth's surface.

TERRESTRIAL ELLIPSOID: An ellipsoid closest to the shape of the earth excluding the atmosphere. The international ellipsoid adopted in 1924 by the International Union of Geodesy and Geophysics is recommended for use.

TERRESTRIAL PRIMARY LINE: Intersection of a primary plane with the surface of the earth.

TERRESTRIAL PRINCIPAL LINE: Intersection of a principal plane with the surface of the earth.

TGL: Terrestrial Sun-Glint Point. (see Sun-Glint Point)

TILT (τ): The angle at the perspective center between the camera optical-axis and the local vertical.

TILT GRID: A grid consisting of two sets of isolines on an image plane. They vary solely with the tilt, and the satellite height has nothing to do with the grid determination. For the precise rectification purposes, isolines of horizontal and nadir angles are used.

TILT INDICATOR: A tilt indicator is a graph for measuring tilt from projected images of earth having horizons. A library of tilt indicators is prepared for discrete increments of satellite height, the usual increment being 25 statute miles (approximately 15 km).

TIME OF FIX (t_F): The moment when the rotational motion of the earth is fixed to establish the coordinates referring to the rotation-free earth.

TIME OF MAXIMUM SATELLITE NADIR-ANGLE (t_S^{MAX}): The time when maximum value of satellite nadir angle occurs.

TIME OF MINIMUM SATELLITE NADIR-ANGLE (t_S^{MIN}): The time when minimum value of satellite nadir angle occurs.

TIME PAST ASCENDING NODE: The amount of time for a body in orbit to advance from the last ascending node to an arbitrary position.

TIME PAST PERIGEE: The amount of time for a body in orbit to advance from the last perigee to an arbitrary position.

TIROS: Abbreviation for Television Infra Red Observation Satellite.

TOA: Terrestrial Optical-Axis Point. (see Optical-Axis Point)

TOA': Terrestrial Optical-Axis Antipode. (see Optical-Axis Point)

TOT: Teletype code for the time of minimum satellite nadir-angle.

TPM: Terrestrial Primary Point. (see Primary-Point)

TPP: Terrestrial Principal Point. (see Principal-Point)

TRACK: A line connecting successive positions of a moving point. This term is used with a 3-letter designator. IPP track, TSP track are the examples.

TRACK DISTANCE (η_T , d_T): The distance between a subsatellite point and the TPM track. The distance is measured as the nadir angle (η_T) viewed from the satellite or the distance of arc (d_T).

TRANSFER GRID: A transfer grid is a quadrilateral grid, constructed to the scale of a geographic map, whose grid net bears a one-to-one correspondence to the net of a perspective grid. The transfer grid has the principal point and the principal line indicated on it.

TRUE ANOMALY (ν): The geocentric angle of a satellite measured in the orbital plane from its perigee in the direction of motion.

TSA: Terrestrial Spin-Axis Point. (see Spin-Axis Point)

TSA': Terrestrial Spin-Axis Antipode. (see Spin-Axis Point)

TSP: Terrestrial Subsatellite Point. (see Subsatellite Point)

TSS: Terrestrial Subsolar Point. (see Subsolar Point)

VERNAL EQUINOX: (Also called the first of Aries). The point of intersection of the celestial equator with the ecliptic, at the point where the sun crosses from the south to the north side of the equator.

VERTICAL ANGLE (ζ): The angle between the local vertical and an oblique plane. The direction of the vertical plane, which is perpendicular to the oblique plane, defines the orientation of the vertical angle.

~~VIDICON: A photoconductive image pickup or television type tube. Each television~~ camera in the satellite consists of a set of optic, a focal plane shutter and a vidicon tube. The image is focused on the vidicon screen by the lens, and the

vidicon scanner transforms the image to an electric signal which can be transmitted or recorded on magnetic tape.

ACKNOWLEDGEMENTS

The author wishes to thank Messrs. James E. Arnold, Joseph L. Goldman, Dr. Soren H. H. Larsen and other staff members of the Mesometeorology Project, Department of Geophysical Sciences, University of Chicago, for their assistance. As to the technical matters, useful suggestions and comments were given by Mr. Linwood F. Whitney, Meteorological Satellite Laboratory, U. S. Weather Bureau, and Mr. William R. Bandeen, National Aeronautics and Space Administration. Without their assistance this report would not have been completed. Sincere gratitude should be expressed to Dr. Morris Tepper, Director of Meteorological Systems, National Aeronautics and Space Administration, and Mr. David S. Johnson, Deputy Director of the Meteorological Satellite Laboratory, for their encouragements and suggestions.

REFERENCES

1. Bandeen, W. R. and W. P. Manger, 1960: Angular motion of the spin axis of the TIROS I meteorological satellite due to magnetic and gravitational torques. Journal of Geophysical Research, 65, 2992-2995.

2. Danby, J. M. A., 1962: Fundamentals of Celestial Mechanics, Macmillan Co.

3. Davis, R. J., F. L. Whipple and J. B. Zirker, 1956: The orbit of a small earth satellite. Scientific Uses of Earth Satellites, second edition 1-22. University of Michigan Press.

4. Fujita, T., 1961: Outline of a technique for precise rectification of satellite cloud photographs. Mesometeorology Research Paper No. 3, University of Chicago.

5. Glaser, A. H., 1960: A system for the meteorological use of satellite television observations. Chapter IV, GRD Research Notes No. 36. Geophysics Research Directorate.

6. Hubert, L. F., 1961: TIROS I: Camera attitude data, analysis of location errors and derivation of correction for calibration. Meteorological Satellite Laboratory Report No. 5, U. S. Weather Bureau.

7. Hubert, L. F., 1961: Canadian grids for TIROS I; Additional orientation data; Errata. Supplement to Meteorological Satellite Laboratory Report No. 5, U. S. Weather Bureau.

8. Kozai, Y., 1959: The motion of a close earth satellite. Astronomical Journal, 9, 367-377.

9. RCA, 1960-62: Alignment and calibration data for the TIROS I-V meteorological satellites. Radio Corporation of America, Princeton.

10. Spitzer, L., 1950: Perturbation of a satellite orbit. Journal of British Interplanetary Society 9, 131.

11. Stafford, W. H., R. M. Croft and G. C. Marshall 1961: Artificial earth satellites and successful solar probes, 1957-60. National Aeronautics and Space Administration Technical Note D-601.

12. Stroud, W. G., 1961: The TIROS satellites. Proceedings of International Meteorological Satellite Workshop, Washington, D. C. 31-43.